

ACCELERATING THE THROUGHPUT OF MASS SPECTROMETRY
ANALYSIS BY ADVANCED WORKFLOW AND INSTRUMENTATION

A Dissertation

Submitted to the Faculty

of

Purdue University

by

Zhuoer Xie

In Partial Fulfillment of the

Requirements for the Degree

of

Doctor of Philosophy

August 2020

Purdue University

West Lafayette, Indiana

THE PURDUE UNIVERSITY GRADUATE SCHOOL
STATEMENT OF DISSERTATION APPROVAL

Dr. R. Graham Cooks, Chair

Department of Chemistry

Dr. Christina W. Li

Department of Chemistry

Dr. Garth J. Simpson

Department of Chemistry

Dr. Hilkka I. Kenttämä

Department of Chemistry

Approved by:

Dr. Christine A. Hrycyna

Head of the School Graduate Program

To the past, and to the unknown future.

ACKNOWLEDGMENTS

In the first place, I would like to thank my family for their perpetual support and unconditional love. I have lost track of how many times I missed the family gathering on traditional festivals, and what comforts my nostalgia is the jar of chopped peppers brought from home. I wish to express my special gratitude to my grandfather, Qilong He, who suffered from wars in his early life but has made it out alive. He wished to witness my graduation but I did not succeed in finishing before his passing away in April. But those summer days we spent cultivating in his garden are the best memory of my childhood. I will keep his diligence and perseverance in mind and live up to it.

I am grateful to my advisor, Prof. R. Graham Cooks, who offers me opportunity to conduct my graduate study in his group. He has not only presented the magnificent world of mass spectrometry but also taught invaluable life lessons to me. I would not accomplish this journey without Graham's encouragement and criticism.

I am deeply indebted to Dr. Zhenwei Wei for his mentoring in my research. All those meals Zhenwei hosted are short but fabulous getaways. Dr. Christina R. Ferreira has been patiently guiding me through the entire work of MRM-profiling and expanding my knowledge in metabolomics. Thank you both for bettering my understanding of being a researcher.

My sincere appreciation goes to previous group members for the initial training and generous guidance on my research: Dr. Pu Wei, Dr. Chris Pulliam, Dr. Valentina Pirro, Zezhen Zhang, Dr. Mei Zhang, Dr. Tianyang Guo, Dr. Karen Yannell, Prof. Wen-ping Peng, Dr. Jing Yi, Dr. Steve Ayrton, Dr. Ryan Bain, Dr. Xinming Huo,

Dr. Adam Hollerbach, Dr. Hong Zhang, Dr. Patrick Fedick, Dr. Dalton Snyder, Dr. Clint Alfaro, Dr. David Logsdon, Dr. Kiran Iyer, and Dr. Fan Pu. The most recent person who left Aston Labs is Brandy McMasters. She managed to organize everything and made our life much easier throughout the years.

I am also thankful to current group members for all the discussions and time we shared: Robert Schrader, Tsdale Mehari, Yangjie Li, Xingshuo Chen, Hannah Brown, Lucas Szalwinski, Sangeeta Pandey, Rong Chen, Saquib Rahman, Lingqi Qiu, Edwin Gonzalez, Nicolás Morato Gutiérrez, Yanyang Hu, Kai-Hung Huang, Phoebe Le, and Dylan Holden. Wish you a meaningful graduate life, though it is meant to be busy and challenging.

I thank Prof. Garth Simpson, Dr. Christina Li, and Dr. Hilka Kenttämä for being on my defense committee. Likewise, I would also like to thank professors of course that I took and members of the Amy facility for consulting and problem solving when I was confused.

TABLE OF CONTENTS

	Page
LIST OF TABLES	ix
LIST OF FIGURES	x
ABSTRACT	xvi
CHAPTER 1. MASS SPECTROMETRY-BASED LIPIDOMICS	1
1.1 Overview	1
1.2 Lipids	2
1.2.1 Classification	2
1.2.2 Isomerism and Shorthand Notation	4
1.3 Current Exploratory Lipidomics Platforms	6
1.3.1 Chromatography Coupled to Mass Spectrometry	7
1.3.2 Direct Injection Mass Spectrometry	9
1.3.3 Mass Spectrometry Imaging	9
1.4 Analytical Challenges and Concerns in Lipidomics	10
1.4.1 Dark Lipidome and Reproducibility Between Platforms	11
1.4.2 Pursuit of Ultimate Structural Elucidation and Separation	12
1.4.3 Faulty Annotation and Assignment	13
1.5 References	14
CHAPTER 2. MULTIPLE REACTION MONITORING (MRM-PROFILING)	
WORKFLOW	20
2.1 Background to MRM-Profiling	20
2.2 Preparation for MRM-Profiling	21
2.2.1 Precursor Ion Scan and Neutral Loss Scan	21
2.2.2 Method Library	25
2.3 Discovery Stage	35
2.3.1 Worklist Generation	36
2.3.2 Data Processing	41
2.3.3 MRM Method Development for Screening Stage	41
2.4 Screening Stage	42
2.4.1 Worklist Generation	43
2.4.2 Data Processing and Statistical Analysis	43
2.5 Identification Stage	44

	Page
2.6 An Example: Milk from Human, Cow, and Soy	44
2.7 Summary	46
2.8 References	53
 CHAPTER 3. QUANTITATIVE ANALYSIS OF PHOSPHOLIPIDS IN OOCYTES AND BLASTOCYSTS BY MRM-PROFILING	
3.1 Abstract	54
3.2 Introduction	55
3.3 Materials and Methods	56
3.3.1 Cultivation of Samples	56
3.3.2 Chemicals	59
3.3.3 Lipid Extraction	59
3.3.4 MRM-Profiling	61
3.3.5 Data Analysis	61
3.3.6 Normalization Methods	62
3.4 Results and Discussion	64
3.4.1 Evaluation of Quantitative Data on Lipids in Oocytes	64
3.4.2 Comparison of Relative and Absolute Normalization of Lipids in Bovine Oocytes and Blastocysts	72
3.5 Conclusions	75
3.6 References	78
 CHAPTER 4. MRM-PROFILING OF LIPIDS TO DISTINGUISH STRAIN- LEVEL DIFFERENCES IN MICROBIAL RESISTANCE IN <i>ESCHERICHIA</i> <i>COLI</i>	
4.1 Abstract	80
4.2 Introduction	81
4.2.1 Antimicrobial Resistance	81
4.2.2 Clinical Identification and Diagnosis	81
4.2.3 Lipid Analysis	82
4.3 Experimental Section	83
4.3.1 Chemicals	83
4.3.2 Bacterial Culture	83
4.3.3 Minimum Inhibitory Concentration Test	84
4.3.4 Sample Preparation	85
4.3.5 Multiple Reaction Monitoring Profiling	85
4.3.6 Statistical Analysis	87
4.4 Results and Discussion	88
4.4.1 Lipid Analysis of Non-Resistant Strains	88
4.4.2 Lipid Profile Differences Between Non-Resistant and Resistant Bacterial Strains	89
4.5 Conclusions	97
4.6 References	97

	Page
CHAPTER 5. HIGH-THROUGHPUT BIOASSAYS USING "DIP-AND-GO" MULTIPLYED ELECTROSPRAY MASS SPECTROMETRY	101
5.1 Abstract	101
5.2 Introduction	102
5.3 Experimental Section	104
5.3.1 Chemicals	104
5.3.2 Reactions	104
5.3.3 Dip-and-Go System	106
5.3.4 Mass Spectrometry Setup	106
5.4 Performance of System	107
5.4.1 Reaction Screening	107
5.4.2 Capability of Bioassays	109
5.4.3 High-Throughput Bioassays	119
5.5 Discussions on Electrophoretic Cleaning and Ion Stacking	123
5.6 Summary	125
5.7 References	125
VITA	128
PUBLICATIONS	129

LIST OF TABLES

Table	Page
2.1 Parameters and details of scan methods in library for lipids.	26
2.2 Parameters and details of scan methods in library for metabolites.	31
2.3 Details of MRM methods based on LipidMaps database in library.	35
3.1 Information of lipid internal standards	60
3.2 Parameters of instrument for MRM-profiling	63
3.3 List of MRMs used for analysis and corresponding <i>RSDs</i>	65
3.4 Quantified amount of lipid of each class per oocyte	72
4.1 MIC results of each strain	85
4.2 Significant MRM transitions from different statistical analysis of control set	91
4.3 Significant MRM transitions from different statistical analysis of samples treated with amoxicillin/clavulanate at half MIC	94
4.4 Postulated classification of transitions selected from <i>t</i> test and ROC curve	95
5.1 Comparison of inductive nESI with and without field amplification micro- CZE of serum sample in isolation scan mode from Figure 5.7.	110

LIST OF FIGURES

Figure	Page
1.1 Classification system recommended by LIPID MAPS®. Eight classes are shown in each panel: fatty acyls (FA), prenol lipids (PR), glycerolipids (GL), saccharolipids (SL), sterol lipids (ST), sphingolipids (SP), glycerophospholipids (GP), and polyketides (PK). One typical molecular structure is illustrated in each class. Major subdivisions are also listed out under each category. The diversity in structure can be visually observed.	3
1.2 Classification and structure sketch of glycerophospholipids (GP) recommended by LIPID MAPS®. Six main subclasses are shown in the top panel: glycerophosphate (PA), glycerophosphocholine (PC), glycerophosphoethanolamine (PE), glycerophosphoglycerol (PG), glycerophosphoinositol (PI), and glycerophosphoserine (PS). The headgroup of each subclass is highlighted in purple. The bottom panel contains three possible results after phosphorylation of PI occurring at 3', 4', and/or 5', producing glycerophosphoinositol mono-/bis-/trisphosphates (PIP, PIP ₂ , PIP ₃ , respectively). Each has a representative structure attached.	5
2.1 Typical workflow of MRM-profiling contains three stages: Discovery, Screening, and Identification. Discovery stage is a process of profiling based on chemical functional groups. Screening stage uses MRM transitions determined from Discovery stage to analyze different groups of samples and produces a panel of molecules/ions that are responsible for the differences between samples. Identification stage focuses on the characterization of molecules/ions from significant or responsible MRM transitions.	21
2.2 Configuration of QqQ (a) and four operation modes: (b) product ion scan, (c) precursor ion scan, (d) neutral loss scan, and (e) multiple reaction monitoring. The operation of Q1 and Q3 can be either <i>Fix</i> or <i>Scan</i>	22
2.3 Illustration of four MS/MS operations on QqQ projected onto a 2D domain.	24

Figure	Page
2.4 Two worklist arrangements of an experiment with two samples and three methods. (a) Apply all methods to the same sample first and then screen the next sample. (b) Apply the same method to all samples first and then screen all samples by the next method.	38
2.5 Overlaid chromatogram of QC samples from two experiments. (a) Experiment 1 with 16 injections of QC. (b) Experiment 2 with 43 injections of QC. In both cases, the time between each two QCs were 10 injections of samples (about 30 min). The curves in shaded area between 0.6 min to 1.4 min are used to calculate the area under curve in Figure 2.6.	39
2.6 Distribution of normalized area under curve (AUC) values of QC samples from the two experiments in Figure 2.5, Experiment 1 and 2 (abbreviated as Exp 1 and 2, respectively). All the areas are normalized to the maximum AUC value in each experiment.	40
2.7 Mass spectra of NL 271 of milk samples from (a) cow, (b) human, and (c) soy. The label and corresponding normalized intensity are shown in the top right corner in each panel. Zoom-in mass spectra of shaded m/z regions I, II, and III are shown in Figure 2.8.	47
2.8 Zoom-in mass spectra of NL 271 of samples from cow (a-c), human (d-f), and soy (g-i) from Figure 2.7. Three typical m/z regions are selected as shown in each column. The normalized intensity is the same as the corresponding value from Figure 2.7. Potential characteristic peaks are highlighted by yellow solid lines with m/z 's labeled.	48
2.9 Mass spectra of NL 273 of milk samples from (a) cow, (b) human, and (c) soy. The label and corresponding normalized intensity are shown in the top right corner in each panel. Zoom-in mass spectra of shaded m/z regions I, II, and III are shown in Figure 2.10.	49
2.10 Zoom-in mass spectra of NL 273 of samples from cow (a-c), human (d-f), and soy (g-i) from Figure 2.9. Three typical m/z regions are selected as shown in each column. The normalized intensity is the same as the corresponding value from Figure 2.9. Potential characteristic peaks are highlighted by yellow solid lines with m/z 's labeled.	50
2.11 Mass spectra of NL 299 of milk samples from (a) cow, (b) human, and (c) soy. The label and corresponding normalized intensity are shown in the top right corner in each panel. Zoom-in mass spectra of shaded m/z regions I, II, and III are shown in Figure 2.12.	51

Figure	Page
2.12 Zoom-in mass spectra of NL 299 of samples from cow (a-c), human (d-f), and soy (g-i) from Figure 2.11. Three typical m/z regions are selected as shown in each column. The normalized intensity is the same as the corresponding value from Figure 2.11. Potential characteristic peaks are highlighted by yellow solid lines with m/z 's labeled.	52
3.1 Relationship between the number of oocytes introduced and the total amount of SM, PS, PG, PE, and PC (from top to bottom) lipids quantified using internal standards. Four concentrations of oocytes extract equivalent to 1.6, 3.2, 4.8 and 6.4 per injection were used. Each point in plot is an average of three measurements.	73
3.2 PLS-DA results for oocyte and blastocyst discrimination using different normalization methods: normalized to modified total ion count (TIC) and normalized to corresponding internal standard (IS). (a) Oocyte normalized to TIC. (b) Oocyte normalized to IS. (c) Blastocyst normalized to TIC. (d) Blastocyst normalized to IS. The two colors represent differences in the nanoparticles applied during culturing, red and blue for group A and group B, respectively. Sample size of each group in (a) and (b) is $N = 11$, and $N = 12$ in (c) and (d). The shaded ellipses represent the calculated 95% confidence range.	74
3.3 Boxplots showing comparisons between two normalization methods of three MRM transitions in blastocyst samples. Top row is result of normalization to corresponding internal standard (IS) and bottom row is result of normalization to modified total ion current (TIC)..	76
3.4 Boxplots showing comparisons between two normalization methods of three MRM transitions in oocyte samples. Top row is result of normalization to corresponding internal standard (IS) and bottom row is result of normalization to modified total ion current (TIC).	77
4.1 Distribution of MRMs selected for screening stage in positive mode. Altogether 1,900 transitions were reorganized into 9 MRM methods.	87
4.2 Distribution of MRMs selected for screening stage in negative mode. Altogether 429 transitions were reorganized into 2 MRM methods.	87
4.3 PCA scores plots of non-resistant bacterial strains (a) ATCC 25922 and (b) ATCC 4157 after various antibiotic treatments. The color-shaded areas are the calculated range with 95% confidence. Amoxicillin and clavulanate are abbreviated as Amox and Clav, respectively.	89
4.4 PCA scores plots of control samples (no amoxicillin or amoxicillin/clavulanate applied) using transitions selected from (a) ANOVA and (b) t test. Color-shaded areas are the calculated range with 95% confidence.	91

Figure	Page
4.5 ROC curves significant transitions (AUC > 0.9) from control set.	92
4.6 PCA score plots of samples treated with amoxicillin/clavulanate at half MIC using transitions selected from (a) ANOVA and (b) <i>t</i> test. The color-shaded areas are the calculated range with 95% confidence.	94
4.7 ROC curves significant transitions (AUC > 0.9) from samples treated with amoxicillin/clavulanate at half MIC.	95
4.8 Distribution of transitions selected from <i>t</i> test between controls and sample treated with amoxicillin/clavulanate at half MIC. "Saturated Chain" refers to the saturated fatty acyl chain residues. "Unsaturated Chain" refers to fatty acyl chain residues with degree of unsaturation ranging from 1 to 5.	96
5.1 Instrumentation for dip-and-go multiplexed HTS bioassay. The emitter holder has 12 channels which can hold 12 emitters designed to fit the 96-well plate format. Step 1 is the "dip" step used for sample introduction. The emitters are immersed into water, sample solution and water in turn (the figure only shows dip into sample solution) to load the leading and trailing zones with pure water and the mid zone with sample solution. In Step 2 the holder is installed on a 1D moving stage and subjected to 10 s electrophoretic cleaning. In Step 3, the emitters are moved into position for inductive nESI-MS analysis.	105
5.2 Screening of Claisen-Schmidt reactions in 96-well plate to test the analytical performance of the dip-and-go multiplexed system. Reactions between 6-hydroxyindanone and 5-substituted benzaldehydes were tested. The final reaction mixture in each well was: 25 mM 6-hydroxyindanone, 25 mM aldehyde, and 450 mM KOH. Reactions were run for 30 min and quenched with 10× dilution by methanol in each of the 5 rows for the subsequent inductive nESI analysis. Each point in the Hammett plot is the average of 5 measurements. The inductive nESI is performed under non-accelerating conditions (distance from emitter tip to MS inlet is 2 mm).	108
5.3 Confirmation of non-accelerating analysis conditions of inductive nESI. The reaction solution was mixed for 30 s followed by analysis of both nESI and inductive nESI; the product/reagent ratio is less than 3%.	109
5.4 Full scan mass spectra using inductive nESI analysis of KTEEISEVNL (<i>m/z</i> 581.5) with internal standard KTEEISEVN(L- ¹³ C ₇) (<i>m/z</i> 585.0) in different biological matrices with and without field amplification micro-electrophoretic clean-up. Reaction buffer is 2 nM BACE1 enzyme, 6 mM sodium acetate, 1.5% glycerol, 0.25% DMSO, 3 ppm Brij-27 and 1% formic acid.	111

Figure	Page
5.5 Test of LoQ of KTEEISEVNL (m/z 581.5) with its internal standard KTEEISEVN(L- $^{13}\text{C}_7$) (m/z 585.0) using inductive nESI with field amplification micro-CZE. The concentration of each peptide is 150 nM in reaction buffer of 2 nM BACE1 enzyme, 6 mM sodium acetate, 1.5% glycerol, 0.25% DMSO, 3 ppm Brij-27 and 1% formic acid.	112
5.6 Calibration curve of the dip-and-go analysis for KTEEISEVNL (m/z 581.5) with 150 nM KTEEISEVN(L- $^{13}\text{C}_7$) (m/z 585.0) as internal standard in reaction buffer system (2 nM BACE1 enzyme, 6 mM sodium acetate, 1.5% glycerol, 0.25% DMSO, 3 ppm Brij-27 and 1% formic acid). The intensity of ions at m/z 581.5 and m/z 585.0 are directly read from full scan mass spectra. The curve shows a good linear dynamic range from 150 nM to 4000 nM.	113
5.7 Comparison of inductive nESI with and without field amplification micro-CZE in isolation scan mode. In this mode, we isolated ions in range of m/z 578 - 588, which covers the target and internal standard peptide. The spectra and results of peptides in different human serum matrix system after analysis are shown for comparison.	114
5.8 HTS bioassays of KTEEISEVNL (m/z 581.5) with 250 nM KTEEISEVN(L- $^{13}\text{C}_7$) (m/z 585.0) as internal standard in reaction buffer (2 nM BACE1 enzyme, 6 mM sodium acetate, 1.5% glycerol, 0.25% DMSO, 3 ppm Brij-27 and 1% formic acid) using the dip-and-go multiplexed system. The intensity of KTEEISEVNL and IS are from the full scan MS. The screening rate is 4s/sample and the total analysis time for one row is ca. 50s. The average deviation for row A is 11.0% and for row B is 6.1%	115
5.9 Test of carryover using one emitter for multiple measurements. For all the samples with odd numbers, we spiked the target molecule (TM) KTEELSEVNL and internal standard (IS) in a ratio of 4:1 (1000 nM and 250 nM) in reaction buffer (2 nM BACE1 enzyme, 6 mM sodium acetate, 1.5% glycerol, 0.25% DMSO, 3 ppm Brij-27 and 1% formic acid). For all the samples with even numbers, the ratio of TM to IS is 1:4 (250 nM and 1000 nM). We used the same emitter for dip-and-go measurements of Samples 1 to 10. The spectra are shown. The average deviation of experimental ratio from expected ratio is 2.5%, indicating very small carryover when reusing one emitter multiple times.	116

Figure	Page
5.10 Process of field amplification micro-electrophoresis. (a) Ion migration in each step (note that electroneutrality will be maintained over the whole solution volume including Zones 1, 2, and 3 while each individual zone can have a net charge). (b) Electrode voltage vs. time in the process. (c) TIC over course of the process. (d) Ion map of the process. (e) Typical mass spectra from the three zone.)	118
5.11 (a) MS/MS spectrum of precursor ions in range of m/z 578 to m/z 588. The collision energy used is 30 (nominal value). This range covers the doubly charged precursor ions of KTEEISEVNL (m/z 581.5) and IS (m/z 585.0). The spiked ratio of the KTEEISEVNL and IS is 1 : 1. (b) Typical TIC and EIC of dip-and-go analysis of one row of samples. (c) IC_{50} of inhibitor OM99-2 to BACE1 determined using the dip-and-go system. . .	120
5.12 Inductive nESI spectra with field amplification micro-CZE for analysis of KTEEISEVNL (m/z 581.5 in full scan, m/z 246.1 in product ion scan) after uninhibited and fully inhibited reaction with 150 nM KTEEISEVN(L- $^{13}C_7$) (m/z 585.0 in full scan, m/z 253.1 in product ion scan) as internal standard. The left column shows the spectra in isolation scan mode and the right shows product ion scan spectra. The SNRs in product ion spectra are much better than isolation scan spectra, so can be used for quantification. The determined concentration of KTEEISEVNL after uninhibited reaction is 272 nM after fully inhibited reaction is 3.0 nM.	121
5.13 IC_{50} of OM99-2 to BACE1 determined by LC-TOF-MS. This figure is from one measurement (12 samples). Each sample took ca. 8 min for analysis. The total analysis time is ca. 1.5 h.	122
5.14 Break-up of binding of Brij-27 and sodium formate clusters before and after clean-up indicates the stacking of cations and anions in different zones after electrophoretic clean-up.	124

ABSTRACT

Xie, Zhuoer Ph.D., Purdue University, August 2020. Accelerating the Throughput of Mass Spectrometry Analysis by Advanced Workflow and Instrumentation. Major Professor: R. Graham Cooks.

The exploratory profiling and quantitative bioassays of lipids, small metabolites, and peptides have always been challenging tasks. The most popular instrument platform deployed to solve these problems is chromatography coupled with mass spectrometry. However, it requires large amounts of instrument time, intensive labor, and frequent maintenance, and usually produces results with bias. Thus, the pace of exploratory research is one of poor efficacy and low throughput. The work in this dissertation provides two practical tactics to address these problems. The first solution is multiple reaction monitoring profiling (MRM-profiling), a new concept intended to shift the exploratory research from current identification-centered metabolomics and lipidomics to functional group screening by taking advantage of precursor ion scan and product ion scan. It is also demonstrated that MRM-profiling is capable of quantifying the relative amount of lipids within the same subclass. Besides, an application of the whole workflow to investigate the strain-level differences of bacteria is described. The results have zeroed in on several potential lipid biomarkers and corresponding MRM transitions. The second strategy is aimed to increase the throughput of targeted bioassays by conducting induced nanoelectrospray ionization (nESI) in batch mode. A novel prototype instrument named "Dip-and-Go" system is presented. Characterization of its ability to carry out reaction screening and bioassays exhibits the versatility of the system. The distinct electrophoretic cleaning mecha-

nism contributes to the removal of salt during ionization, which assures the accuracy of measurement.

CHAPTER 1. MASS SPECTROMETRY-BASED LIPIDOMICS

1.1 Overview

In the past several decades of explosion in technologies, the emergence of suffix "-ome" and "-omic" attached to conventional classes of biologically significant molecules has expanded the horizon from focusing on isolated single (or a few) molecule to the big picture of the whole organism. Driven by a vast investment of labors and wealth in instrumentation, software, data science, and collaboration of multiple science disciplines, the strategic and analytical infrastructure in the kingdoms of genomics and proteomics has been systematically constructed and has profoundly undermined the traditional methods in bioanalytical chemistry and even in clinical applications. However, lipids being located at the bottom of the omic cascade, are conventionally considered to be containers for proteins and genes but not directly genetically encoded.^[1] This and their extraordinary structural complexity means that they have not been well explored until the past decade. The definitions of *lipidome* and *lipidomics* were not included in the IUPAC Gold Book until the latest version in 2018^[2] and they are explained as:

Lipidome Complete set of lipid species and their metabolites present within a particular cell type, tissue, or body fluid.

Lipidomics Systematic and comprehensive study aimed at the identification, profiling, and quantification of lipidome.

From the above material, one can conclude that there are three basic aspects in lipidomics study: identification, profiling, and quantification. In this chapter, a brief introduction of lipid structure and an overview on critical instrumentation developments, and the range of current workflows in mass spectrometry-based lipidomics are presented. Two future directions in lipidomics are suggested and techniques/strategies with outstanding potential will be evaluated at the end. The discussion is based on the consensus definitions.

1.2 Lipids

1.2.1 Classification

There is not a universal definition of lipids, but grouping like molecules is approachable based on structures. The most accepted classification system is the LIPID MAPS® Lipid Classification System, which contained 43,645 individual lipid structures in its database as of March 2020. These lipids exist in mammals, lipids, bacteria, etc. According to the hierarchy in this system, the domain of lipids is divided into eight classes: fatty acids (FA), glycerolipids (GL), glycerophospholipids (GP), sphingolipids (SP), sterol lipids (ST), prenol lipids (PR), saccharolipids (SL), and polyketides (PK). Each class has subclasses and they all have distinct labels in the system. The representative molecules and subclasses are shown in Figure 1.1.

For some classes of lipids, the structures have common features as a result of the similar synthetic pathway inside cells. In light of the structure, it seems that lipids are based on several precursors in biological synthesis (not the same "precursor" as in "precursor ion scan" from mass spectrometry). The most typical class is GP as shown in the top panel of Figure 1.2, which can be regarded as a complex of a glycerol, a phosphate, a headgroup, and up to two fatty acyl chains. The classification of GP is based on headgroups (shown in parentheses), including glycerophosphate (PA, proton, H^+), glycerophosphocholine (PC, choline, $C_5H_{14}NO^+$), glycerophospho-

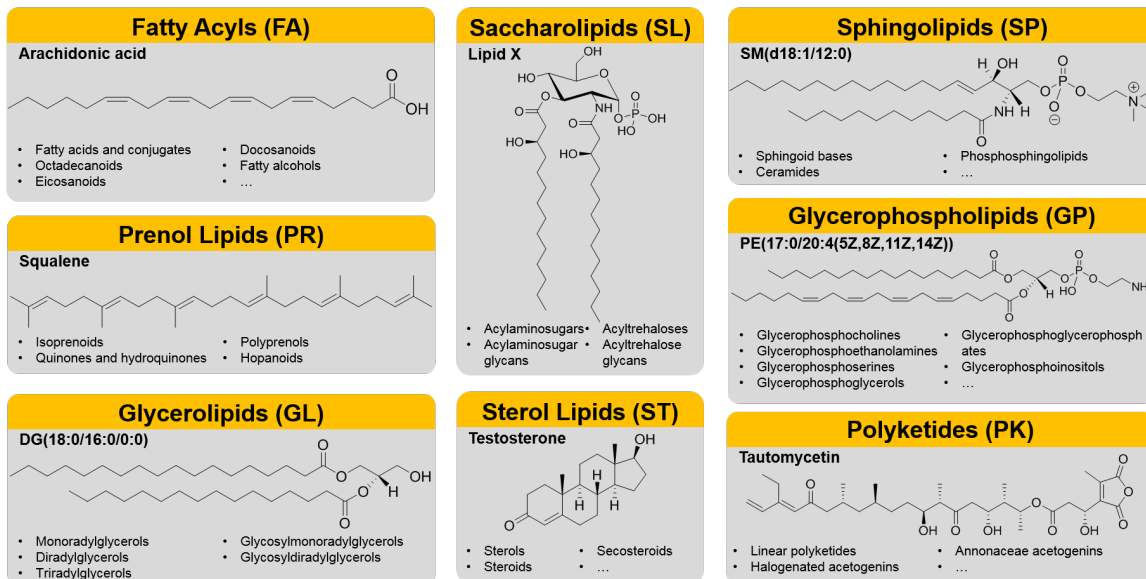


Figure 1.1. Classification system recommended by LIPID MAPS®. Eight classes are shown in each panel: fatty acyls (FA), prenol lipids (PR), glycerolipids (GL), saccharolipids (SL), sterol lipids (ST), sphingolipids (SP), glycerophospholipids (GP), and polyketides (PK). One typical molecular structure is illustrated in each class. Major subdivisions are also listed out under each category. The diversity in structure can be visually observed.

ethanolamine (PE, ethanolamine, C_2H_7NO), glycerophosphoglycerol (PG, glycerol, $C_3H_8O_3$), glycerophosphoinositol (PI, inositol, $C_6H_{12}O_6$), and glycerophosphoserine (PS, serine, $C_3H_7NO_3$). By further attachment to the headgroup, the list of subclasses can be extended to a great degree. For example, in PI, one of the six hydroxyl groups (1') in inositol is occupied by glycerol phosphate. The other three hydroxyl groups at 3', 4' and 5', which are not adjacent to the functionalized location, are still available for further modification by one, two, or three phosphates to produce glycerophosphoinositol mono-/bis-/trisphosphates (PIP, PIP₂, PIP₃, respectively). Representative structures are included in the bottom panel of Figure 1.2. In light of different combinations of the locations of substitution, these subclasses can be described by PIP[3'], PIP[4'], PIP[5'], PIP₂[3', 4'], PIP₂[3', 5'], PIP₂[4', 5'], and PIP₃[3', 4', 5'], altogether six subordinate classes.

1.2.2 Isomerism and Shorthand Notation

Isomerism is a hallmark of lipidomics. Variations in chain length, the presence of branched chain or cyclic structures, the degree of unsaturation, the location of any double bonds, geometric isomerism (i.e. *cis-trans* isomerism) about double bonds, and modification by additional functional groups strikingly enrich the number of possible structures. Rules for the shorthand notation of lipids were suggested by Liebisch et al.,^[3] then adopted by LIPID MAPS and accepted by many researchers. Currently, they are systematically applied to subclasses of GP, GL, and SP. Different levels of annotations can be applied to the same molecule.

1. The subclass of a lipid is presented by a unique abbreviation, such as PC.
2. The elemental composition can be determined so that the total number of carbon atoms and number of carbon-carbon double bonds in fatty acyl chains positions can be attached to indicate further details, such as PC(32:4) denoting a PC lipid with a total number of 32 carbon atoms and 4 C=C double bonds in fatty acyl chains at sn-1 and sn-2 positions.

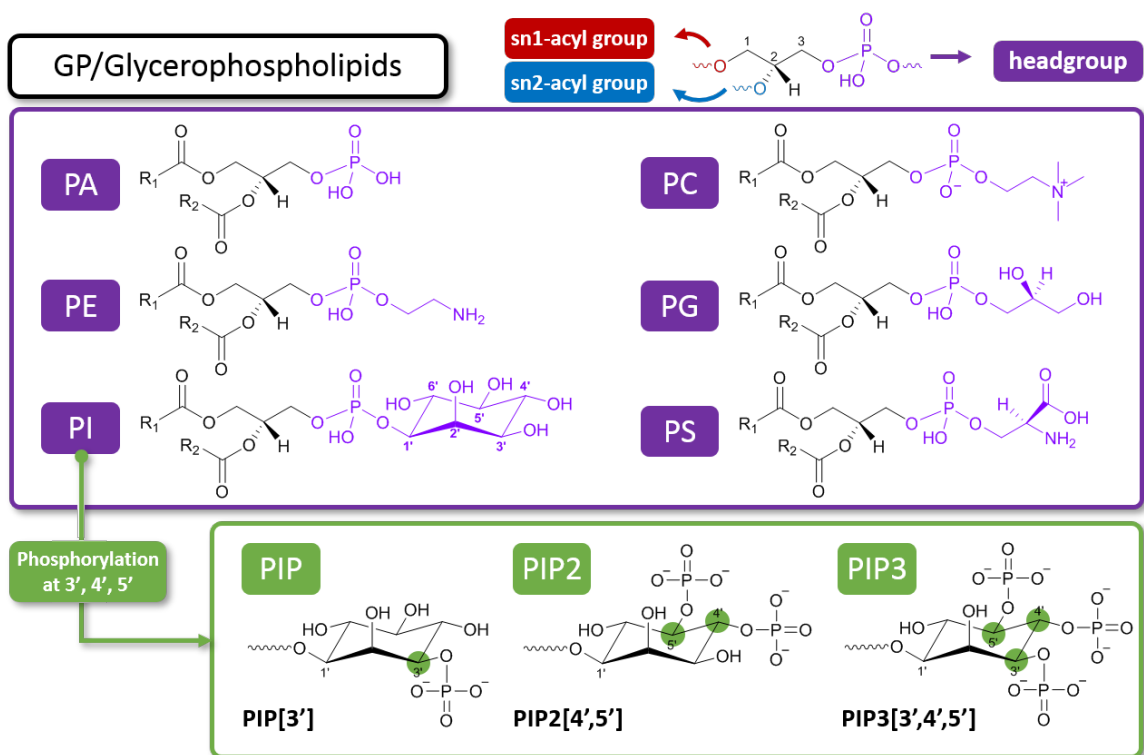


Figure 1.2. Classification and structure sketch of glycerophospholipids (GP) recommended by LIPID MAPS®. Six main subclasses are shown in the top panel: glycerophosphate (PA), glycerophosphocholine (PC), glycerophosphoethanolamine (PE), glycerophosphoglycerol (PG), glycerophosphoinositol (PI), and glycerophosphoserine (PS). The headgroup of each subclass is highlighted in purple. The bottom panel contains three possible results after phosphorylation of PI occurring at 3', 4', and/or 5', producing glycerophosphoinositol mono-/bis-/trisphosphates (PIP, PIP₂, PIP₃, respectively). Each has a representative structure attached.

3. If the length and number of fatty acyl chains are known, the details can be represented in the parentheses. For example, PC(32:4) has 11 matches in LIPID MAPS Structure Database, one of which could be PC(12:0_20:4), noting the chain length and number of C=C bonds in two fatty acyl chains without definitive positional information. Two possibilities are PC(12:0/20:4) and PC(20:4/12:0) in form of PC(sn-1/sn-2).
4. For each C=C bond in the sn-1 chain, location is shown using Δ -nomenclature and geometric isomerism designated by E/Z are recorded as PC(20:4(5Z,8Z,11Z,14Z)/12:0).
5. If applicable, the linkage at sn-1 can be clarified for plasmanyl species with alkyl ether bond (prefix O-) and plasmenyl species (or plasmalogen) with (1Z)-alkenyl ether bond (prefix P-), such as PC(P-16:0/18:2(9Z,12Z)).

More specific rules have been set up for each class of lipids, but the level of annotation is essentially decided by which analytical tool is applied. Most MS-based analytical methods can prove the existence of a certain kind of ions observed, but cannot rule out the possibility of missing other compounds in a mixture.

1.3 Current Exploratory Lipidomics Platforms

The foremost question to be answered in lipidomics is “what is the goal/expected outcome of the study?”. Three major tasks are identification, profiling, and quantification. Obviously, the experimental design needs to match the goal of study. If a project involves a specific molecule, the goal might be method development and optimization to separate, identify, and quantify this target molecule. Thus, lipid profiling techniques might not be suitable in this case. For large-scale study in biomarker discovery and screening of clinical samples, profiling of the lipidome should be high-throughput with a broad coverage instead of determining the quantity and identity of each chemical species. Since abilities of instrument and methodology in identification, profiling and quantification take the form of a trade-off, these tasks are closely

related in different workflows and share certain common solutions. However, there is no universal method to unravel all the questions at one time.

In general, a typical workflow for a lipidomics study is comprised of sample preparation (e.g. lipid extraction,^[4-6] internal standard selection,^[7,8] and derivatization^[9-11]), separation (e.g. chromatography and ion mobility spectroscopy), MS analysis (e.g. full scan, high resolution MS, and tandem MS), and data interpretation (e.g. database match and univariate/multivariate statistics^[12,13]). As the principal method in the workflow, MS is indispensable in any form of lipidomics studies. Currently, there are three mainstream strategies that are well known in this field: (1) chromatography coupled to MS, often as LC-MS/MS, (2) direct injection MS, almost always with MS/MS, and (3) MS imaging. The following sections are intended to provide an overview of current methodologies of the general format and directions instead of specific innovations, with emphasis on exploratory lipidomics.

1.3.1 Chromatography Coupled to Mass Spectrometry

Chromatography contains a large set of techniques including thin-layer chromatography (TLC), liquid chromatography (LC), and gas chromatography (GC). Regardless of what the stationary phase, mobile phase, and modifier are used, every platform with chromatography basically shares the same goal – to completely separate the analytes into as many groups as possible and then subject these groups of molecules to downstream MS analysis. GC-MS is commonly used for volatile lipids such as ST and FA. However, derivatization is frequently applied to these classes.^[10,11] LC-MS is complementary to GC-MS and more versatile in terms of coverage of lipids. High-performance liquid chromatography (HPLC) and ultra-high-performance liquid chromatography (UHPLC), with much greater pressure inside the columns, have taken over of the whole LC-MS market. Three main types of HPLC widely applied in lipidomics are hydrophilic interaction LC (HILIC),^[14,15] normal-phase HPLC (NP-HPLC),^[16,17] and reversed-phase HPLC (RP-HPLC).^[18,19] HILIC and NP-HPLC

separate lipids based on their headgroups (e.g. differences in polarities of different subclasses of GP), while RP-HPLC separates by the properties of the moieties of fatty acyl chains (e.g. hydrophobicity, chain length, and number of double bonds). Although the separation of lipids with different headgroups can be achieved with ease using automation, study to further resolve lipids with more detailed structural information can be retarded by the binary choice of separation based on headgroups or fatty acyl chains in single stage of HPLC. Accordingly, combining RP-HPLC with either one of HILIC and NP-HPLC has been introduced. In two-dimensional HPLC (2D-HPLC),^[20-22] coelutions from the first dimension can be further separated in the second column 2D-HPLC expands the number of lipids of analysis but also requires more time for method development and analysis. Another valuable chromatographic technique undergoing revival is supercritical fluid chromatography (SFC),^[23-25] which has higher throughput than HPLC^[26] and can be coupled with subsequent separations.^[27]

Even though commonly used, there are limitations of sample chromatography for exploratory analysis. A typical chromatographic separation usually takes about tens of minutes or up to an hour or more. The retention time drift and signal fluctuation after lengthy operation time can jeopardize the reliability and reproducibility of data and even lead to wrong conclusions. This influence can be corrected by peak alignment before data analysis,^[28] but still requires continuous monitoring throughout the process. Another regular occurrence in chromatography is the sample loss and carry-over from the interactions between mobile phase and stationary phase.^[29] As for the more powerful 2D-HPLC, it is more challenging and time-consuming for operation and maintenance. Consequently, LC-MS platforms are more helpful for target analysis and quantification but often lack high-throughput needed for profiling.

1.3.2 Direct Injection Mass Spectrometry

Direct injection of samples has become popular due to its low cost, short time, easy operation, and rich information in lipid structures. Compared to LC-MS platforms, direct injection has higher throughput, but the tradeoff between resolution in scan spectra and specificity in identifying each peak is considered as the main weakness of the method with low-resolution mass analyzers.^[30,31] Issues such as ion suppression and complexity of multiple forms of adducts can be mitigated by proper experimental design, but appropriate selection of internal standard for quantification^[7] and deconvoluting peak overlapping of isobaric ions^[32,33] are frequently required. Even for HRMS, one cannot completely get rid of this ambiguity in mass.^[34-36] However, as a strategy more suitable for profiling with prior knowledge and partially capable of identification and quantification, applications of direct injection MS have proved its capability and potential in metabolite- and lipid-related disease analysis of clinical samples.

1.3.3 Mass Spectrometry Imaging

Different from the previous two strategies, MS imaging (MSI) focuses on acquiring the spatial distribution of lipids in samples, while for LC- and direct injection MS the samples undergo homogenization prior to analysis. Various ionization methods have been created and applied for imaging purpose. Three main types of them are matrix-assisted laser desorption/ionization (MALDI), desorption electrospray ionization (DESI), and secondary ion mass spectrometry (SIMS). The lipid profile that can be acquired depends on the mechanism of each method and the spatial resolution.

MALDI uses a laser to transfer energy to the matrix that is added to aid the ionization of analytes in sample. So, the spatial resolution (typically around 10 μm) mostly depends on the radius of the laser beam and the coverage of lipid profile is predominantly affected by matrix. In DESI, charged droplets generated by electrospray pick

up analytes from samples surface for analysis. The typical spatial resolution is 150 μm to 250 μm but can be optimized for better resolution (down to 30 μm). The current application of DESI-MSI concentrates on the biomarker discovery and diagnosis of disease based on multivariate statistics of lipid profile.^[37-39] SIMS has the best spatial resolution (<1 μm) out of these three solutions and matches the scale of single cells. The ion beam is focused on the surface of sample and continuously removes materials from the surface for analysis.^[38,40] Other innovative ionization techniques available for lipidomics (although some are not suitable for imaging) using direct liquid extraction have been reviewed by Laskin et al.^[37] More interests in this field have been extended to in situ analysis (e.g. MasSpec Pen^[41] and SpiderMass^[42]) and intraoperative evaluation.^[43-45]

In MSI, the lipid profile (sometimes also metabolite profiles in the low mass region) at each pixel defined by the method of choice is recorded and then used for reconstruction of distribution image by extracting the intensity of a desired m/z at each pixel from the sample. Except for the usual tradeoff between the analysis time and resolution of mass spectra, another tradeoff between spatial resolution and sampling amount matters in this strategy. The higher the spatial resolution, the smaller the sampling amount. On one hand, spatial resolution is intrinsically determined by the mechanism of each ionization method and corresponding physical parameters, which can both also affect the profile to be observed from mass spectrometer. On the other hand, analysis of minute sample is challenging the limit of detection and sensitivity of the downstream MS. Thus, the balance between these factors are crucial in MSI experiment.

1.4 Analytical Challenges and Concerns in Lipidomics

Literature reviews in recent five years^[4,6,7,13,23,31,38,40,46-71] have put forward many challenges in lipidomics. But there are several problems stand out as we are more versed in lipids. One of most concern is the reproducibility of exploratory lipidomics

on different platforms and/or at different laboratories. Besides, the structural elucidation has long been troubling the characterization experiment, but fortunately some MS-based methods have been invented and applied. Another problem is the annotation of lipids, which, if not done properly, can lead to wrong conclusions. These are three major haunting problems for the reviews above.

1.4.1 Dark Lipidome and Reproducibility Between Platforms

Even though the structure and nomenclature of lipids is now basically harmonized, an overall measurement of entire lipid classes present in a given sample still requires the application of a range of analytical approaches due to the chemical diversity of lipids. Another analytical challenge is the “dark” lipidome, i.e. the lipids not yet reported for biological samples. According to Lipid Maps, there are 20,000 lipid entries that have been detected and curated. Another 20,000 lipids in the database have been computationally generated. Nonetheless, there is a database of 1,300,000 simulated lipids, which represents lipids that may (or may not) exist, or the dark lipidome.

The huge number of lipids in lipidome also results in the fact that it is nearly impossible to know how many lipids are there to be detected in a given sample. Considering such assorted instruments and methodologies in MS-based lipidomics, the reliability of data and reproducibility of protocols across various platforms and laboratories stand out as lipidomics keeps growing. Several laboratories have cross-validated the data among different platforms and protocols and have achieved harmonized results after statistical analysis.^[72-75] In 2017, NIST has globally distributed the same standard reference material to 31 laboratories for profiling lipids.^[76] The result showed that 1,527 unique lipids were measured, but only 339 were identified by at least five laboratories. This astonishingly poor result regarding the same sample has suggested the inherent bias determined by the workflow of each measurement. A recent position paper on developing accepted guidelines in standard workflows on lipidomics of hu-

man plasma was published by multiple scholars, which has systematically elaborated different stages of analytics using MS.^[77] This is a good starting point for building and regulating the relationship between lipidomics and clinical applications. On the strategic side, most efforts have been put into separating each component by separation from HPLC or different accurate mass from HRMS. It is true that HPLC and HRMS can help the identification, but the sacrifice in throughput and sensitivity in profiling stage do not suggest this as a rational move for profiling.

1.4.2 Pursuit of Ultimate Structural Elucidation and Separation

There are several methods that can characterize the stereoisomerism involving the regioisomers in *sn*-position and *cis-trans* isomer in an unsaturated chain. By reactions at double bonds and fragmentation, the chain structure can be recognized from different product ions. Available representative techniques include Ozone induced dissociation (OzID),^[78,79] Paterò-Büchi reaction,^[80,81] ultraviolet photodissociation (UVPD),^[82] electron impact excitation of ions from organics (EIEIO),^[83,84] and gas-phase ion/ion charge inversion reaction.^[85,86] All of the above methods have been detailly reviewed,^[87] except for the last method involving ion/ion reaction in gas phase. A doubly positively charged tris-phenanthroline alkaline earth metal complex is introduced to combine with a trapped single negatively charged ion to form a larger complex with flipped single positive charge. CID in positive mode can locate the double bonds in fatty acyls. More recently, a new mechanism of autoxidation occurring in unsaturated lipids has been proposed.^[88] The authors proved that Criegee intermediates, formed by initial addition of hydroxyl radical (HO•) to C=C bonds, play a significant role in propagation of the radical chain reaction. This HO• triggered process is also valid in the presence of water and the rate of autoxidation was not to be neglected. Although this is a mechanism study, the cleavage at C=C bonds can provide unique information potentially to be applied to structural elucidation.

Another large family of emerging techniques is ion mobility spectrometry (IMS). The mobility of ions in bath gas (mostly He or N₂) and the applied electrical field collaboratively determine the drift time of each ion. Several types in lipidomic study are high field asymmetric waveform IMS (FAIMS), drift-tube IMS (DT-IMS), traveling wave IMS (TW-IMS), and trapped IMS (TIMS), commercialized by different vendors. Although the range of methods is extremely huge, the most surprising point brought by IMS is the information on isomeric lipids that used to complicate the lipid identification in any form.^[67-69] The m/z vs. arrival times plot unveils a much more complicated world in biological samples. More recently, a device named structures for lossless ion manipulations (SLIM) was invented, aiming at tackling multi-omic analysis and ultra-separation of biomolecules.^[89] Using an ultra-long path for separation, PC lipids with differences in double bond positions and cis/trans isomerism can be differentiated in arrival time as well as glycolipids with hydroxyl group at equatorial or axial positions.^[90] As path length increases, isotopomers (isotopic stereoisomers with the same number of each isotope but varying in positions) can be further separated.^[91] It is promising by combing ultimate separation and high resolution, the precision of identification will be promoted to an elevated level as the number of systems on which information is acquired goes down.

1.4.3 Faulty Annotation and Assignment

Although the rules for annotation different levels of structures in lipids have been well established, excessive annotation and false assignment of lipids in the literature can still occur during data analysis, either manually or automatically retrieved from library search.^[48,92] For example, an experiment using simple full mass scan HRMS should never report lipids with sn-1/sn-2 assignments. . . they are simply guesses. Besides, one should be extremely cautious about the lipid assignments in light of known biochemistry in samples so that the structures are relevant to the biogenesis of these lipids. Another caveat caused by software vendors is an annotation that exceeds the

information in the spectrum. When this occurs, the reported name should be abandoned without further characterization.^[48] It was reported in the same survey from NIST^[93] that only 57% of participants are accepting the annotation rules by LIPID MAPS. Given the unclear underlying mechanism of identification by commercial software, the number of laboratories that can correctly assign the structures might be fewer than half. To avoid the consequences by erroneous annotations, standards still need to be adjusted and promoted in lipidomics community. More importantly, the researcher should be aware of to what extent the involving methodology and instrument platform are capable of reporting the lipid profile. If unexpected annotations occur, it could be caused by either experimental defects (e.g. contamination in samples, deficit coverage of algorithm used by library search), or a novel finding in science.

1.5 References

- [1] M. R. Wenk, *Cell* **2010**, *143*, 888–895.
- [2] J. Labuda, R. P. Bowater, M. Fojta, G. Gauglitz, Z. Glatz, I. Hapala, J. Havliš, F. Kilar, A. Kilar, L. Malinovská, H. M. M. Sirén, P. Skládal, F. Torta, M. Valachovič, M. Wimmerová, Z. Zdráhal, D. B. Hibbert, *Pure and Applied Chemistry* **2018**, *90*, 1121–1198.
- [3] G. Liebisch, J. A. Vizcaíno, H. Köfeler, M. Trötzmüller, W. J. Griffiths, G. Schmitz, F. Spener, M. J. Wakelam, *Journal of Lipid Research* **2013**, *54*, 1523–1530.
- [4] S. Pati, B. Nie, R. D. Arnold, B. S. Cummings, *Biomedical Chromatography* **2016**, *30*, 695–709.
- [5] K. Jurowski, K. Kochan, J. Walczak, M. Barańska, W. Piekoszewski, B. Buszewski, *TrAC Trends in Analytical Chemistry* **2017**, *86*, 276–289.
- [6] T. Züllig, M. Trötzmüller, H. C. Köfeler, *Analytical and Bioanalytical Chemistry* **2020**, *412*, 2191–2209.
- [7] M. Wang, C. Wang, X. Han, *Mass Spectrometry Reviews* **2017**, *36*, 693–714.
- [8] M. Holčapek, G. Liebisch, K. Ekroos, *Analytical Chemistry* **2018**, *90*, 4249–4257.
- [9] X. Zhao, S. Zhu, H. Liu, *Journal of Separation Science* **2020**, jssc.201901346.
- [10] T. Řezanka, K. Pádřová, K. Sigler in *Encyclopedia of Lipidomics*, (Ed.: M. R. Wenk), Springer Netherlands, Dordrecht, **2016**, pp. 1–9.

- [11] S. W. J. Shields, C. R. Canez, K. V. Wasslen, H. Lee, D. Stalinski, L. Trouborst, S. Joudan, S. Whitton, H. P. Weinert, J. M. Manthorpe, J. C. Smith in *NATO Science for Peace and Security Series A: Chemistry and Biology*, (Eds.: J. H. Banoub, R. M. Caprioli), NATO Science for Peace and Security Series A: Chemistry and Biology 9789402411126, Springer Netherlands, Dordrecht, **2017**, pp. 177–206.
- [12] J. L. Griffin, S. Liggi, Z. Hall in *New Developments in Mass Spectrometry, Vol. 2020-Janua*, 7, The Royal Society of Chemistry, **2020**, pp. 25–48.
- [13] H. Tsugawa, K. Ikeda, M. Arita, *Biochimica et Biophysica Acta (BBA) - Molecular and Cell Biology of Lipids* **2017**, 1862, 762–765.
- [14] E. D. Tague, B. M. Woodall, J. R. Harp, A. T. Farmer, E. M. Fozo, S. R. Campagna, *Metabolomics* **2019**, 15, 53.
- [15] C. D. Calvano, G. Ventura, A. M. M. Sardanelli, L. Savino, I. Losito, G. De Michele, F. Palmisano, T. R. Cataldi, *International Journal of Molecular Sciences* **2019**, 20, 3341.
- [16] S. Abreu, A. Solgadi, P. Chaminade, *Journal of Chromatography A* **2017**, 1514, 54–71.
- [17] R. Cruz, S. Casal, *Journal of Chromatography A* **2018**, 1565, 81–88.
- [18] R. C. Barrientos, Q. Zhang, *Analytical Chemistry* **2019**, 91, 9673–9681.
- [19] M. Ovčáčíková, M. Lísa, E. Cífková, M. Holčapek, *Journal of Chromatography A* **2016**, 1450, 76–85.
- [20] A. Baglai, A. F. Gargano, J. Jordens, Y. Mengerink, M. Honing, S. van der Wal, P. J. Schoenmakers, *Journal of Chromatography A* **2017**, 1530, 90–103.
- [21] W. Lv, X. Shi, S. Wang, G. Xu, *TrAC Trends in Analytical Chemistry* **2019**, 120, 115302.
- [22] D. R. Stoll, P. W. Carr, *Analytical Chemistry* **2017**, 89, 519–531.
- [23] C. Chollet, S. Boutet-Mercey, L. Laboureur, C. Rincon, M. Méjean, J. Jouhet, F. Fenaille, B. Colsch, D. Touboul, *Journal of Mass Spectrometry* **2019**, 54, 791–801.
- [24] M. Lísa, E. Cífková, M. Khalikova, M. Ovčáčíková, M. Holčapek, *Journal of Chromatography A* **2017**, 1525, 96–108.
- [25] D. Wolrab, M. Chocholoušková, R. Jirásko, O. Peterka, M. Holčapek, *Analytical and Bioanalytical Chemistry* **2020**, 412, 2375–2388.
- [26] M. Lísa, M. Holčapek, *Analytical Chemistry* **2015**, 87, 7187–7195.
- [27] L. Yang, H. Nie, F. Zhao, S. Song, Y. Meng, Y. Bai, H. Liu, *Analytical and Bioanalytical Chemistry* **2020**, 412, 2225–2235.
- [28] C. A. Smith, E. J. Want, G. O’Maille, R. Abagyan, G. Siuzdak, *Analytical Chemistry* **2006**, 78, 779–787.

- [29] C. J. DeLong, P. R. Baker, M. Samuel, Z. Cui, M. J. Thomas, *Journal of Lipid Research* **2001**, *42*, 1959–1968.
- [30] X. Han, K. Yang, R. W. Gross, *Mass Spectrometry Reviews* **2012**, *31*, 134–178.
- [31] F.-F. F. Hsu, *Analytical and Bioanalytical Chemistry* **2018**, *410*, 6387–6409.
- [32] Z. Zhou, S. R. Marepally, D. S. Nune, P. Pallakollu, G. Ragan, M. R. Roth, L. Wang, G. H. Lushington, M. Visvanathan, R. Welti, *Lipids* **2011**, *46*, 879–884.
- [33] G. Liebisch, B. Lieser, J. Rathenberg, W. Drobnik, G. Schmitz, *Biochimica et Biophysica Acta (BBA) - Molecular and Cell Biology of Lipids* **2004**, *1686*, 108–117.
- [34] C. Bielow, G. Mastrobuoni, M. Orioli, S. Kempa, *Analytical Chemistry* **2017**, *89*, 2986–2994.
- [35] E. Ryan, G. E. Reid, *Accounts of Chemical Research* **2016**, *49*, 1596–1604.
- [36] T. Kind, O. Fiehn, *BMC Bioinformatics* **2006**, *7*, 1–10.
- [37] J. Laskin, I. Lanekoff, *Analytical Chemistry* **2016**, *88*, 52–73.
- [38] Y. H. Rustam, G. E. Reid, *Analytical Chemistry* **2018**, *90*, 374–397.
- [39] Q. Zheng, H. Chen, *Annual Review of Analytical Chemistry* **2016**, *9*, 411–448.
- [40] K. Yang, X. Han, *Trends in Biochemical Sciences* **2016**, *41*, 954–969.
- [41] J. Zhang, J. Rector, J. Q. Lin, J. H. Young, M. Sans, N. Katta, N. Giese, W. Yu, C. Nagi, J. Suliburk, J. Liu, A. Bensussan, R. J. DeHoog, K. Y. Garza, B. Ludolph, A. G. Sorace, A. Syed, A. Zahedivash, T. E. Milner, L. S. Eberlin, *Science Translational Medicine* **2017**, *9*, eaan3968.
- [42] B. Fatou, P. Saudemont, E. Leblanc, D. Vinatier, V. Mesdag, M. Wisztorski, C. Focsa, M. Salzet, M. Ziskind, I. Fournier, *Scientific Reports* **2016**, *6*, 25919.
- [43] E. R. St John, M. Rossi, P. Pruski, A. Darzi, Z. Takats, *TrAC Trends in Analytical Chemistry* **2016**, *85*, 2–9.
- [44] D. R. Ifa, L. S. Eberlin, *Clinical Chemistry* **2016**, *62*, 111–123.
- [45] H. M. Brown, V. Pirro, R. G. Cooks, *Clinical Chemistry* **2018**, *64*, 628–630.
- [46] A. Checa, C. Bedia, J. Jaumot, *Analytica Chimica Acta* **2015**, *885*, 1–16.
- [47] D. Schwudke, A. Shevchenko, N. Hoffmann, R. Ahrends, *Journal of Biotechnology* **2017**, *261*, 131–136.
- [48] J. P. Koelmel, C. Z. Ulmer, C. M. Jones, R. A. Yost, J. A. Bowden, *Biochimica et Biophysica Acta (BBA) - Molecular and Cell Biology of Lipids* **2017**, *1862*, 766–770.
- [49] Z. Zhou, J. Tu, Z.-J. Zhu, *Current Opinion in Chemical Biology* **2018**, *42*, 34–41.
- [50] Z. Ni, L. Goracci, G. Cruciani, M. Fedorova, *Free Radical Biology and Medicine* **2019**, *144*, 110–123.

- [51] F. M. Vaz, M. Pras-Raves, A. H. Bootsma, A. H. C. van Kampen, *Journal of Inherited Metabolic Disease* **2015**, *38*, 41–52.
- [52] T. Cajka, O. Fiehn, *Analytical Chemistry* **2016**, *88*, 524–545.
- [53] R. W. Gross, *Biochimica et Biophysica Acta (BBA) - Molecular and Cell Biology of Lipids* **2017**, *1862*, 731–739.
- [54] K. Jurowski, K. Kochan, J. Walczak, M. Barańska, W. Piekoszewski, B. Buszewski, *Critical Reviews in Analytical Chemistry* **2017**, *47*, 418–437.
- [55] T. Hu, J.-L. L. Zhang, *Journal of Separation Science* **2018**, *41*, 351–372.
- [56] J. Wang, C. Wang, X. Han, *Analytica Chimica Acta* **2019**, *1061*, 28–41.
- [57] A. Triebel, J. Hartler, M. Trötz Müller, H. C. Köfeler, *Biochimica et Biophysica Acta (BBA) - Molecular and Cell Biology of Lipids* **2017**, *1862*, 740–746.
- [58] T. Hyötyläinen, L. Ahonen, P. Pöhö, M. Orešič, *Biochimica et Biophysica Acta (BBA) - Molecular and Cell Biology of Lipids* **2017**, *1862*, 800–803.
- [59] H.-C. C. Lee, T. Yokomizo, *Biochemical and Biophysical Research Communications* **2018**, *504*, 576–581.
- [60] X. Zheng, R. D. Smith, E. S. Baker, *Current Opinion in Chemical Biology* **2018**, *42*, 111–118.
- [61] C. Hu, Q. Duan, X. Han, *PROTEOMICS* **2019**, *1900070*, 1900070.
- [62] T. Porta Siegel, K. Ekroos, S. R. Ellis, *Angewandte Chemie International Edition* **2019**, *58*, 6492–6501.
- [63] M. Wang, C. Wang, R. H. Han, X. Han, *Progress in Lipid Research* **2016**, *61*, 83–108.
- [64] C. Hu, M. Wang, X. Han, *Redox Biology* **2017**, *12*, 946–955.
- [65] S. Tumanov, J. J. Kamphorst, *Current Opinion in Biotechnology* **2017**, *43*, 127–133.
- [66] M. Ghaste, R. Mistrik, V. Shulaev, *International Journal of Molecular Sciences* **2016**, *17*, 816.
- [67] G. Paglia, M. Kliman, E. Claude, S. Geromanos, G. Astarita, *Analytical and Bioanalytical Chemistry* **2015**, *407*, 4995–5007.
- [68] C. Hinz, S. Liggi, J. L. Griffin, *Current Opinion in Chemical Biology* **2018**, *42*, 42–50.
- [69] F. Zandkarimi, L. M. Brown in *Advances in experimental medicine and biology*, Vol. 1140, **2019**, pp. 317–326.
- [70] E. B. Yalcin, S. M. de la Monte, *Journal of Histochemistry & Cytochemistry* **2015**, *63*, 762–771.

- [71] C. R. Ferreira, A. K. Jarmusch, V. Pirro, C. M. Alfaro, A. F. González-Serrano, H. Niemann, M. B. Wheeler, R. A. C. Rabel, J. E. Hallett, R. Houser, A. Kaufman, R. G. Cooks, *Reproduction Fertility and Development* **2015**, *27*, 621–637.
- [72] T. Cajka, J. T. Smilowitz, O. Fiehn, *Analytical Chemistry* **2017**, *89*, 12360–12368.
- [73] K. Contrepois, S. Mahmoudi, B. K. Ubhi, K. Papsdorf, D. Hornburg, A. Brunet, M. Snyder, *Scientific Reports* **2018**, *8*, 17747.
- [74] I. Matraszek-Zuchowska, B. Wozniak, A. Posyniak, *Chromatographia* **2016**, *79*, 1003–1012.
- [75] A. Triebel, B. Burla, J. Selvalatchmanan, J. Oh, S. H. Tan, M. Y. Chan, N. A. Mellet, P. J. Meikle, F. Torta, M. R. Wenk, *Journal of Lipid Research* **2020**, *61*, 105–115.
- [76] J. A. Bowden, A. Heckert, C. Z. Ulmer, C. M. Jones, J. P. Koelmel, L. Abdullah, L. Ahonen, Y. Alnouti, A. M. Armando, J. M. Asara, T. Bamba, J. R. Barr, J. Bergquist, C. H. Borchers, J. Brandsma, S. B. Breitkopf, T. Cajka, A. Cazenave-Gassiot, A. Checa, M. A. Cinel, R. A. Colas, S. Cremers, E. A. Dennis, J. E. Evans, A. Fauland, O. Fiehn, M. S. Gardner, T. J. Garrett, K. H. Gotlinger, J. Han, Y. Huang, A. H. Neo, T. Hyötyläinen, Y. Izumi, H. Jiang, H. Jiang, J. Jiang, M. Kachman, R. Kiyonami, K. Klavins, C. Klose, H. C. Köfeler, J. Kolmert, T. Koal, G. Koster, Z. Kuklennyik, I. J. Kurland, M. Leadley, K. Lin, K. R. Maddipati, D. McDougall, P. J. Meikle, N. A. Mellett, C. Monnin, M. A. Moseley, R. Nandakumar, M. Oresic, R. Patterson, D. Peake, J. S. Pierce, M. Post, A. D. Postle, R. Pugh, Y. Qiu, O. Quehenberger, P. Ramrup, J. Rees, B. Rembiesa, D. Reynaud, M. R. Roth, S. Sales, K. Schuhmann, M. L. Schwartzman, C. N. Serhan, A. Shevchenko, S. E. Somerville, L. St. John-Williams, M. A. Surma, H. Takeda, R. Thakare, J. W. Thompson, F. Torta, A. Triebel, M. Trötz Müller, S. J. K. Ubhayasekera, D. Vuckovic, J. M. Weir, R. Welti, M. R. Wenk, C. E. Wheelock, L. Yao, M. Yuan, X. H. Zhao, S. Zhou, *Journal of Lipid Research* **2017**, *58*, 2275–2288.
- [77] B. Burla, M. Arita, M. Arita, A. K. Bendt, A. Cazenave-Gassiot, E. A. Dennis, K. Ekroos, X. Han, K. Ikeda, G. Liebisch, M. K. Lin, T. P. Loh, P. J. Meikle, M. Orešič, O. Quehenberger, A. Shevchenko, F. Torta, M. J. O. Wakelam, C. E. Wheelock, M. R. Wenk, *Journal of Lipid Research* **2018**, *59*, 2001–2017.
- [78] M. C. Thomas, T. W. Mitchell, D. G. Harman, J. M. Deeley, J. R. Nealon, S. J. Blanksby, *Analytical Chemistry* **2008**, *80*, 303–311.
- [79] M. R. L. Paine, B. L. J. Poad, G. B. Eijkel, D. L. Marshall, S. J. Blanksby, R. M. A. Heeren, S. R. Ellis, *Angewandte Chemie International Edition* **2018**, *57*, 10530–10534.
- [80] X. Ma, Y. Xia, *Angewandte Chemie - International Edition* **2014**, *53*, 2592–2596.

- [81] X. Xie, Y. Xia, *Analytical Chemistry* **2019**, *91*, 7173–7180.
- [82] E. Ryan, C. Q. N. Nguyen, C. Shiea, G. E. Reid, *Journal of The American Society for Mass Spectrometry* **2017**, *28*, 1406–1419.
- [83] T. Baba, J. L. Campbell, J. C. Y. Le Blanc, P. R. S. Baker, K. Ikeda, *Journal of Lipid Research* **2018**, *59*, 910–919.
- [84] J. L. Campbell, T. Baba, *Analytical Chemistry* **2015**, *87*, 5837–5845.
- [85] C. E. Randolph, D. J. Foreman, S. K. Betancourt, S. J. Blanksby, S. A. McLuckey, *Analytical Chemistry* **2018**, *90*, 12861–12869.
- [86] C. E. Randolph, S. J. Blanksby, S. A. McLuckey, *Analytical Chemistry* **2020**, *92*, 1219–1227.
- [87] S. E. Hancock, B. L. Poad, A. Batarseh, S. K. Abbott, T. W. Mitchell, *Analytical Biochemistry* **2017**, *524*, 45–55.
- [88] M. Zeng, N. Heine, K. R. Wilson, *Proceedings of the National Academy of Sciences* **2020**, *117*, 4486–4490.
- [89] L. Deng, Y. M. Ibrahim, E. S. Baker, N. A. Aly, A. M. Hamid, X. Zhang, X. Zheng, S. V. B. Garimella, I. K. Webb, S. A. Prost, J. A. Sandoval, R. V. Norheim, G. A. Anderson, A. V. Tolmachev, R. D. Smith, *ChemistrySelect* **2016**, *1*, 2396–2399.
- [90] R. Wojcik, I. K. Webb, L. Deng, S. V. Garimella, S. A. Prost, Y. M. Ibrahim, E. S. Baker, R. D. Smith, *International Journal of Molecular Sciences* **2017**, *18*, 1–12.
- [91] R. Wojcik, G. Nagy, I. K. Attah, I. K. Webb, S. V. Garimella, K. K. Weitz, A. Hollerbach, M. E. Monroe, M. R. Ligare, F. F. Nielson, R. V. Norheim, R. S. Renslow, T. O. Metz, Y. M. Ibrahim, R. D. Smith, *Analytical Chemistry* **2019**, *91*, 11952–11962.
- [92] G. Liebisch, K. Ekroos, M. Hermansson, C. S. Ejsing, *Biochimica et Biophysica Acta (BBA) - Molecular and Cell Biology of Lipids* **2017**, *1862*, 747–751.
- [93] J. A. Bowden, C. Z. Ulmer, C. M. Jones, J. P. Koelmel, R. A. Yost, *Metabolomics* **2018**, *14*, 53.

CHAPTER 2. MULTIPLE REACTION MONITORING (MRM-PROFILING) WORKFLOW

2.1 Background to MRM-Profiling

As introduced in Chapter 1, three current platforms for exploratory lipidomics are LC-MS, direct injection MS, and MSI. These methods regard each molecule as an individual compound. The dynamic fluctuation of such entities in side a living cell results in various phenotypes. The analysis of such samples requires complex sample preparation and separation techniques in current exploratory workflow. However, molecule information undergoes huge loss or dilution in the separation-based workflow due to the sample loss and polarity selection by extraction and column. Ionization prior to introduction into the MS makes abundant or highly ionizable molecules easily observed in the full scan mode, while others are suppressed.

What has been long ignored in many exploratory analytical workflows is the role of functional groups in metabolic pathways. Functional groups are part of the main properties in a molecule and they drive the chemical reactions both in a drug synthesis plant and endoplasmic reticulum of a cell. Thus, a new tactic, multiple reaction monitoring profiling (MRM-profiling), has been invented to expedite the screening of biological samples and focus on the functional group characteristics. MRM-profiling uses direct injection to introduce samples and alternative MS/MS scans or MRM transitions to characterize functional groups in sample. In this approach, the explicit annotation of structure is not the focus until the final stage. Instead, the main goal is to narrow down the candidate molecules/ions that account for the prominent

differences in the lipid functional group profile between various groups of samples. The method is divided into three stages: Discover, Screening, and Identification. A typical workflow of MRM-profiling is generalized in Figure 2.1.

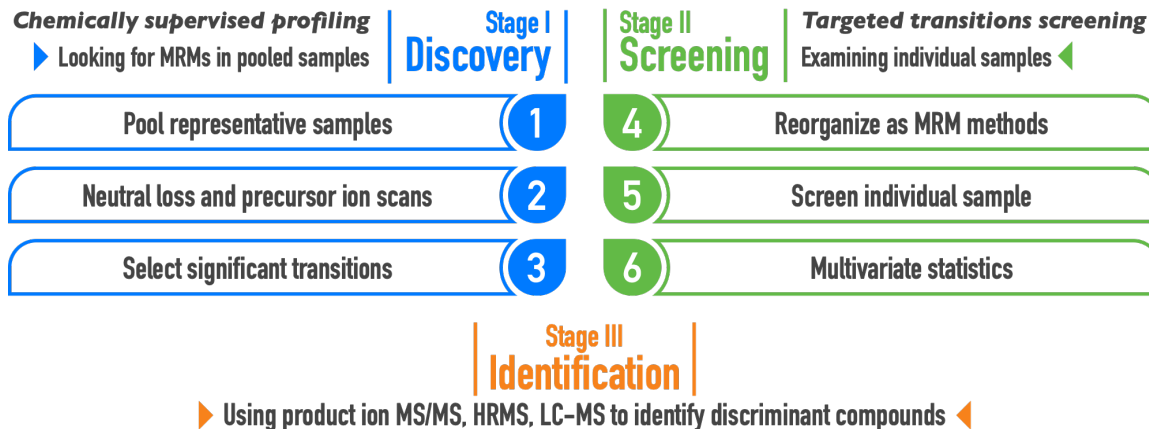


Figure 2.1. Typical workflow of MRM-profiling contains three stages: Discovery, Screening, and Identification. Discovery stage is a process of profiling based on chemical functional groups. Screening stage uses MRM transitions determined from Discovery stage to analyze different groups of samples and produces a panel of molecules/ions that are responsible for the differences between samples. Identification stage focuses on the characterization of molecules/ions from significant or responsible MRM transitions.

2.2 Preparation for MRM-Profiling

2.2.1 Precursor Ion Scan and Neutral Loss Scan

The core instrument in MRM-profiling is the triple quadrupole mass spectrometer (QqQ). Quadrupole refers to four parallel metal rods that are connected in pairs and powered by DC and RF voltages, so that it can either be used to isolate ions of a specific m/z by fixed voltages or to scan ions by ramping a particular voltage, named quadrupole mass filter. For QqQ, there are three such quadrupoles, of which the first (Q1) and the third (Q3) quadrupoles serve as mass filters, while the second quadrupole

(q2) is where collision-induced dissociation (CID) occurs. The configuration is shown in Figure 2.2(a). Ions that exit Q1 are termed *precursor ions* and fragments that

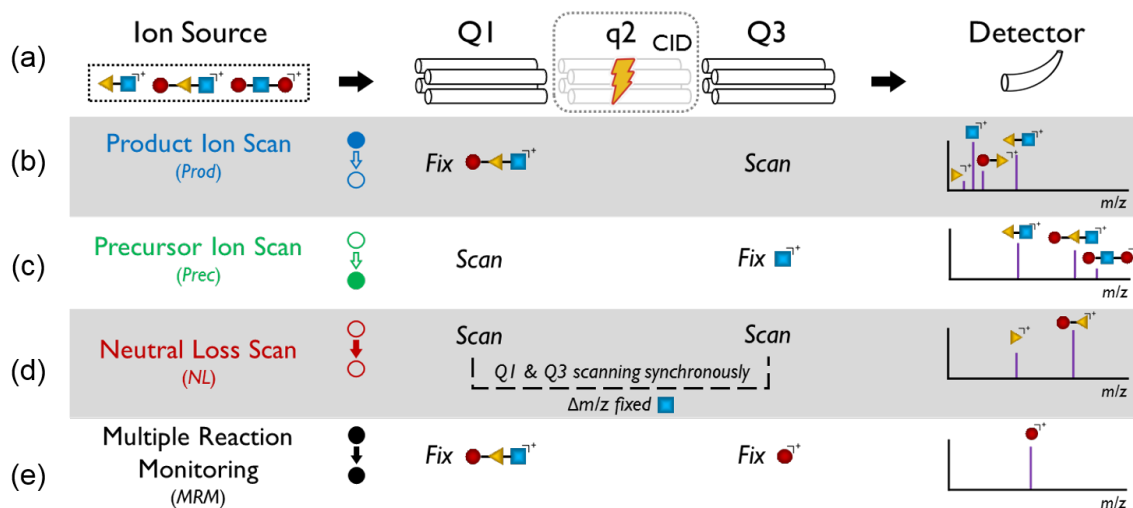


Figure 2.2. Configuration of QqQ (a) and four operation modes: (b) product ion scan, (c) precursor ion scan, (d) neutral loss scan, and (e) multiple reaction monitoring. The operation of Q1 and Q3 can be either *Fix* or *Scan*.

enter Q3 are termed *product ions*. For a pair of singly charged precursor ion and product ion, the m/z difference between them can be regarded as losing a group of atoms that does not carry charge and is termed *neutral loss*. By combining the two operations (fix or scan) of Q1 and Q3, four MS/MS operation modes can be carried out on QqQ: product ion scan (Prod), precursor ion scan (Prec), neutral loss scan (NL), and multiple reaction monitoring (MRM).

Prod mode in Figure 2.2(b) is the most used one in tandem mass spectrometry, where Q1 (fix) isolates a specific m/z for fragmentation in q2 and then mass analysis in Q3 (scan). This mode can provide rich structural information on ions with the same m/z .

In Prec mode shown in Figure 2.2(c), the operation of Q1 and Q3 are switched, compared to Prod, so that Q1 (scan) is transferring ions in a certain order to q2 for fragmentation and then Q3 (fix) for detection of the m/z of a specific fragment. The resulting spectrum reveals all the detectable ions with this same feature. For example, the phosphocholine headgroup ($C_5H_{15}NO_4P^+$, note the charge) in PC lipids often generates a peak at m/z 184.1 and Prec of 184.1 can be used to figure out the molecules functionally related to phosphocholine.

In NL mode shown in Figure 2.2(d), both Q1 and Q3 are scanned synchronously with a constant m/z difference between them. This constant value can be regarded as a neutral group of atoms that are lost during CID, and so is called neutral loss. For example, the fatty acyl chains in TAG, originally from fatty acids, can be easily lost as $RCOONH_4$ when ammonium salts dominates the solution.

In MRM mode shown in Figure 2.2(e), both Q1 and Q3 are fixed at a pair of m/z 's, also termed *transition*. This operation enables the selection of a specific precursor ion in Q1 and records the signal intensity of a desired product ion selected by Q3. MRM is frequently used for quantification of a known transition due to its high sensitivity.

All four operations can be projected onto a 2D domain as lines (Prod, Prec, NL) or points (MRM), as illustrated in Figure 2.3. For more operations in tandem mass spectrometry, readers are directed to reference [1] that has explored all possible combinations and their analytical meanings. It is obvious that Prec and NL scans can provide more insight in functional group screening, which suits the goal of MRM-profiling. The discovery stage and screening stage will be focused on picking out the most characteristic and statistically important points from each scan line.

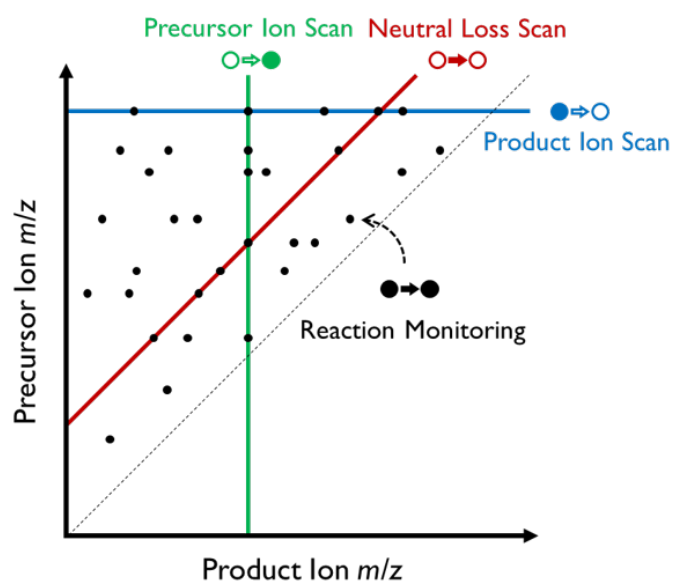


Figure 2.3. Illustration of four MS/MS operations on QqQ projected onto a 2D domain.

2.2.2 Method Library

The fragmentation mechanism of glycerophospholipids has already been extensively introduced and summarized.^[2] Two types of methods are included: scan-based and MRM-based. The scan-based methods are numbered from 1 - 65 for lipids and 66 - 110 for metabolites, as tabulated in Tables 2.1 and 2.2, respectively. As for MRM-based methods, they were inferred from information in the LipidMaps database. The molecular information was downloaded from the database. Because the molecular composition and lipid class are given for a specific molecule, it was easy to reason the major fragments after CID. These fragments can provide a strategy for fast screening of common lipids. The information of all the MRM-based methods are tabulated in Table 2.3.

Table 2.1. Parameters and details of scan methods in library for lipids.

#	Target Functional Group ^a	Scan Type	Mode	Collision Energy ^b	Mass Range	References
1	PC; SM	Prec 184.1	+	20/21/22/23	600 - 1200	[3]
2	PE	NL 141	+	19/20/21/22	500 - 1200	[3]
3	PS	NL 185	+	19/20/21/22	600 - 1200	[3]
4	PI	NL 277	+	19/20/21/22	500 - 1200	[4]
5	PA	NL 115	+	16/17/25/26	500 - 1200	[5, 6]
6	PA; LysoPG	NL 153	-	19/20/21/22	500 - 1200	[3]
7	GIPC	NL 179	+	19/20/21/22	500 - 1200	[5, 6]
8	PG	NL 189	+	19/20/21/22	500 - 1200	[4]
9	Cer(d20:1)	Prec 292.1	+	20/21/22/23	500 - 1200	[7]
10	Cer(d18:1)	Prec 264.1	+	20/21/22/23	500 - 1200	[7, 8]
11	Cer(d18:0)	Prec 266.1	+	20/21/22/23	500 - 1200	[7, 8]
12	Cer(t18:0)	Prec 282.1	+	20/21/22/23	500 - 1200	[7, 8]
13	Acyl-carnitines	Prec 85.1	+	28/29/30/31	200 - 800	[9]
14	Sulfatide	Prec 97.1	-	28/29/30/31	500 - 1200	[9]

continued on next page^aThis is tentative assignment of functional group or lipid class by mass.^bCollision energy is in manufacturer's units

Table 2.1. *continued*

#	Target Functional Group	Scan Type	Mode	Collision Energy	Mass Range	References
15	Cholesteryl esters	Prec 369.1	+	16/17/18/19	500 - 1000	[10]
16	Fatty Acyl Chain 12:0 (pos)	NL 217	+	19/20/21/22	500 - 1200	[11]
17	Fatty Acyl Chain 14:0 (pos)	NL 245	+	19/20/21/22	500 - 1200	[11]
18	Fatty Acyl Chain 14:1 (pos)	NL 223	+	19/20/21/22	500 - 1200	[11]
19	Fatty Acyl Chain 16:0 (pos)	NL 273	+	19/20/21/22	500 - 1200	[11]
20	Fatty Acyl Chain 16:1 (pos)	NL 271	+	19/20/21/22	500 - 1200	[11]
21	Fatty Acyl Chain 18:0 (pos)	NL 301	+	19/20/21/22	500 - 1200	[11]
22	Fatty Acyl Chain 18:1 (pos)	NL 299	+	19/20/21/22	500 - 1200	[11]
23	Fatty Acyl Chain 18:2 (pos)	NL 297	+	19/20/21/22	500 - 1200	[11]
24	Fatty Acyl Chain 18:3 (pos)	NL 295	+	19/20/21/22	500 - 1200	[11]
25	Fatty Acyl Chain 20:0 (pos)	NL 329	+	19/20/21/22	500 - 1200	[11]
26	Fatty Acyl Chain 20:1 (pos)	NL 327	+	19/20/21/22	500 - 1200	[11]
27	Fatty Acyl Chain 20:2 (pos)	NL 325	+	19/20/21/22	500 - 1200	[11]
28	Fatty Acyl Chain 20:3 (pos)	NL 323	+	19/20/21/22	500 - 1200	[11]
29	Fatty Acyl Chain 20:4 (pos)	NL 321	+	19/20/21/22	500 - 1200	[11]
30	Fatty Acyl Chain 20:5 (pos)	NL 319	+	19/20/21/22	500 - 1200	[11]

continued on next page

Table 2.1. *continued*

#	Target Functional Group	Scan Type	Mode	Collision Energy	Mass Range	References
31	Fatty Acyl Chain 22:0 (pos)	NL 357	+	19/20/21/22	500 - 1200	[11]
32	Fatty Acyl Chain 22:1 (pos)	NL 355	+	19/20/21/22	500 - 1200	[11]
33	Fatty Acyl Chain 22:2 (pos)	NL 353	+	19/20/21/22	500 - 1200	[11]
34	Fatty Acyl Chain 22:3 (pos)	NL 351	+	19/20/21/22	500 - 1200	[11]
35	Fatty Acyl Chain 22:4 (pos)	NL 349	+	19/20/21/22	500 - 1200	[11]
36	Fatty Acyl Chain 22:5 (pos)	NL 347	+	19/20/21/22	500 - 1200	[11]
37	Fatty Acyl Chain 22:6 (pos)	NL 345	+	19/20/21/22	500 - 1200	[11]
38	Fatty Acyl Chain 24:0 (pos)	NL 385	+	19/20/21/22	500 - 1200	[11]
39	Fatty Acyl Chain 26:0 (pos)	NL 413	+	19/20/21/22	500 - 1200	[12]
40	Fatty Acyl Chain 28:0 (pos)	NL 441	+	19/20/21/22	500 - 1200	[12]
41	Fatty Acyl Chain 12:0 (neg)	Prec 199.1	-	28/29/30/31	400 - 1200	[12]
42	Fatty Acyl Chain 14:0 (neg)	Prec 227.1	-	28/29/30/31	400 - 1200	[12]
43	Fatty Acyl Chain 14:1 (neg)	Prec 225.1	-	28/29/30/31	400 - 1200	[12]
44	Fatty Acyl Chain 16:0 (neg)	Prec 255.1	-	28/29/30/31	400 - 1200	[12]
45	Fatty Acyl Chain 16:1 (neg)	Prec 253.1	-	28/29/30/31	400 - 1200	[12]
46	Fatty Acyl Chain 18:0 (neg)	Prec 283.1	-	28/29/30/31	400 - 1200	[12]

continued on next page

Table 2.1. *continued*

#	Target Functional Group	Scan Type	Mode	Collision Energy	Mass Range	References
47	Fatty Acyl Chain 18:1 (neg)	Prec 281.1	-	28/29/30/31	400 - 1200	[12]
48	Fatty Acyl Chain 18:2 (neg)	Prec 279.1	-	28/29/30/31	400 - 1200	[12]
49	Fatty Acyl Chain 18:3 (neg)	Prec 277.1	-	28/29/30/31	400 - 1200	[12]
50	Fatty Acyl Chain 20:0 (neg)	Prec 311.1	-	28/29/30/31	400 - 1200	[12]
51	Fatty Acyl Chain 20:1 (neg)	Prec 309.1	-	28/29/30/31	400 - 1200	[12]
52	Fatty Acyl Chain 20:2 (neg)	Prec 307.1	-	28/29/30/31	400 - 1200	[12]
53	Fatty Acyl Chain 20:3 (neg)	Prec 305.1	-	28/29/30/31	400 - 1200	[12]
54	Fatty Acyl Chain 20:4 (neg)	Prec 303.1	-	28/29/30/31	400 - 1200	[12]
55	Fatty Acyl Chain 20:5 (neg)	Prec 301.1	-	28/29/30/31	400 - 1200	[12]
56	Fatty Acyl Chain 22:0 (neg)	Prec 339.1	-	28/29/30/31	400 - 1200	[12]
57	Fatty Acyl Chain 22:1 (neg)	Prec 337.1	-	28/29/30/31	400 - 1200	[12]
58	Fatty Acyl Chain 22:2 (neg)	Prec 335.1	-	28/29/30/31	400 - 1200	[12]
59	Fatty Acyl Chain 22:3 (neg)	Prec 333.1	-	28/29/30/31	400 - 1200	[12]
60	Fatty Acyl Chain 22:4 (neg)	Prec 331.1	-	28/29/30/31	400 - 1200	[12]
61	Fatty Acyl Chain 22:5 (neg)	Prec 329.1	-	28/29/30/31	400 - 1200	[12]
62	Fatty Acyl Chain 22:6 (neg)	Prec 327.1	-	28/29/30/31	400 - 1200	[12]

continued on next page

Table 2.1. *continued*

#	Target Functional Group	Scan Type	Mode	Collision Energy	Mass Range	References
63	Fatty Acyl Chain 24:0 (neg)	Prec 367.1	-	28/29/30/31	400 - 1200	[12]
64	Fatty Acyl Chain 26:0 (neg)	Prec 395.1	-	28/29/30/31	400 - 1200	[12]
65	Fatty Acyl Chain 28:0 (neg)	Prec 423.1	-	28/29/30/31	600 - 1200	[12]

Table 2.2. Parameters and details of scan methods in library for metabolites.

#	Target Functional Group ^a	Scan Type	Mode	Collision Energy ^b	Mass Range
66	NH ₃ - aliphatic amines and oximes	NL 17	+	15/20/25/30	80 - 1200
67	H ₂ O - carboxylic acids; aldehydes; ester	NL 18	+	15/20/25/30	80 - 1200
68	H ₂ O - amines; aromatic nitrile - aminosulphonic acids	NL 27	+	15/20/25/30	80 - 1200
69	CO - carboxylic acids; aldehydes	NL 28	+	15/20/25/30	80 - 1200
70	H ₂ CN - nitroaromatics NO - nitroaromatics	NL 30	+	15/20/25/30	80 - 1200
71	CH ₂ O - aldehydes CH ₄ O - methyl esters	NL 32	+	15/20/25/30	80 - 1200
72	H ₂ S - thiols	NL 34	+	15/20/25/30	80 - 1200
73	HCl - chlorides	NL 36	+	15/20/25/30	80 - 1200
74	CO ₂ - carboxylic acids; carbamates	NL 44	+	15/20/25/30	80 - 1200
75	NO ₂ - nitroaromatics CH ₂ O ₂ - carboxylic acids	NL 46	+	15/20/25/30	80 - 1200

continued on next page

^aThis is tentative assignment of functional group or target class of metabolites by mass. The asterisk (*) denotes this group as conjugate
^bCollision energy is in manufacturer's units

Table 2.2. *continued*

#	Target Functional Group	Scan Type	Mode	Collision Energy	Mass Range
76	CH ₄ OS - methionine sulfoxide	NL 64	+	15/20/25/30	80 - 1200
77	C ₃ H ₅ NO - serine residue	NL 71	+	15/20/25/30	80 - 1200
78	C ₃ H ₆ S - methionine side chain	NL 74	+	15/20/25/30	80 - 1200
79	SO ₃ - sulfonic acids	NL 80	+	15/20/25/30	200 - 1200
	HPO ₃ - phosphates				
80	HSO ₃ - sulfonic acids	NL 81	+	15/20/25/30	200 - 1200
81	H ₂ SO ₃ - sulfonate group	NL 82	+	15/20/25/30	200 - 1200
82	H ₃ PO ₄ - phosphates	NL 98	+	15/20/25/30	200 - 1200
83	C ₃ H ₇ NO ₂ S - cysteine(*)	NL 121	+	15/20/25/30	200 - 1200
84	HI - aromatic iodides	NL 128	+	15/20/25/30	200 - 1200
85	C ₆ H ₁₀ O ₃ - dideoxyhexoside	NL 130	+	15/20/25/30	200 - 1200
86	C ₅ H ₈ O ₄ - pentoside	NL 132	+	15/20/25/30	200 - 1200
87	C ₆ H ₁₀ O ₄ - deoxyhexoside	NL 146	+	15/20/25/30	200 - 1200
	C ₅ H ₁₀ N ₂ O ₃ - gamma-GluCys(*) ; glutathione				
88	C ₆ H ₁₀ O ₅ - hexoside	NL 162	+	15/20/25/30	200 - 1200
89	C ₅ H ₉ NO ₃ S - N-acetylcysteine(*)	NL 163	+	15/20/25/30	200 - 1200

continued on next page

Table 2.2. *continued*

#	Target Functional Group	Scan Type	Mode	Collision Energy	Mass Range
90	C ₆ H ₈ O ₆ - glucoronides	NL 176	+	15/20/25/30	200 - 1200
91	C ₆ H ₁₀ O ₇ - glucoronides (benzylic)	NL 194	+	15/20/25/30	200 - 1200
92	C ₈ H ₁₃ NO ₅ - N-acetylglucosamine (benzylic)(*)	NL 203	+	15/20/25/30	300 - 1200
93	C ₈ H ₁₅ NO ₆ - N-acetylglucosamine(*)	NL 221	+	15/20/25/30	300 - 1200
94	C ₉ H ₁₂ O ₈ - malonylglucoronides	NL 248	+	15/20/25/30	300 - 1200
95	C ₈ H ₁₄ N ₂ O ₅ S - gamma-GluCys(*)	NL 250	+	15/20/25/30	300 - 1200
96	C ₉ H ₁₄ O ₉ - malonylglucoronides (benzylic)	NL 266	+	15/20/25/30	300 - 1200
97	C ₁₀ H ₁₇ N ₃ O ₆ S - glutathione(*)	NL 307	+	15/20/25/30	350 - 1200
98	H ₂ O - amines; aromatic nitrile - aminosulphonic acids	NL 27	-	15/20/25/30	80 - 1200
99	CO - carboxylic acids; aldehydes	NL 28	-	15/20/25/30	80 - 1200
100	H ₂ CN - nitroaromatics NO - nitroaromatics CH ₂ O - aldehydes	NL 30	-	15/20/25/30	80 - 1200
101	CO ₂ - carboxylic acids; carbamates	NL 44	-	15/20/25/30	80 - 1200
102	NO ₂ - nitroaromatics	NL 46	-	15/20/25/30	80 - 1200

continued on next page

Table 2.2. *continued*

#	Target Functional Group	Scan Type	Mode	Collision Energy	Mass Range
	CH ₂ O ₂ - carboxylic acids				
103	SO ₂ - sulfonic acids, sulfonates	NL 64	-	15/20/25/30	80 - 1200
104	SO ₃ - sulfonic acids	NL 80	-	15/20/25/30	100 - 1200
105	C ₃ H ₇ NO ₂ S - cysteine(*)	NL 121	-	15/20/25/30	200 - 1200
106	C ₆ H ₁₀ O ₄ - deoxyhexoside	NL 146	-	15/20/25/30	200 - 1200
107	C ₆ H ₁₂ O ₅ - rhamnoside	NL 164	-	15/20/25/30	200 - 1200
108	C ₆ H ₈ O ₆ - glucoronides	NL 176	+	15/20/25/30	200 - 1200
109	C ₈ H ₁₃ NO ₅ - N-acetylglucosamine (benzylic)(*)	NL 203	+	15/20/25/30	250 - 1200
110	C ₈ H ₁₄ N ₂ O ₅ S - gamma-GluCys(*)	NL 250	-	15/20/25/30	300 - 1200

Table 2.3. Details of MRM methods based on LipidMaps database in library.

#	Target Functional Group	Scan Type	Mode
MRM-1	PC; SM (odd carbon number)	MRM	+
MRM-2	PE (odd carbon number)	MRM	+
MRM-3	PG (odd carbon number)	MRM	+
MRM-4	PI (odd carbon number)	MRM	+
MRM-5	PS (odd carbon number)	MRM	+
MRM-6	PC; SM (even carbon number)	MRM	+
MRM-7	PE (even carbon number)	MRM	+
MRM-8	PG (even carbon number)	MRM	+
MRM-9	PI (even carbon number)	MRM	+
MRM-10	PS (even carbon number)	MRM	+
MRM-11	Free Fatty Acids	MRM	-
MRM-12	Acyl-carnitines	MRM	+
MRM-13	Ceramides	MRM	+

2.3 Discovery Stage

In this part, Agilent 6410 Triple Quadrupole is employed as an example to show how worklist generation and experimental design are accomplished. The method development might need few changes when carried out on a different vendor's platform.

The goal of Discovery stage is to determine which MRMs are important to discriminate different samples based on functional group screening by various scans. This can be accomplished using literature data in method library (see Tables 2.1, 2.2, and 2.3), or experiment as addressed in this section. Discovery stage is accomplished using a triple quadrupole mass spectrometer. Few labeled representative samples that contain the common features of sample sets are analyzed by considerable Prec and NL scans. Such representative samples can be acquired by a strategy like sample pooling. Some of the applied scans are tabulated in Tables 2.1 and 2.2. Head groups and fatty acyl chain residues are the two main classes of molecular features to be investigated for phospholipids. Data from scans is then extracted and filtered

based on the absolute intensity and relative intensity compared to control samples (e.g. above a certain threshold comparing to that in blank sample). For each scan, a list of precursor/product ion pairs can be acquired, these are MRM transitions. This assorted list of intense MRM transitions are the chemical features that show significant signals in MS but their importance in discriminating different groups is not evaluated yet. The data filter is supposed to remove scans or MRM transitions that did not originate from the biological system of interest, while also keeping as much information as possible. For example, a reasonable evaluation of bacteria can be made between the bacteria and the corresponding culture medium with the same lipid extraction protocol. Then the overlapping MRM transitions can be removed to generate a characteristic set of MRM features for the bacteria.

2.3.1 Worklist Generation

The first step of Discovery stage is to set up a worklist for the instrument system to arrange the samples and methods in desired order. The worklist file (*.wkl) is generated using Agilent MassHunter Acquisition Worklist Editor. However, Microsoft Excel is more user-friendly for generating a worklist with repeated information. Either way is acceptable. A valid worklist at least contains the following information: Sample Name, Sample Position, Method, and Data File.

Sample Name It contains all the samples to be analyzed. Wash solutions and quality controls are also included at a constant frequency. The use of QC will be discussed in the next section.

Sample Position This is the place for robot to locate the desired sample vial.

Method Designated *.m file as described in previous section. It can be either MRM method or scan method.

Data File The name of the data file for each sample per method is assigned in form of [SampleName]_[Method].d.

The order of the worklist can be organized according to either samples or names as shown in Figure 2.4, in which two samples are screened by three methods. When the worklist is created in order of samples in Figure 2.4(a), Sample 1 is analyzed by three methods and then those methods are applied to Sample 2. In another regime shown in Figure 2.4(b), samples are alternately analyzed by each method. The total number of injections in both cases is six, but each tactic has pros and cons. In the former one, the influence from carryover can be minimized because of much fewer switching between samples. However, when the number of sample increases, the time gap between injections of the first and last samples using the same method can be as long as hours. This could possibly introduce errors from fluctuation of instrument performance after long runtime. In the latter case, the influence from instrument error can be well controlled with minimal time difference between samples. But the frequent switching would fail the data acquisition and result in carryover effect if any injection is delayed.

One way to avoid carryover is to introduce wash solvent whenever a different sample is introduced. Obviously, the former worklist (one wash introduced between Sample 1 and Sample 2) is better than the latter one (altogether at least five wash introduced between each adjacent pair of injections) due to the shorter total time increase in analysis.

As for the fluctuation of instrument status, it is not possible to cancel the influence in unknown samples. Thus, the best we can do is introduce quality control to monitor the stability of instrument. A QC sample is injected every constant period of time or constant number of injections (usually one QC for every 30 min or every 10 injections). The chromatogram can be used to evaluate how the instrument is behaving. For example, Figure 2.5 shows the overlaid chromatograms of all the QC samples in two experiments, Experiment 1 and Experiment 2, with 16 injections and 43 injections of QC samples, respectively. Visually, one can draw the conclusion that the instrument behaved better in Experiment 1 by Figure 2.5(a) due to the perfect overlapping of all

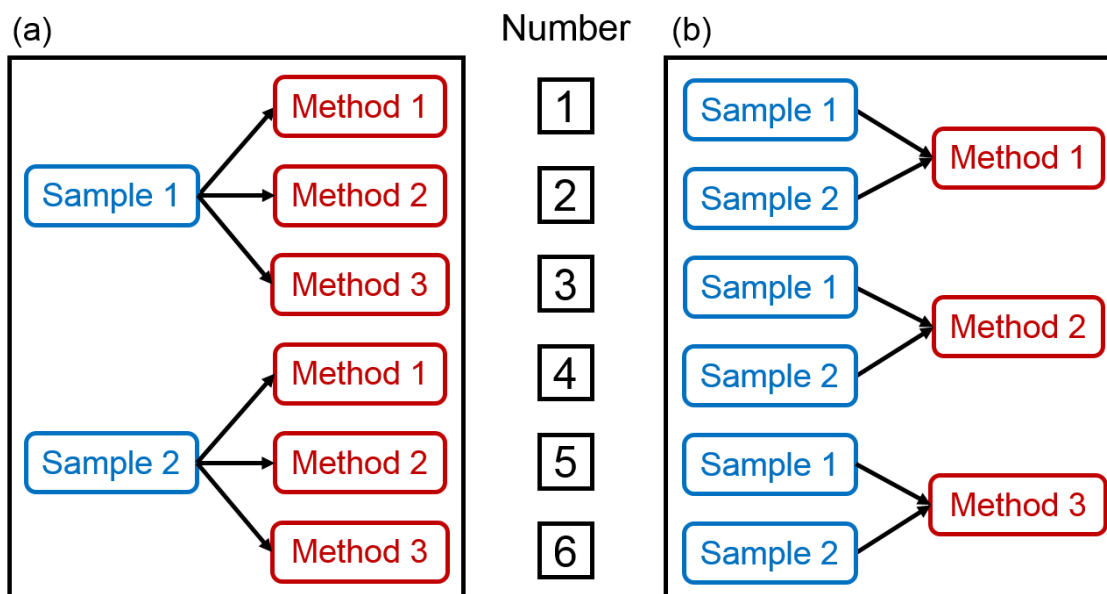


Figure 2.4. Two worklist arrangements of an experiment with two samples and three methods. (a) Apply all methods to the same sample first and then screen the next sample. (b) Apply the same method to all samples first and then screen all samples by the next method.

the layers. The simultaneous rise of signal at around 0.65 min and similar shape of signal decay prove the instrument did not exhibit significant fluctuation across over the whole analysis. However, the signal underwent large variations in Experiment 2 shown in Figure 2.5(b). The spikes at beginning and end indicate that capillary might be clogged or leaking might occur during elution. These possible reasons also resulted in the wide spread of the intensities from 5×10^4 counts to 2×10^5 counts. The area under curve (AUC) value of each chromatogram between 0.6 min to 1.4 min can be calculated. These AUC results are plotted in Figure 2.6. The AUCs of each experiment was normalized to the maximum. The distribution of Experiment 1 is apparently wider than Experiment 2, indicating the latter one is more stable. Thus, constant injections of QC are beneficial and essential for confirming the status of instrument and evaluating the reliability of results. This is also helpful to avoid wasting instrument time and carry out trouble shooting.

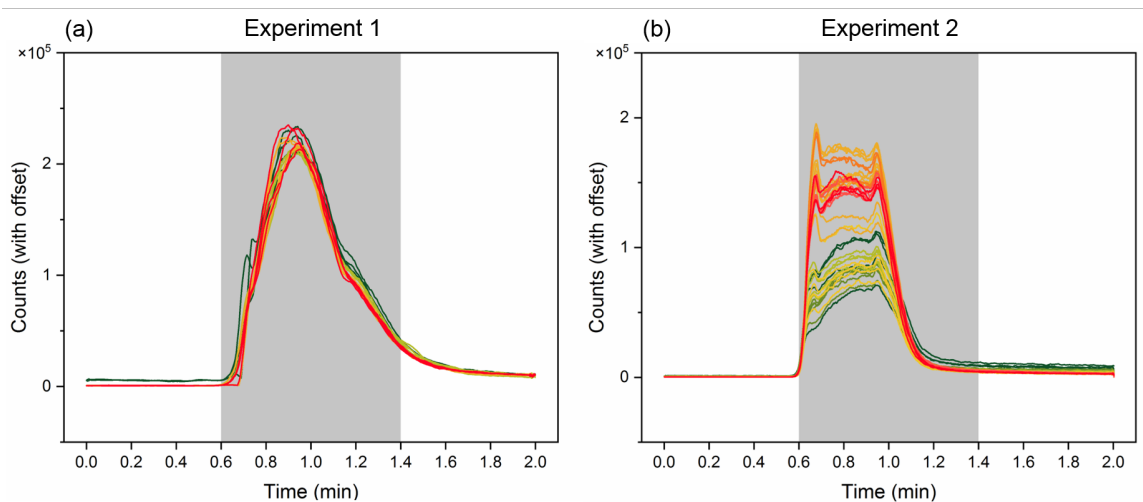


Figure 2.5. Overlaid chromatogram of QC samples from two experiments. (a) Experiment 1 with 16 injections of QC. (b) Experiment 2 with 43 injections of QC. In both cases, the time between each two QCs were 10 injections of samples (about 30 min). The curves in shaded area between 0.6 min to 1.4 min are used to calculate the area under curve in Figure 2.6.

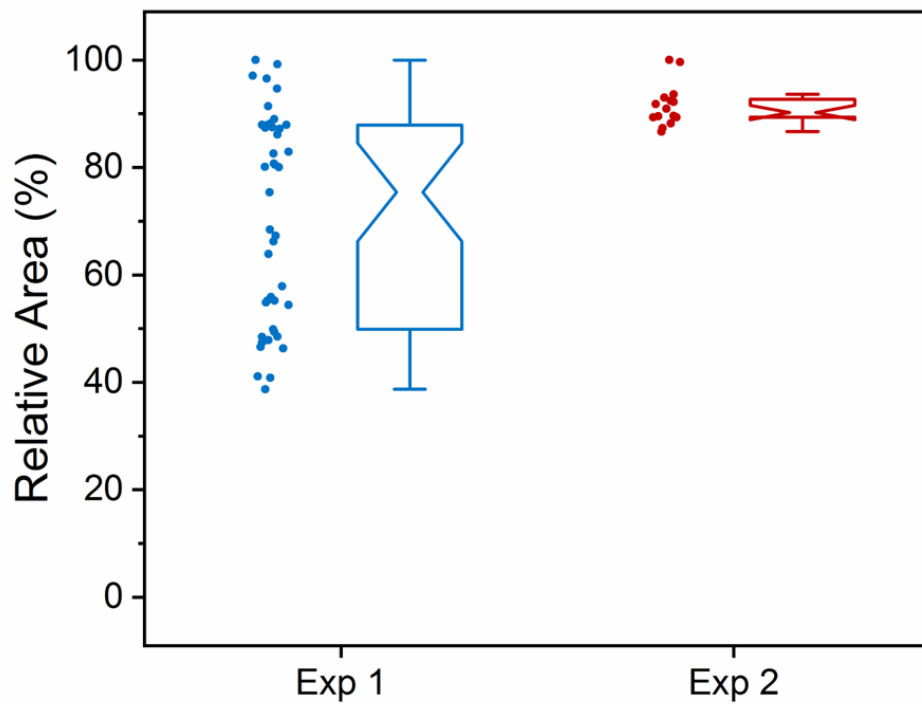


Figure 2.6. Distribution of normalized area under curve (AUC) values of QC samples from the two experiments in Figure 2.5, Experiment 1 and 2 (abbreviated as Exp 1 and 2, respectively). All the areas are normalized to the maximum AUC value in each experiment.

2.3.2 Data Processing

Raw MS data from the triple quadrupole instrument is usually stored with an increment of 0.1 Da in precursor's m/z for Prec and NL scans. Given the resolution of the instrument is unit-resolution, it is rational to pre-process by data binning. A common bin width is 1 Da. In this case, the intensity of a specific whole number m/z M is averaged or summed from m/z M to m/z ($M + 0.9$) so that the new m/z M represents the nominal mass of the averaged or summed data. An alternative is to set the range of whole number m/z M as from m/z ($M - 0.5$) to m/z ($M + 0.4$) and the new m/z M becomes the rounded values of all data involved. A smaller bin width such as 0.3 Da or 0.5 Da is also practical, but the data binning strategy needs to be consistent throughout the data analysis and should not jeopardize the quality of data.

Several filters can be applied once data is binned. The most straightforward one is filtering by comparing the absolute counts to control sample or blank sample. For example, peaks that are 30% higher than that of blank sample will survive for further filtering. The threshold can be adjusted to maintain the trade-off between the number of peaks and corresponding chemical information. Another way of filtering is to normalize data from each scan to the maximum intensity first, and then to compare in the same way as addressed above. After filtering, all peaks, now in MRM transitions format, are gathered together and duplicate entries can be removed. Most duplicates result from their occurrences in both Prec and NL scans under the same ion mode.

2.3.3 MRM Method Development for Screening Stage

After processing of data from Discovery stage, the feature MRMs that are rich in chemical information are retained. Given the limited capability of the instrument program, one MRM method can at most accommodate about 300 individual MRMs,

considering the need of recording and averaging the MRM for at least 10 times. Theoretically, these transitions can be randomly grouped as 200 - 300 for methods. But it is preferred that transitions with the same ion mode and/or with similar precursor ion are put in the same method to reduce the error brought by instrument.

Essential parameters for a transition include: Precursor Ion, Product Ion, Dwell, Fragmentor, Collision Energy, Polarity. Again, as long as the parameters of a transition is set, it is supposed to be consistent for all samples. Most information can be retrieved from corresponding scan method.

Precursor Ion & Product Ion Both are m/z values.

Dwell The time lasts for the signal of one MRM transition to be recorded.

Fragmentor The voltage controls the velocity of ions passing through the middle pressure region from ambient pressure ESI sprayer to high vacuum mass spectrometer.

Collision Energy The value in manufacturer's unit determines the degree of fragmentation during CID.

Polarity Represents the ion mode of a transition, positive or negative.

2.4 Screening Stage

In the Screening stage, more samples will be interrogated using fewer numbers of MRM transitions compared to the Discovery stage. The goal is to find a panel of transitions that maximize the differences among groups. By applying previously determined characteristic MRM transitions and carrying out statistical analysis, the candidates can be selected in an efficient manner.

2.4.1 Worklist Generation

Samples with different labels are supposed to be prepared in duplicates so that they can be analyzed and averaged to reduce the errors resulting from instrument instability and increase the reliability of data. With much fewer MRM transitions, each sample can be screened in a fast pace to allow more analyses. The recommended arrangement of worklist still follows what is applied to Discovery stage as shown in Figure 2.4(a). But this time, replicates will be included. For example, if there are 10 replicates for both Sample 1 and Sample 2, the samples with the same labels are supposed to be analyzed successively to avoid contamination or fluctuation. Thus, the hierarchy of order is screening Sample 1A by all methods first, cleaning by wash solvent, screening Sample 1B by all methods, ... , screening Sample 2A by all methods, cleaning, ... It is also recommended to introduce intermittent QCs for status check.

2.4.2 Data Processing and Statistical Analysis

The data processing is simply grouping all the data together in a matrix of MRM transitions vs. intensities of each sample. Whether to normalize the data still remains a question. For most studies, statistics are carried out based on the original data, data normalized to total ion counts, and data normalized to maximum counts. As a preliminary result of investigating the effect of different normalization methods, Chapter 3 demonstrates that in an embryo or blastocyst system, the results are similar for the latter two methods.

Univariate and multivariate statistics can then be applied, including but not limited to Student's t-test, analysis of variance (ANOVA), principal component analysis (PCA), and linear discriminant analysis (LDA), depending on the purposes of research. How to carry out statistical analysis and the method to implement them will not be discussed here because they should be considered for individual set of data. No matter what statistics, the outcome of Screening stage is a panel of MRMs, con-

taining information of potential molecules that can be used as diagnostic factor or for biomarker study. The analysis can be halted here if the purpose is only to build a model for differentiation. It is noteworthy that these features are still represented by m/z 's in the form of MRMs, but structures have not yet been identified. Accordingly, for more intricate study of each MRM other than pattern research, an Identification stage is required.

2.5 Identification Stage

Based on a smaller set of significant MRM transitions from Screening stage, elaborate study on separation and structure of these candidates can be carried out, as called the Identification stage. The whole process of zeroing in on final candidates can be achieved in much shorter time since the Discovery phase has already ruled out the less informative transitions and the Screening phase is focused on the more meaningful ones. The identification of a specific MRM transition can be accomplished through more sophisticated targeted methods. Although this stage is not the core of MRM-profiling concept, the characterization of a molecule responsible for a transition will strengthen the conclusion. Separation techniques such as HPLC and IMS are beneficial to isolate the target molecule from other analytes for downstream analysis and HRMS of full scan and product ion scan is helpful to infer the molecular composition. There are also other innovative analytical tools for tackling the problem as reviewed in Chapter 1.

2.6 An Example: Milk from Human, Cow, and Soy

Milk is rich in glycerides, which is composed of a glycerol and one to three fatty acids. Three common fatty acids are palmitic acid ($C_{16}H_{32}O_2$, FA(16:0), 256.43 g/mol), palmitoleic acid ($C_{16}H_{30}O_2$, FA(16:1), 254.41 g/mol), and oleic acid ($C_{18}H_{34}O_2$, FA(18:1), 282.47 g/mol). For a mono-/di-/triacylglyceride, one type of NL from the loss of a fatty acyl chain can be observed. In this particular experiment, ammonium salt was

added to promote ionization and substitute the proton in fatty acid loss to form a neutral entity. As a result, the corresponding NL scan of FA(16:0), FA(16:1), and FA(18:1) uses 273, 271, and 299 Da, respectively. Thus, theoretically, applying these three NL scans to the lipid extracts of milk will unveil the profiles of lipids containing these three molecular features.

Three different types of milk were selected: cow milk, human milk, and soy milk. After lipid extraction and drying overnight, each sample was redissolved for analysis by NL scans. The result of performing NL 271 is shown in Figure 2.7 and note that the m/z axis refers to the precursor ion. The common feature of the distribution is that no peak occurs over m/z 900. The constant general gap of 28 Da indicates the biological origin of the three samples. As for the distribution patterns, the three kinds of milk are distinct. Visually, cow milk sample exhibits a wide coverage of m/z . High intensity peaks tend to center around m/z 650 and expand to m/z 750, starting from which much lower intensity peaks locate. For human milk sample, the coverage is a little narrower than cow milk, but the intensity generally rises as the m/z increases and reaches its maximum at around m/z 875. The soy milk sample, however, only has two groups of peaks observable and is totally different from the previous two. Three zones labeled I, II, and III are zoomed in and shown in Figure 2.8. Zone I as shown in the first column from left in Figure 2.8 can differentiate cow sample from the other two with m/z 654.5 being the most characteristic. So the transition m/z 654.5 \rightarrow m/z 383.5 can be definitely included in the panel of significant MRMs. Moving on to Zone II in the middle column of Figure 2.8, human milk sample has more featured peaks, such as m/z 792.6. Other less intense peaks at m/z 790.6, m/z 793.6, and m/z 794.6 are also candidates and could be kept if they meet the threshold cut. The last column in Figure 2.8 contains Zone III, which is complicated for human milk and soy milk samples. It might not be intuitive if only this zone is provided when classifying samples, but the relative abundance in this region is valuable for statistics or other chemical profiling purpose. So, to retain as much chemical information as possible,

in these three zones, the peaks of interest are highlighted in yellow solid lines and labeled at the top. By subtracting 271 Da, the product ion m/z can be calculated for constructing the MRM method file intended to be used in Screening stage.

The results of NL 273 are shown in Figure 2.9 and Figure 2.10, and those of NL 299 are shown in Figure 2.11 and Figure 2.12. By comparing results among different scans of the same sample, the distribution pattern is consistent and can be used to determine the origin of sample. The NL scans are sensitive enough to capture such pattern differences between samples. In the three typical zones, all the peaks that are supposed to be picked out and transferred for next stage analysis are highlighted in yellow. But there are more peaks, or better termed as transitions, spreading in ranges other than these. Combining all the MRMs that survive after filtering makes the full list for Screening stage.

2.7 Summary

MRM-profiling is a concept that emphasizes the chemically important functional groups and their contribution to distinguishing samples. Most current exploratory lipidomics studies by LC-MS focus on splitting the integrated m/z feature into several parts, where this “split” can complicate the whole data analysis and introduce loss of information in detection. The m/z is already an important feature as it is characteristic of an individual compound. It is the connections between m/z values or transitions that characterize functional groups. This metabolic signature, we argue, is the most efficient way of characterizing differences between samples as a lipid profiling strategy. MRM-profiling is definitely not the best tool for acquiring deeper structure information and has restricted quantification performance. Nevertheless, without complicated dataset and bias, it is a valuable profiling strategy for large-scale study.

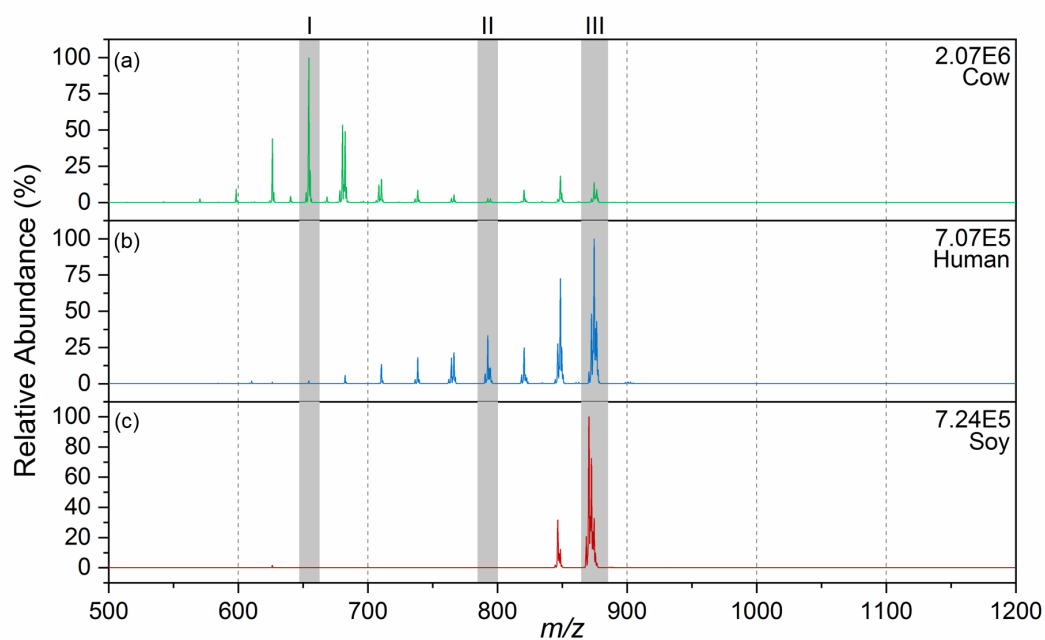


Figure 2.7. Mass spectra of NL 271 of milk samples from (a) cow, (b) human, and (c) soy. The label and corresponding normalized intensity are shown in the top right corner in each panel. Zoom-in mass spectra of shaded m/z regions I, II, and III are shown in Figure 2.8.

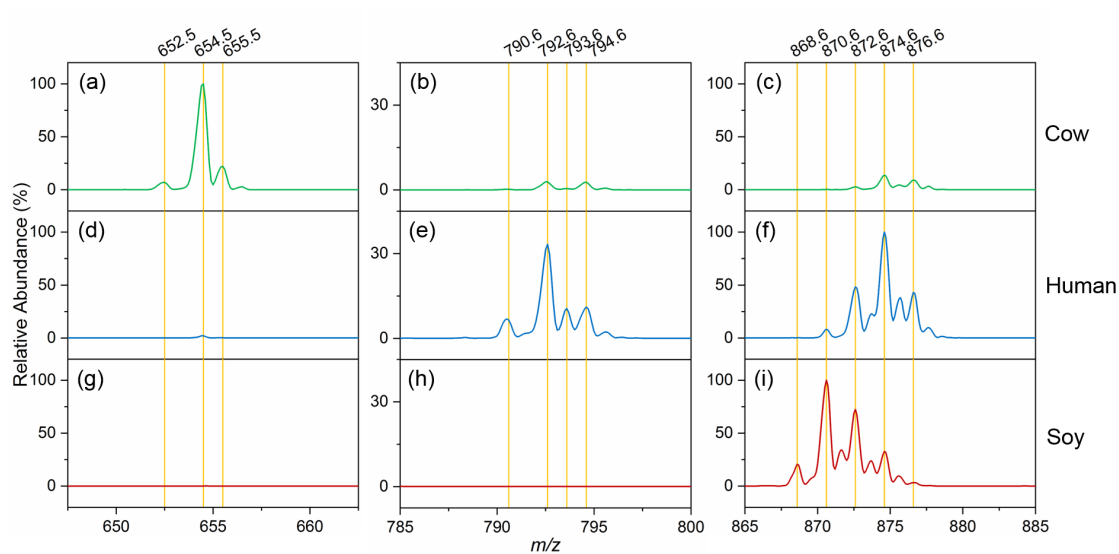


Figure 2.8. Zoom-in mass spectra of NL 271 of samples from cow (a-c), human (d-f), and soy (g-i) from Figure 2.7. Three typical m/z regions are selected as shown in each column. The normalized intensity is the same as the corresponding value from Figure 2.7. Potential characteristic peaks are highlighted by yellow solid lines with m/z 's labeled.

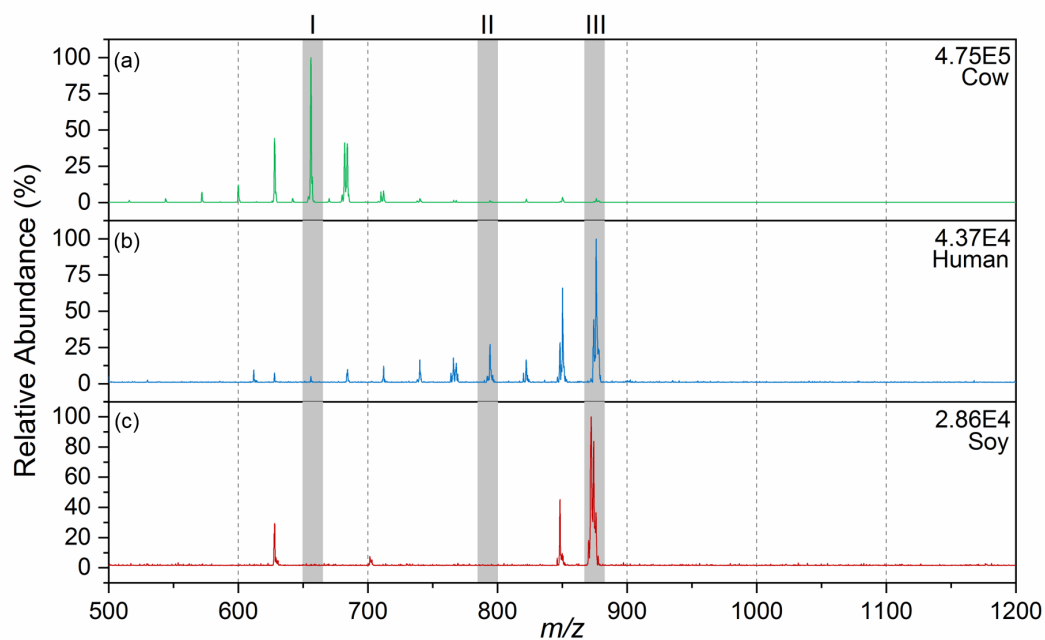


Figure 2.9. Mass spectra of NL 273 of milk samples from (a) cow, (b) human, and (c) soy. The label and corresponding normalized intensity are shown in the top right corner in each panel. Zoom-in mass spectra of shaded m/z regions I, II, and III are shown in Figure 2.10.

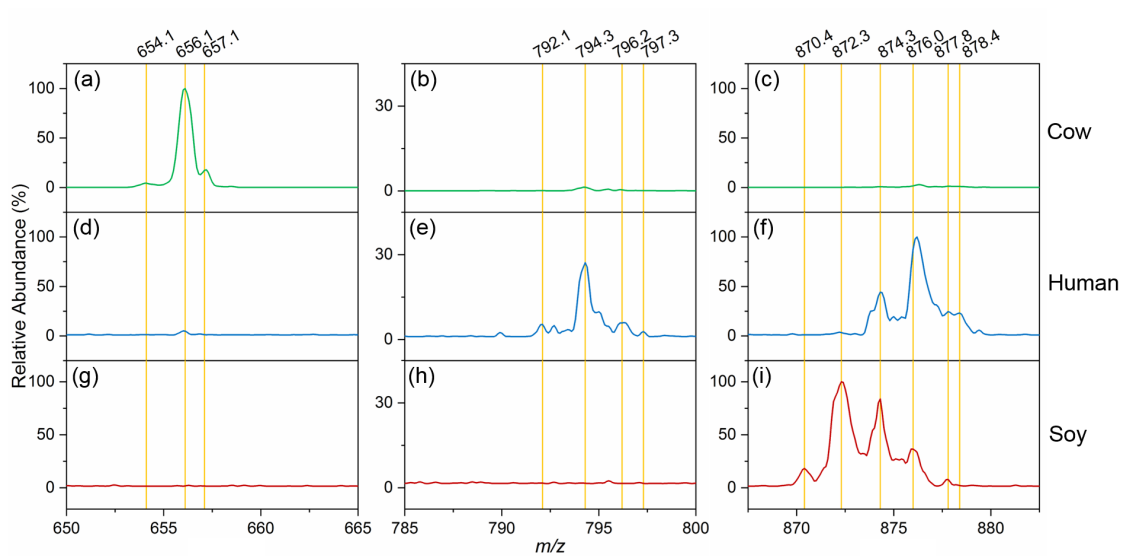


Figure 2.10. Zoom-in mass spectra of NL 273 of samples from cow (a-c), human (d-f), and soy (g-i) from Figure 2.9. Three typical m/z regions are selected as shown in each column. The normalized intensity is the same as the corresponding value from Figure 2.9. Potential characteristic peaks are highlighted by yellow solid lines with m/z 's labeled.

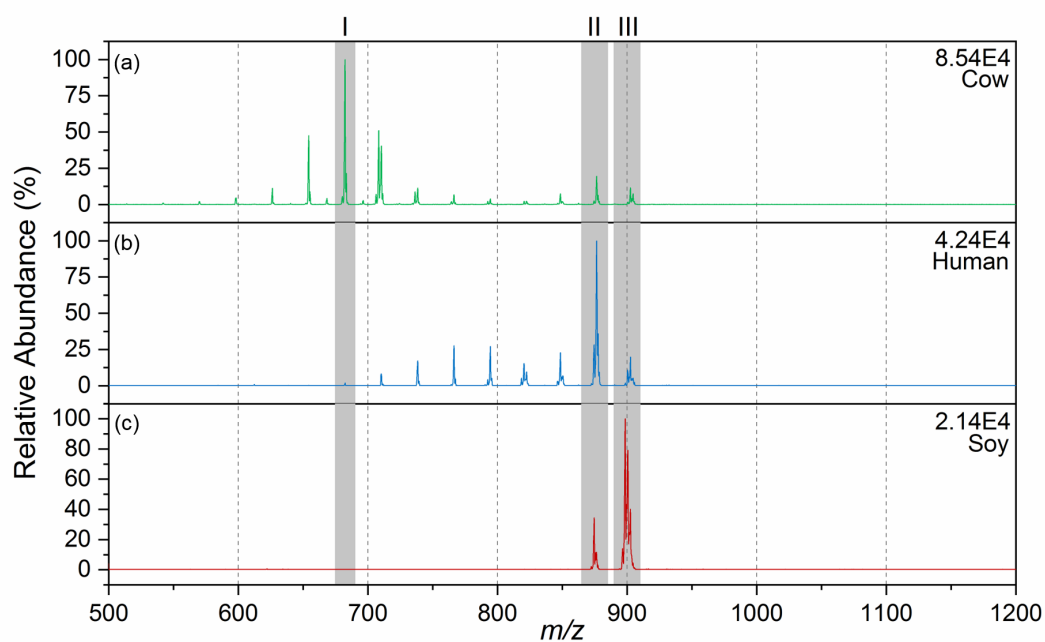


Figure 2.11. Mass spectra of NL 299 of milk samples from (a) cow, (b) human, and (c) soy. The label and corresponding normalized intensity are shown in the top right corner in each panel. Zoom-in mass spectra of shaded m/z regions I, II, and III are shown in Figure 2.12.

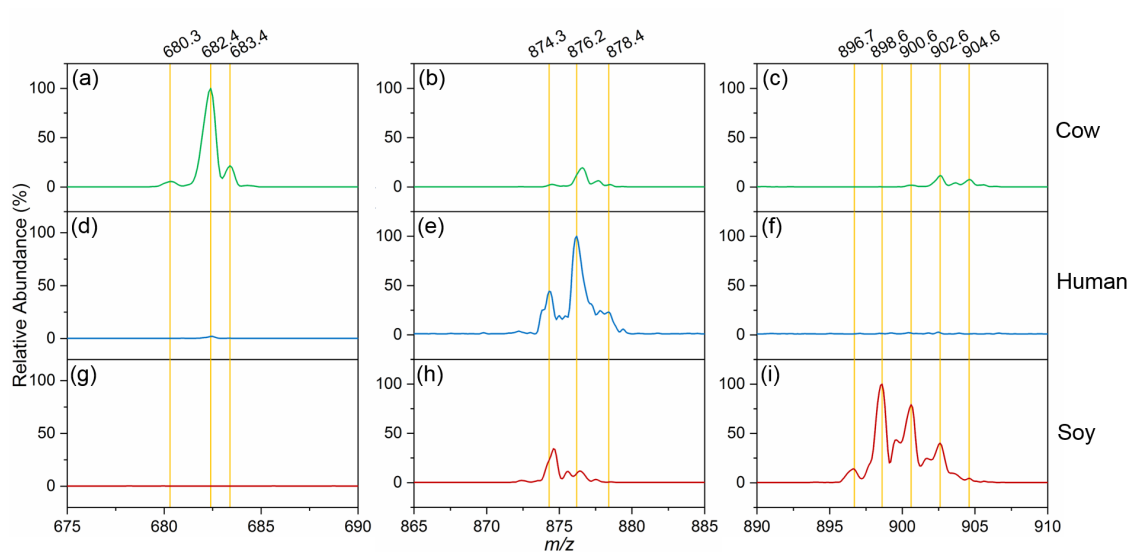


Figure 2.12. Zoom-in mass spectra of NL 299 of samples from cow (a-c), human (d-f), and soy (g-i) from Figure 2.11. Three typical m/z regions are selected as shown in each column. The normalized intensity is the same as the corresponding value from Figure 2.11. Potential characteristic peaks are highlighted by yellow solid lines with m/z 's labeled.

2.8 References

- [1] J. C. Schwartz, A. P. Wade, C. G. Enke, R. G. Cooks, *Analytical Chemistry* **1990**, *62*, 1809–1818.
- [2] R. C. Murphy in *Tandem Mass Spectrometry of Lipids: Molecular Analysis of Complex Lipids*, 4, Royal Society of Chemistry, **2014**, pp. 130–193.
- [3] B. Brugger, G. Erben, R. Sandhoff, F. T. Wieland, W. D. Lehmann, *Proceedings of the National Academy of Sciences* **1997**, *94*, 2339–2344.
- [4] T. Houjou, K. Yamatani, M. Imagawa, T. Shimizu, R. Taguchi, *Rapid Communications in Mass Spectrometry* **2005**, *19*, 654–666.
- [5] S. Xiao, W. Gao, Q.-F. Chen, S.-W. Chan, S.-X. Zheng, J. Ma, M. Wang, R. Welti, M.-L. Chye, *The Plant Cell* **2010**, *22*, 1463–1482.
- [6] How Lipid Profiling Works - Kansas Lipidomics Research Center.
- [7] A. H. Merrill Jr., M. C. Sullards, J. C. Allegood, S. Kelly, E. Wang, *Methods* **2005**, *36*, 207–224.
- [8] B. Colsch, C. Afonso, I. Popa, J. Portoukalian, F. Fournier, J.-C. Tabet, N. Baumann, *Journal of Lipid Research* **2004**, *45*, 281–286.
- [9] X. Han, R. W. Gross, *Mass Spectrometry Reviews* **2005**, *24*, 367–412.
- [10] G. Liebisch, M. Binder, R. Schifferer, T. Langmann, B. Schulz, G. Schmitz, *Biochimica et Biophysica Acta (BBA) - Molecular and Cell Biology of Lipids* **2006**, *1761*, 121–128.
- [11] M. Li, E. Butka, X. Wang, *Scientific Reports* **2015**, *4*, 6581.
- [12] Y. Ma, T. Kind, D. Yang, C. Leon, O. Fiehn, *Analytical Chemistry* **2014**, *86*, 10724–10731.

CHAPTER 3. QUANTITATIVE ANALYSIS OF PHOSPHOLIPIDS IN OOCYTES AND BLASTOCYSTS BY MRM-PROFILING

3.1 Abstract

Quantification of lipids in minute samples such as oocytes and embryos challenges the limits of bioanalytical chemistry. As an alternative to conventional mass spectrometry methods that incorporate chromatographic separation, MRM-profiling has been developed as a high sensitivity exploratory method. First, the method uses precursor ion scans and neutral loss scans to target specific chemical functionalities from which significant MRM transitions are identified (discovery stage). It then applies these MRM transitions to individual samples (screening stage). MRM-profiling has been applied to multiple scientific and clinical models as an indicator of up-/down-regulation in molecular composition or a classifier for diseased/healthy status. Here we show that by introducing internal standards, MRM-profiling can be successfully used for quantification of phospholipids. Bovine *in vitro*-matured oocytes and *in vitro*-produced blastocysts were collected and processed using a single lipid extraction step. Internal standards were added to the lipid extracts for quantitation by lipid class. We demonstrate that: (1) different classes of phospholipids in oocytes can be quantified at levels corresponding to the contents of just two oocytes; (2) the lipid content of selected MRM transitions by class in oocytes varies from 4.5 ng to 0.7 ng; (3) both relative (using modified total ion count from selected transitions) and absolute (using ion intensity from internal standard) normalization methods were successful in distinguishing oocytes (and blastocysts) cultured in different environments.

3.2 Introduction

Mammalian cell membranes are composed of a variety of glycerophospholipids and sphingolipids that differ in headgroup and acyl-chain composition.^[1] Alterations in the lipid composition of cells have been reported during stem cell differentiation and in various pathological conditions including cancer, neurodegeneration and diabetes.^[2,3] In reproductive biology, dietary lipids have been shown to impact ovarian follicle and corpus luteum size^[4] as well as the content of lipids in oocytes of dairy cows.^[5] Thus, monitoring and quantifying phospholipids in small numbers of cells is of special interest for exploring cellular subpopulations since membrane processes are key to cellular differentiation and to preimplantation development and uterine implantation.^[6-8] Moreover, cryopreservation of cells and embryos is an important biotechnology and phospholipids are among the structures that are most sensitive to freezing.^[9-11]

Various methods and techniques have been developed for quantitation of phospholipids by chemical class, including those based on chromatography, MS, and NMR.^[12-14] One of the most widely used methods relies on coupling MS to liquid or gas chromatography, e.g. LC-MS or GC-MS, along with such variants as high-performance LC, tandem MS, and high resolution MS.^[15,16] Although these solutions have proved valuable in quantitative analysis, exploratory lipidomic studies on microscopic samples still require complex separation and use of time-consuming protocols. Besides, many unknown lipids remain undetected even after laborious work in extraction, purification, and separation. Our group has demonstrated lipid profiling of single mammalian oocytes and preimplantation embryos using DESI-MS.^[17-19] However, DESI-MS is not a quantitative method on this scale and quantification of phospholipids remains challenging in such minute samples.

MRM-profiling is a two-stage method based on functional group screening using MRMs without chromatographic separation. It starts with a discovery stage that applies precursor ion (Prec) and neutral loss (NL) MS/MS scans, or predicted MRM

transitions of lipids from a library, to representative samples. Prec and NL scans are both specific to lipid functional groups. MRM transitions that are significant in intensity can be determined using customized data filters. In the second stage, by applying these MRMs to a larger set of individual sample, a panel of differentiating molecular features and potential biomarkers can be derived. Statistical analysis can then be used to build up a classifier for validation or prediction of sample properties. MRM-profiling has been applied to the analysis of lipids, including phospholipids and triacylglycerols from biofluids^[20-25] or cell lysates,^[26,27] where it exhibits excellent sensitivity and allows rapid analysis of samples in small amounts while producing data consistent with results from traditional reference methods. In a previous study of profiling lipids in oocytes and embryos,^[26] MRM-profiling was shown to allow characterization of different phospholipids in these samples. As a follow-up study, here we use internal standards in MRM-profiling to quantify lipids at the 2 to 6 oocyte level. We used this information to investigate the effects of different normalization methods using model bovine oocytes and blastocysts from vitrification with cryoprotective molecules distributed within the organism.

3.3 Materials and Methods

3.3.1 Cultivation of Samples

Collection of Oocytes Bovine ovaries were collected from a slaughterhouse and transported to the laboratory in 0.9% physiological saline supplemented with 0.05 g/L streptomycin at 35 °C. Antral follicles (3 mm to 8 mm) from ovaries were aspirated with 18-gauge needles adapted to 20 mL syringes. Cumulus-oocyte complexes (COCs) were morphologically evaluated under a stereomicroscope and those with at least three compact layers of cumulus cells were selected and washed several times in tissue culture medium/4-(2-hydroxyethyl)-1-piperazineethanesulfonic acid (TCM/HEPES) supplemented with 50 mg/L gentamycin and 0.1% bovine serum albumin (BSA).

***In vitro* Maturation** Pools of 20 COCs were cultured in drops of 100 μ L in Petri dishes covered with 3.5 mL of mineral oil at 38.8 °C for 22 hours in a humidified atmosphere containing 5% CO₂. The maturation medium was HEPES-buffered tissue culture medium-199 (TCM-199, Gibco/BRL, Grand Island, NY, USA) supplemented with 0.2 mM sodium pyruvate, 100 IU/mL penicillin G, 100 μ g/mL streptomycin, 0.5 μ g/mL follicle stimulating hormone (Folltropin-Bioniche, Canada), 5 μ g/mL luteinizing hormone (Lutropin-Bioniche, Canada) and 1 μ g/mL 17 β -estradiol. Fetal bovine serum (FBS, Invitrogen Gibco/BRL) was added to the standard TCM at 10% (*v/v*). After *in vitro* maturation (IVM), oocytes were stripped of cumulus cells by gentle successive pipetting in 100 μ L drops of 0.5% hyaluronidase over a period of 5 min. Completely denuded and morphologically undamaged oocytes were removed from the microdrops and washed from residual cumulus cells three times in a Petri dish containing 200 μ L TCM supplemented with 5% FBS. Immediately, oocytes were checked for first polar body extrusion to verify that maturation occurred (oocytes in metaphase II stage). Procedures were performed at 38.5 °C and immediately after polar body analyses, oocytes were stabilized during 60 min in IVM medium before sample preparation. Mature oocytes (metaphase II stage) were washed in five microdrops (100 μ L each) of MeOH/H₂O solution (1 : 3, *v/v*) and transferred to 1.5 mL tubes (Axygen, DNase and RNase-free grade) in a minimal volume of 1 μ L to 2 μ L.

***In vitro* Fertilization** COCs were washed in *in vitro* fertilization (IVF) medium and inseminated with thawed spermatozoa obtained by the Percoll method using the modified Brackett and Oliphant medium (BO-Sperm medium, Invitro – Assisted Reproductive Technologies Ltd.) supplemented with 6 mg/mL BSA fraction V. Fertilization was performed in microdrops of BO-IVF medium (Invitro Assisted Reproductive Technologies Ltd.) supplemented with 20 μ g/mL heparin and 6 mg/mL fatty acid-free BSA under mineral oil. Twenty COCs in the BO-IVF medium were co-incubated with the sperm suspension at a final concentration of 1×10^6 spermcells/mL for 18 h in a 100 μ L microdrop under mineral oil at 38.5 °C, in a humidified atmo-

sphere containing 5% CO₂. At the end of the fertilization period, presumptive zygotes were partially denuded by pipetting, washed three times in synthetic oviductal fluid (SOF) medium and then cultured in a microdrop of SOF medium with 2.5% FBS and 1 mg/mL BSA (20 to 25 embryos per 50 μ L) under mineral oil at 38.8 °C for 10 days in a water-saturated atmosphere of 5% CO₂. The culture medium was changed every 48 h. Embryonic cleavage rates (ratio of the number of cleaved zygotes to the total number of the oocytes subjected to IVF) and blastocyst rates (ratio of the number of blastocysts to the number of fertilized oocytes cultured) were evaluated at day 3 and day 7-8, respectively.

Embryo Preparation Day 7 blastocysts were first exposed to equilibration solution (ES) consisting of 7.5% ethylene glycol (EG, Sigma), 7.5% DMSO (Sigma), and 20% fetal calf serum in TCM-199 for 8 min at room temperature, and then transferred into a vitrification solution consisting of 15% EG, 15% DMSO, 0.5 M sucrose, and 20% fetal calf serum (FCS) in TCM-199 for 1 min at room temperature. Within 1 min, up to five blastocysts were placed on a sheet of each vitrification device (Ingamed, Maringá, Brazil) in a small volume of the vitrification solution (<1 μ L) and the device was plunged into liquid nitrogen. Two types of nanoparticles, labeled A and B, served as vitrification media supplements. Group A contained phospholipids and antioxidants while group B contained fatty acids. After storage in liquid nitrogen, the blastocysts were warmed by immersing the device into 1 mL of 0.5 M sucrose in the TCM-199 and 20% FCS for 30 s at 37 °C, and then transferred to the TCM-199 and 20% FCS. The blastocysts were washed three times at 5-min intervals with the TCM-199 and 20% FCS at 37 °C and cultured in 100 μ L of the SOF medium for 72 h at 38.5 °C in 5% CO₂ in air. Blastocysts with a re-expanded blastocoel cavity were considered as surviving.

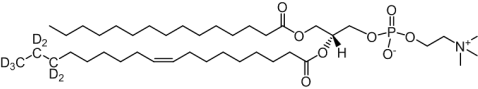
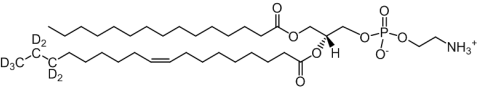
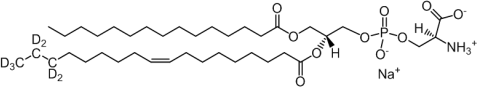
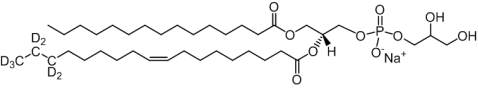
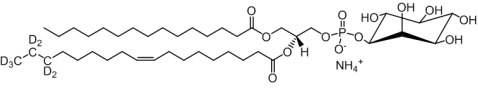
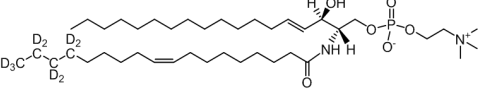
3.3.2 Chemicals

Vendors of chemicals used in cultivation and treatment are elaborated in previous paragraphs. MeOH, ACN, and $\text{NH}_4\text{CH}_3\text{CO}_2$ were purchased from Millipore Sigma (St. Louis, MO). Internal standard, SPLASH[®] LIPIDOMIX[®] Mass Spec Standard, was purchased from Avanti Polar Lipids (Alabaster, AL). The internal standards that were used for quantitation are listed in Table 3.1. Bovine *in vitro*-matured oocytes and *in vitro*-produced blastocysts were provided by Invitra – Assisted Reproductive Technologies Ltd. (Ribeirão Preto, SP, Brazil). The *in vitro*-produced blastocysts were subjected to different vitrification treatments in terms of media supplementation to the equilibration solution. Two types of nanoparticles, labeled A and B, served as vitrification media supplements. Group A contained phospholipids and antioxidants while group B contained fatty acids. Detailed information on sample collection, cultivation, and treatment is included in the following sections. After warming, the surviving cells were collected for lipid extraction.

3.3.3 Lipid Extraction

Lipid extraction of oocyte and embryo samples was carried out by one-step pure methanol protocol. Samples treated with MeOH were washed three times in 50 μL microdroplets of MeOH/ H_2O (1 : 3, *v/v*). Then the oocytes were transferred to 2 μL MeOH/ H_2O and were immediately coated with 10 μL to 20 μL MeOH. After complete evaporation of the solvent for 60 min, the microtubes were vacuum sealed and stored in a freezer at -30°C until samples were transported. After being received, dry lipid extracts were stored under -80°C until mass spectrometry analysis. The lipid extracts were redissolved in ACN/MeOH/300 mM $\text{NH}_4\text{CH}_3\text{CO}_2$ (in H_2O) (3 : 6.65 : 0.35, *v/v/v*) with internal standards.

Table 3.1. Information of lipid internal standards

Compound	Molecular Structure	Transition (m/z)
15:0-18:1(d7) PC (C ₄₁ H ₇₃ D ₇ NO ₈ P)		754.1 → 184.1
15:0-18:1(d7) PE (C ₃₈ H ₆₇ D ₇ NO ₈ P)		711.6 → 570.6
15:0-18:1(d7) PS ^a (C ₃₉ H ₆₆ D ₇ NNaO ₁₀ P)		754.5 → 569.5
15:0-18:1(d7) PG ^a (C ₃₉ H ₆₇ D ₇ NaO ₁₀ P)		758.5 → 569.5
15:0-18:1(d7) PI ^b (C ₄₂ H ₇₅ D ₇ NO ₁₃ P)		846.6 → 569.6
d18:1-18:1(d9) SM (C ₄₁ H ₇₂ D ₉ N ₂ O ₆ P)		738.6 → 184.1

^aThe internal standards of PS and PG are in Na⁺ salt forms.

^bThe internal standard of PI is in NH₄⁺ salt form.

3.3.4 MRM-Profilig

The prepared samples (details in SI, section 2) were investigated by MRM-profilig. The discovery stage was adapted from an earlier study^[26] using bovine oocytes and embryos. In this study, 14,184 MRM transitions were established based on LIPID MAPS Structure Database (<http://www.lipidmaps.org/>) and the expected fragmentation pattern from known Prec and NL scans focusing on lipid functional groups. They were filtered down to 383 significant MRM transitions.^[26] This final MRM list included transitions from phosphatidylcholine (PC), phosphatidylethanolamine (PE), phosphatidylglycerol (PG), phosphatidylserine (PS), and sphingomyelin (SM). In the present study we performed the screening stage analysis using these 383 transitions organized into two methods. For each MRM method, 8 μ L of solution was injected at a flow rate of 20 μ L/min. The data acquisition time for each method was 2 min on a triple quadrupole mass spectrometer (Agilent QQQ 6410, Santa Clara, CA) equipped with an autosampler (Agilent G1367A 1100 series, Santa Clara, CA). Electrospray ionization voltage was 4 kV in positive ion mode. Other parameters are included in SI (Section 3).

3.3.5 Data Analysis

Raw data files were exported as intensity vs. MRM transition lists using custom scripts. A data filter was applied to remove transitions that showed ion intensity less than 30% higher than that of a blank sample. Then, the remaining lipid transitions were grouped together according to the lipid classes. Other instrument parameters are listed in Table 3.2. Each MRM intensity was subject to background correction by subtracting signal intensities from that for pure solvent. For simplicity of expression and reading, the intensity appearing in the following discussion, $I(x)$ where x is a specific MRM, refers to the net (corrected) intensity. Isotope deconvolution was not applied to the intensity profile because the adjacent m/z 's were not monitored. Normalized data sets (as addressed in the paragraph below) were used for statistics.

Ion intensities of these transitions were gathered together for partial least squares discriminant analysis (PLS-DA) that was accomplished by uploading processed data to MetaboAnalyst 4.0 (<http://www.metaboanalyst.ca/>).

3.3.6 Normalization Methods

Two normalization methods were applied to the data for each class of lipids: (1) normalizing to the modified total ion count of the class of lipids to which a specific transition belongs (shown as TIC); (2) normalizing to the ion count of internal standard that is of the same lipid type as the transition (shown as IS). Now take PC(30:0) and its corresponding internal standard PC(15:0/18:1(d7)) as an example to explain how each method was carried out.

Normalization to TIC It should be clarified that the “modified total ion count” refers to the sum of ion counts from all the selected MRMs. The normalization of PC(30:0) can be realized by dividing the ion intensity of the transition for this lipid by the total ion count of the MRM transitions for the whole PC class, so providing the relative fraction of the PC(30:0) signal among its class, denoted by "R" in the subscript in Equation (3.1).

$$PC_R(30 : 0) = \frac{I(PC\ 30 : 0)}{\sum_{x \in PC} I(x)} \quad (3.1)$$

Normalization to IS In the second case, the ion intensity of PC(30:0) was divided directly by that of the corresponding internal standard, indicating the absolute molar ratio between the PC(30:0) and its internal standard, denoted by "A" in the subscript in Equation (3.2).

$$PC_A(30 : 0) = \frac{I(PC\ 30 : 0)}{I(IS)} \quad (3.2)$$

Both normalized data sets were used for statistics to evaluate the performance of internal standards for MRM-profiling. Ion intensities of these transitions were

Table 3.2. Parameters of instrument for MRM-profiling

Parameter Entry	Typical Value		Unit
Electrospray Ionization Voltage	4		kV
Fragmentor Voltage	135		V
Cell Accelerator Voltage	2		V
Dwell Time	25		ms
Sample Injection Volume	8		μ L
Flow Rate	20		μ L/min
Gas Temperature	300		$^{\circ}$ C
Gas Flow	5		L/min
Nebulizer Pressure	17		psi
Stop Time	2		min
MS1 Resolution		Unit Resolution	
MS2 Resolution		Unit Resolution	
	PC	22	
	PE	20	
Collision Energy	PG	22	Manufacturer's Unit
	PS	20	
	SM	22	

gathered for statistical analysis. Comparisons were made between data processed using relative and absolute normalization.

3.4 Results and Discussion

3.4.1 Evaluation of Quantitative Data on Lipids in Oocytes

Quantitative analysis of lipids was accomplished using oocyte lipid extracts. The lipid extract from 64 oocytes was dissolved in 64 μL of solvent containing multiple lipid internal standards. Four different fractions of the solution, containing lipid content from 6, 12, 18 and 24 oocytes, were diluted so that equivalents of 1.6, 3.2, 4.8 and 6.4 oocytes were analyzed per injection, respectively. Due to the minute amount of sample, we combined a small set of MRMs to evaluate different lipid classes in the same sample injection. As noted in Table 3.3, 130 of the 383 significant MRMs were used for quantitation of particular lipid classes, namely 28 from the PC class, 18 from SM, 34 from PE, 19 from PG, and 14 from the PS class. The relative standard deviation (RSD) of absolute intensity from each transition is also shown and supports the excellent reproducibility of the methods. MRMs that showed similar signal intensities to those of blank samples were removed during data processing. The amount of each lipid type was calculated based on the following two assumptions:

1. The net intensity of an MRM, $I(x)$, is proportional to the amount of the precursor ion per injection in moles, $n(x)$,

$$I(x) \propto n(x) \tag{3.3}$$

2. The difference in ionization, ion transfer, and/or fragmentation efficiency between different precursor ions has little influence on the signal intensity. Thus, the ratio of signal intensities of an MRM and its corresponding internal stan-

dard, $\frac{I(x)}{I(\text{IS})}$, is assumed to be equal to the ratio of the amount of the two compounds, $\frac{n(x)}{n(\text{IS})}$,

$$\frac{I(x)}{I(\text{IS})} = \frac{n(x)}{n(\text{IS})} \quad (3.4)$$

Table 3.3. List of MRMs used for analysis and corresponding *RSDs*

Class ^a	Compound ^b	Transition	<i>RSD</i> ^c (%) in Sapmples ^d			
			1.6	3.2	4.8	6.4
PC (28/50)	PC (30:0)	706.5 → 184.1	3.0	2.6	4.1	4.0
	PC (30:1)	704.5 → 184.1	2.3	5.2	3.4	2.6
	PC (30:2)	702.5 → 184.1	5.6	0.5	2.0	6.7
	PC (32:0)	734.6 → 184.1	2.9	1.7	2.4	2.8
	PC (32:2)	730.5 → 184.1	5.9	10.3	4.9	7.3
	PC (32:3)	728.5 → 184.1	14.4	10.3	11.0	14.6
	PC (34:0)	762.6 → 184.1	4.9	5.7	1.8	0.7
	PC (34:1)	760.6 → 184.1	0.7	1.7	0.4	2.1
	PC (34:2)	758.6 → 184.1	1.1	3.1	0.3	1.7
	PC (34:3)	756.6 → 184.1	2.0	3.5	3.7	3.5
	PC (34:4)	754.5 → 184.1	3.7	0.6	0.5	0.4
	PC (34:5)	752.5 → 184.1	2.1	1.8	1.6	0.4
	PC (36:0); PCp(38:6)	790.6 → 184.1	12.6	11.1	8.1	7.6
PC (36:1)	788.6 → 184.1	11.2	4.4	2.3	6.6	

continued on next page

^aThe first and second numbers in parentheses after each lipid class refer to the total numbers of MRM transitions used in analyses of oocytes and embryos, respectively.

^bOnly one or two possible matches of chemical formula is shown in the list. This tentative assignment does not guarantee the actual structures of corresponding ions. The names were acquired from LIPID MAPS Structure Database.

^cTransitions with *RSD* shown in table were used for relative and absolute normalization during comparison, while those with “/” were eliminated during data processing.

^dThe values 1.6, 3.2, 4.8 and 6.4 refer to the equivalent number of oocytes per injection in analysis.

Table 3.3. *continued*

Class	Compound	Transition	<i>RSD</i> (%) in Sapmples			
			1.6	3.2	4.8	6.4
	PC (36:2)	786.6 → 184.1	0.8	3.0	3.5	3.5
	PC (36:3)	784.6 → 184.1	3.9	0.8	2.8	3.4
	PC (36:4)	782.6 → 184.1	5.0	2.3	2.3	1.8
	PC (36:5)	780.6 → 184.1	2.4	10.9	2.4	2.5
	PC (36:8)	774.5 → 184.1	5.8	1.3	1.8	6.2
	PC (38:0)	818.7 → 184.1	17.0	5.8	8.9	13.6
	PC (38:1)	816.6 → 184.1	8.0	8.2	5.8	7.6
	PC (38:2)	814.6 → 184.1	5.4	0.8	3.7	5.3
	PC (38:3)	812.6 → 184.1	5.6	0.8	4.9	7.0
	PC (38:4)	810.6 → 184.1	3.9	2.4	3.4	2.6
	PC (38:5)	808.6 → 184.1	5.4	2.8	4.9	4.1
	PC (38:6)	806.6 → 184.1	11.3	7.9	5.0	5.7
	PC (38:7)	804.6 → 184.1	5.8	9.6	3.6	11.5
	PC (40:5)	836.6 → 184.1	4.0	6.0	8.2	4.0
	PCo(32:1)	718.6 → 184.1	/	/	/	/
	PCo(32:2)	716.6 → 184.1	/	/	/	/
	PCo(32:3)	714.5 → 184.1	/	/	/	/
	PCo(34:0)	748.6 → 184.1	/	/	/	/
	PCo(34:1)	746.6 → 184.1	/	/	/	/
	PCo(34:2)	744.6 → 184.1	/	/	/	/
	PCo(34:3)	742.6 → 184.1	/	/	/	/
	PCo(36:0)	776.6 → 184.1	/	/	/	/
	PCo(36:1)	774.6 → 184.1	/	/	/	/
	PCo(36:2)	772.6 → 184.1	/	/	/	/

continued on next page

Table 3.3. *continued*

Class	Compound	Transition	<i>RSD</i> (%) in Sapmples			
			1.6	3.2	4.8	6.4
	PCo(36:3)	770.6 → 184.1	/	/	/	/
	PCo(36:4)	768.6 → 184.1	/	/	/	/
	PCo(36:5)	766.6 → 184.1	/	/	/	/
	PCo(38:0)	804.7 → 184.1	/	/	/	/
	PCo(38:4)	796.6 → 184.1	/	/	/	/
	PCo(38:5)	794.6 → 184.1	/	/	/	/
	PCo(38:6)	792.6 → 184.1	/	/	/	/
	PCo(40:6)	820.6 → 184.1	/	/	/	/
	PCo(42:6)	848.6 → 184.1	/	/	/	/
	PCp(36:5)	764.6 → 184.1	/	/	/	/
	PCp(40:6)	818.6 → 184.1	/	/	/	/
	PCp(42:6)	846.6 → 184.1	/	/	/	/
SM (18/18)	SM (d16:1/18:1)	701.6 → 184.1	2.6	2.7	2.0	3.9
	SM (d16:1/22:1)	757.6 → 184.1	3.9	2.0	1.9	3.2
	SM (d16:1/24:0)	787.7 → 184.1	3.5	5.2	5.3	3.8
	SM (d16:1/24:1)	785.6 → 184.1	3.2	4.7	5.4	3.9
	SM (d18:0/16:0)	705.6 → 184.1	7.1	8.0	3.8	5.0
	SM (d18:0/18:0)	733.6 → 184.1	6.3	2.3	4.5	2.9
	SM (d18:0/20:0)	761.6 → 184.1	1.3	0.4	0.5	1.7
	SM (d18:0/22:0)	789.7 → 184.1	5.7	2.2	4.4	9.6
	SM (d18:0/24:0)	817.7 → 184.1	7.2	5.8	11.1	6.3
	SM (d18:1/14:0)	675.5 → 184.1	2.2	5.6	5.4	7.5
	SM (d18:1/16:0)	703.6 → 184.1	4.9	1.8	1.5	1.5
	SM (d18:1/18:0)	731.6 → 184.1	3.5	6.0	2.3	2.2

continued on next page

Table 3.3. *continued*

Class	Compound	Transition	<i>RSD</i> (%) in Sapmples			
			1.6	3.2	4.8	6.4
	SM (d18:1/18:1)	729.6 → 184.1	5.6	4.8	12.3	4.7
	SM (d18:1/20:0)	759.6 → 184.1	4.1	4.9	2.6	3.5
	SM (d18:1/24:0)	815.7 → 184.1	4.9	16.2	2.3	2.6
	SM (d18:1/24:1)	813.7 → 184.1	4.9	3.2	2.5	1.5
	SM (d18:2/22:1)	783.6 → 184.1	1.1	1.1	6.2	5.6
	SM (d18:2/24:1)	811.7 → 184.1	4.3	3.0	1.4	5.0
PE (34/36)	PE (18:0)	482.3 → 341.3	5.8	10.5	3.6	9.0
	PE (18:1)	480.3 → 339.3	7.4	9.9	8.9	7.4
	PE (20:1)	508.3 → 367.3	6.1	6.3	8.5	10.1
	PE (20:4)	502.3 → 361.3	6.8	16.4	6.9	8.3
	PE (22:4)	530.3 → 389.3	6.2	5.4	6.1	6.7
	PE (32:1)	690.5 → 549.5	3.3	7.7	3.7	13.6
	PE (34:0)	720.6 → 579.6	3.4	8.4	7.7	17.2
	PE (34:1)	718.5 → 577.5	7.5	0.6	6.9	5.7
	PE (34:2)	716.5 → 575.5	6.4	8.5	9.1	14.8
	PE (36:1)	746.6 → 605.6	4.4	10.4	5.6	5.8
	PE (36:2)	744.6 → 603.6	11.2	4.4	6.0	5.0
	PE (36:3)	742.5 → 601.5	13.1	1.5	3.4	8.8
	PE (36:4)	740.5 → 599.5	10.1	17.5	13.6	5.7
	PE (36:5)	738.5 → 597.5	5.8	5.5	12.6	11.3
	PE (36:8)	732.5 → 591.5	4.3	3.7	7.2	3.0
	PE (38:3)	770.6 → 629.6	3.9	9.0	18.3	9.2
	PE (38:4)	768.6 → 627.6	3.6	2.1	5.1	1.8
	PE (38:5)	766.5 → 625.5	12.0	9.0	3.6	3.6

continued on next page

Table 3.3. *continued*

Class	Compound	Transition	<i>RSD</i> (%) in Sapmples			
			1.6	3.2	4.8	6.4
	PE (38:6)	764.5 → 623.5	0.9	11.7	7.9	0.7
	PE (38:9)	758.5 → 617.5	4.6	7.8	0.3	12.1
	PE (40:2)	772.6 → 631.6	9.8	9.1	8.7	3.1
	PE (40:4)	796.6 → 655.6	0.3	1.0	3.7	6.6
	PE (40:5)	794.6 → 653.6	7.5	19.8	14.0	9.3
	PE (40:6)	792.6 → 651.6	9.6	4.3	4.0	6.3
	PE (40:7)	790.5 → 649.5	3.8	7.8	13.3	4.6
	PEo (34:1)	704.6 → 563.6	11.1	3.4	15.9	8.7
	PEo (34:2)	702.5 → 561.5	9.6	3.3	13.7	7.0
	PEo (36:2)	730.6 → 589.6	1.6	1.2	6.9	16.6
	PEo (36:3)	728.6 → 587.6	2.9	6.9	17.6	3.5
	PEo (36:5)	724.5 → 583.5	6.1	13.5	5.4	9.2
	PEo (38:4)	754.6 → 613.6	2.4	5.8	8.6	11.9
	PEo (38:5)	752.6 → 611.6	3.6	8.3	7.4	6.1
	PEo (38:6)	750.5 → 609.5	2.0	9.2	8.6	1.5
	PEo (40:5)	780.6 → 639.6	6.9	4.5	4.7	3.0
	PEp (36:6)	748.5 → 607.5	/	/	/	/
	PEp (40:7)	774.5 → 633.5	/	/	/	/
PG (19/22)	PG (16:0)	516.3 → 327.3	8.2	14.5	9.2	9.0
	PG (18:0)	530.3 → 341.3	5.5	2.1	5.4	3.5
	PG (20:0)	572.3 → 383.3	4.5	2.1	5.8	12.4
	PG (22:0)	586.4 → 397.4	2.8	4.7	0.9	3.3
	PG (22:6)	574.3 → 385.3	4.0	3.8	3.6	3.3
	PG (24:0)	628.4 → 439.4	4.5	3.3	4.0	3.4

continued on next page

Table 3.3. *continued*

Class	Compound	Transition	<i>RSD</i> (%) in Sapmples			
			1.6	3.2	4.8	6.4
	PG (26:0)	656.4 → 467.4	3.4	2.0	3.2	4.3
	PG (32:0)	740.5 → 551.5	6.7	4.9	10.0	7.3
	PG (34:0)	768.5 → 579.5	3.8	12.5	5.4	11.5
	PG (34:1)	766.5 → 577.5	8.7	6.5	13.1	4.9
	PG (34:2)	764.5 → 575.5	0.8	6.5	2.7	7.4
	PG (36:1)	794.6 → 605.6	2.2	8.6	3.2	16.0
	PG (36:2)	792.5 → 603.5	3.5	6.3	10.2	4.4
	PG (36:3)	790.5 → 601.5	6.2	2.5	5.0	5.0
	PG (36:4)	788.5 → 599.5	4.8	3.1	2.1	3.2
	PG (36:8)	780.5 → 591.5	3.1	5.8	1.7	3.7
	PG (38:3)	818.6 → 629.6	1.6	3.5	2.2	2.2
	PG (38:4)	816.5 → 627.5	1.7	4.4	6.7	1.1
	PG (40:0)	852.6 → 663.6	0.2	1.7	0.1	1.3
	PGo (20:0)	544.4 → 355.4	/	/	/	/
	PGp (20:0)	542.4 → 353.4	/	/	/	/
	PGp (38:6)	796.5 → 607.5	/	/	/	/
PS (14/19)	PS (14:1)	468.2 → 283.2	7.8	8.7	5.6	14.0
	PS (16:0)	512.3 → 327.3	16.9	6.3	16.6	4.5
	PS (28:0)	680.4 → 495.4	4.4	4.5	5.1	25.2
	PS (28:1)	678.4 → 493.4	3.1	0.8	1.3	5.5
	PS (30:2)	704.4 → 519.4	0.2	0.7	0.1	4.3
	PS (32:2)	732.5 → 547.5	5.8	7.5	7.7	5.6
	PS (36:1)	790.6 → 605.6	10.9	9.5	14.3	8.7
	PS (36:2)	788.5 → 603.5	10.2	5.5	12.3	29.2

continued on next page

Table 3.3. *continued*

Class	Compound	Transition	<i>RSD</i> (%) in Sapmples			
			1.6	3.2	4.8	6.4
	PS (36:8)	776.4 → 591.4	4.8	10.1	4.2	10.2
	PS (38:1)	818.6 → 633.6	1.8	5.3	20.3	7.2
	PS (38:2)	816.6 → 631.6	4.2	13.2	13.0	7.2
	PS (38:4)	812.5 → 627.5	5.2	9.1	14.8	6.5
	PS (38:7)	806.5 → 621.5	1.4	2.7	1.7	0.7
	PS (40:4)	840.6 → 655.6	3.2	13.4	4.7	4.1
	PSo (16:0)	484.3 → 299.3	/	/	/	/
	PSo (20:0)	540.4 → 355.4	/	/	/	/
	PSp (16:0)	482.3 → 297.3	/	/	/	/
	PSp (40:6)	820.5 → 635.5	/	/	/	/
	PSp (42:6)	848.6 → 663.6	/	/	/	/

Figure 3.1 shows the linearity between the amount of lipid in each class quantified by this internal standard method and the known number of oocyte equivalents contained in each injected volume. Each point and the corresponding error bar on the curve were calculated based on three replicates. The coefficients of determination (R^2) for PC, PE, PG, PS, and SM are 0.9971, 0.9969, 0.9899, 0.9816 and 0.9996, respectively. The average amount of each lipid class per oocyte, corresponding standard deviation (SD) and relative standard deviation (RSD) were calculated from the curve and are shown in Table 3.4. The RSDs of PC, SM, PG, and PE were around 10%, while PS was significantly higher at 17.3%. Therefore, the use of internal standards to quantify different classes of lipids in MRM-profiling is feasible and the performance of the method is promising even at the not-yet-realized single oocyte level. It is noteworthy that the quantified values are calculated from representative lipids rather than the

entire class of lipids in the samples. The quantitation is based on the monoisotopic molecular composition of a molecule. The samples therefore are expected to contain many more lipids than these calculations.

Table 3.4. Quantified amount of lipid of each class per oocyte

Lipid Class	PC	PE	PG	PS	SM
Average (ng)	4.5	0.67	0.82	2.0	0.74
Standard Deviation (ng)	0.36	0.072	0.091	0.35	0.036
Relative Standard Deviation (%)	8.0	10.8	11.2	17.3	4.9

3.4.2 Comparison of Relative and Absolute Normalization of Lipids in Bovine Oocytes and Blastocysts

MRM-profiling data obtained on oocyte samples was used to quantify lipid classes in these organisms by using internal standards. Scores plots were acquired from oocytes by applying PLS-DA to data normalized using the two different methods as shown in Figure 3.2. Oocytes and blastocysts were cultured with two types of nanoparticles added as supplements to the vitrification media to improve cell viability during cryopreservation, group A containing phospholipids and antioxidants and group B containing fatty acids (red and blue in Figure 3.2, respectively). Sample size was $N = 11$ for each group in oocyte and $N = 12$ for those in blastocyst. The two groups of oocyte samples in Figure 3.2(a) and (b) are mainly distinguished by the first component. (The first two components explain 22% and 35.5% of the variance between two different classes of oocytes when the data from oocyte samples are normalized to modified total ion count and to lipid internal standards, respectively.) The discrimination between the two areas at the 95% confidence level in both cases indicates that the normalization strategy does not have a large effect on the discriminant analysis.

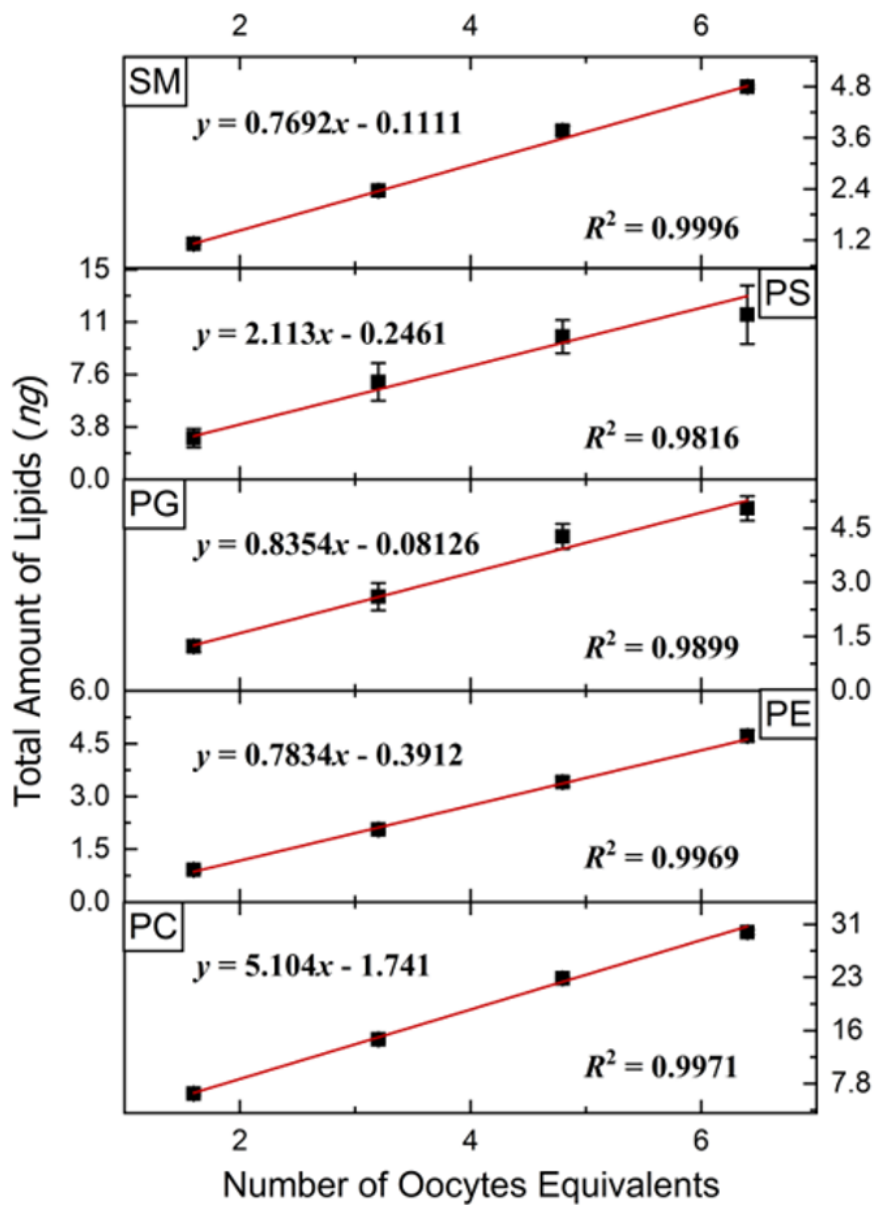


Figure 3.1. Relationship between the number of oocytes introduced and the total amount of SM, PS, PG, PE, and PC (from top to bottom) lipids quantified using internal standards. Four concentrations of oocytes extract equivalent to 1.6, 3.2, 4.8 and 6.4 per injection were used. Each point in plot is an average of three measurements.

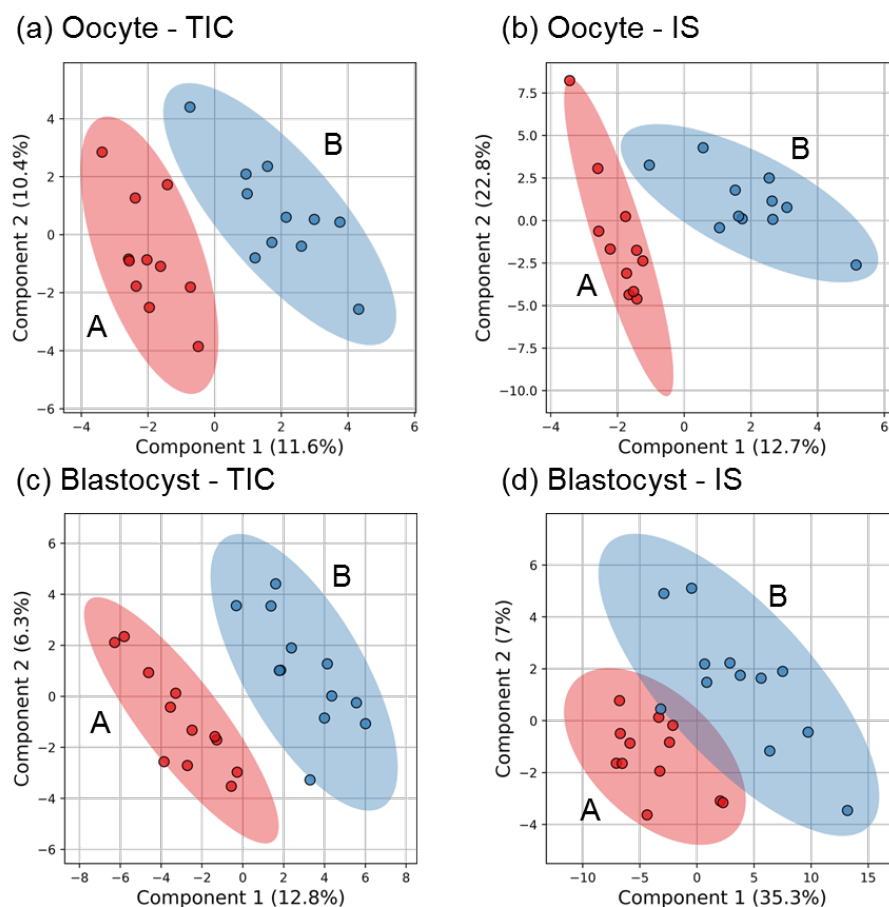


Figure 3.2. PLS-DA results for oocyte and blastocyst discrimination using different normalization methods: normalized to modified total ion count (TIC) and normalized to corresponding internal standard (IS). (a) Oocyte normalized to TIC. (b) Oocyte normalized to IS. (c) Blastocyst normalized to TIC. (d) Blastocyst normalized to IS. The two colors represent differences in the nanoparticles applied during culturing, red and blue for group A and group B, respectively. Sample size of each group in (a) and (b) is $N = 11$, and $N = 12$ in (c) and (d). The shaded ellipses represent the calculated 95% confidence range.

The data from blastocysts were acquired and then processed using the same normalization methods as that of the oocyte data in Figure 2 (c) and (d). In both cases, the two groups of blastocysts are separated by PLS-DA. Overall, the first two principal components explain 19.1% and 42.3% for normalizing to modified total ion count and internal standards, respectively. The fraction of variance that the first component explains when normalizing to internal standards (35.3%) is higher than that from normalization to modified total ion count (12.8%). However, when normalizing to internal standards, overlap occurs between the two elliptical areas at the 95% confidence and one sample from group B tended to be clustering with group A. In Figures 3.3 and 3.4, boxplots of several representative MRM transitions, which were normalized by IS and TIC, show the differences in intensity between groups. Both normalization methods exhibit similar results for each transition.

3.5 Conclusions

In conclusion, the lipid contents of oocytes and blastocysts can be quantitatively measured using MRM-profiling due to the linear response observed with the use of one internal standard per class. We have demonstrated that the lipid analysis using samples as small as the equivalent of 2 bovine oocytes can be achieved. Whether normalization is done with respect to internal standards or modified total ion count has relatively little effect on the statistical results when distinguishing different groups of blastocyst samples. This indicates the feasibility of applying MRM-profiling as a quantitative method for lipid analysis if internal standards and corresponding concentrations are carefully selected.

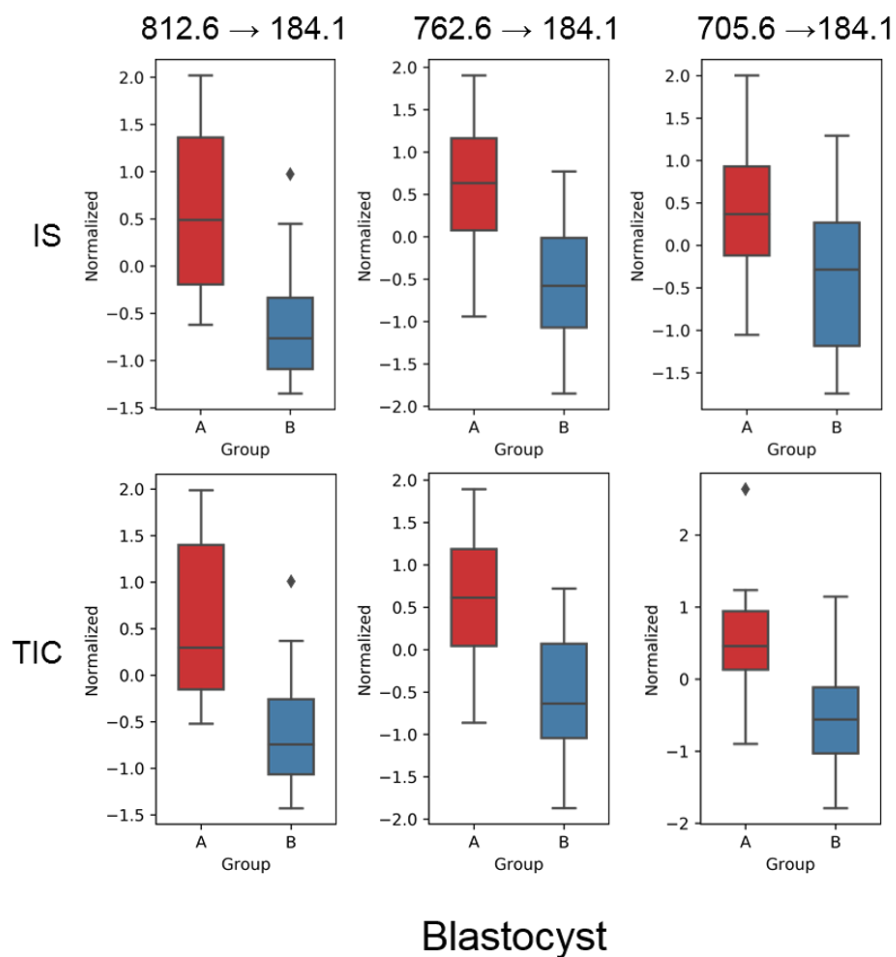


Figure 3.3. Boxplots showing comparisons between two normalization methods of three MRM transitions in blastocyst samples. Top row is result of normalization to corresponding internal standard (IS) and bottom row is result of normalization to modified total ion current (TIC)..

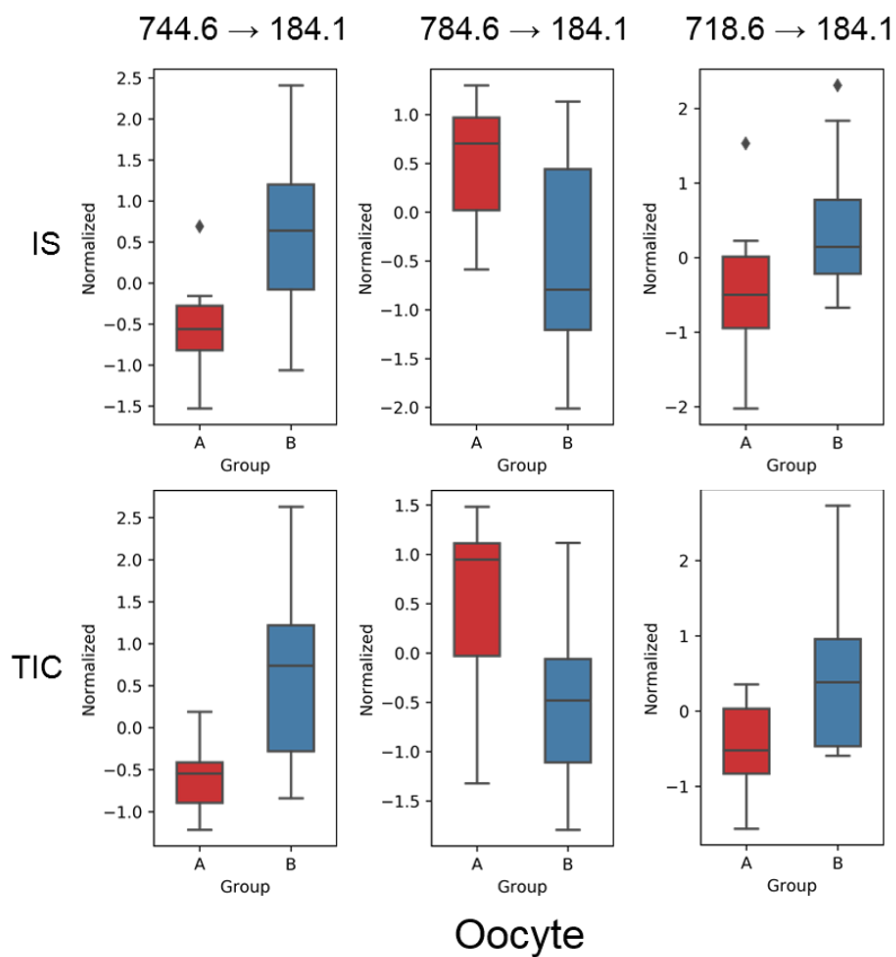


Figure 3.4. Boxplots showing comparisons between two normalization methods of three MRM transitions in oocyte samples. Top row is result of normalization to corresponding internal standard (IS) and bottom row is result of normalization to modified total ion current (TIC).

3.6 References

- [1] H. Ohvo-Rekila, B. Ramstedt, P. Leppimaki, J. P. Slotte, *Progress in Lipid Research* **2002**, *41*, 66–97.
- [2] P. Strzyz, *Nature Reviews Molecular Cell Biology* **2018**, *19*, 141–141.
- [3] A. Mitchell, L. Ashton, X. B. Yang, R. Goodacre, A. Smith, J. Kirkham, *Cytometry Part A* **2015**, *87*, 1012–1019.
- [4] T. Bilby, J. Block, B. do Amaral, O. Sa Filho, F. Silvestre, P. Hansen, C. Staples, W. Thatcher, *Journal of Dairy Science* **2006**, *89*, 3891–3903.
- [5] A. F. González-Serrano, C. R. Ferreira, V. Pirro, A. Lucas-Hahn, J. Heinzmann, K.-G. Haderl, U. Baulain, P. Aldag, U. Meyer, M. Piechotta, G. Jahreis, S. Dänicke, R. G. Cooks, H. Niemann, *Reproduction Fertility and Development* **2016**, *28*, 1326.
- [6] H. Li, P. Balan, A. Vertes, *Angewandte Chemie - International Edition* **2016**, *55*, 15035–15039.
- [7] H. Muhamadali, D. Weaver, A. Subaihi, N. Almasoud, D. K. Trivedi, D. I. Ellis, D. Linton, R. Goodacre, *Analyst* **2016**, *141*, 111–122.
- [8] L. Zhang, A. Vertes, *Angewandte Chemie International Edition* **2018**, *57*, 4466–4477.
- [9] A. Arav, R. Zvi, *Molecular and Cellular Endocrinology* **2008**, *282*, 150–152.
- [10] C. Lin, L. H. Wang, P. J. Meng, C. S. Chen, S. Tsai, *PLoS ONE* **2013**, *8*, (Ed.: K. X. Chai), e57823.
- [11] C. Lin, S. Tsai, *Theriogenology* **2012**, *77*, 1257–1261.
- [12] S. Khoury, C. Canlet, M. Z. Lacroix, O. Berdeaux, J. Jouhet, J. Bertrand-Michel, *Biomolecules* **2018**, *8*, 1–16.
- [13] X. Han, R. W. Gross, *Mass Spectrometry Reviews* **2005**, *24*, 367–412.
- [14] B. Brugger, G. Erben, R. Sandhoff, F. T. Wieland, W. D. Lehmann, *Proceedings of the National Academy of Sciences* **1997**, *94*, 2339–2344.
- [15] T. Cajka, O. Fiehn, *TrAC Trends in Analytical Chemistry* **2014**, *61*, 192–206.
- [16] T. Wang, D. Zhou, *Current Opinion in Food Science* **2017**, *16*, 15–20.
- [17] C. R. Ferreira, A. K. Jarmusch, V. Pirro, C. M. Alfaro, A. F. González-Serrano, H. Niemann, M. B. Wheeler, R. A. C. Rabel, J. E. Hallett, R. Houser, A. Kaufman, R. G. Cooks, *Reproduction Fertility and Development* **2015**, *27*, 621–637.
- [18] V. Pirro, A. K. Jarmusch, C. R. Ferreira, R. G. Cooks in *Lipidomics*, (Ed.: P. Wood), Neuromethods March, Springer New York, New York, NY, **2017**, Chapter 14, pp. 187–210.

- [19] D. Laskowski, G. Andersson, P. Humblot, M. A. Sirard, Y. Sjunnesson, C. R. Ferreira, V. Pirro, R. Båge, *Reproduction Fertility and Development* **2018**, *30*, 1253–1266.
- [20] C. R. Ferreira, K. E. Yannell, B. Mollenhauer, R. D. Espy, F. B. Cordeiro, Z. Ouyang, R. G. Cooks, *Analyst* **2016**, *141*, 5252–5255.
- [21] F. B. Cordeiro, C. R. Ferreira, T. J. P. Sobreira, K. E. Yannell, A. K. Jarmusch, A. P. Cedenho, E. G. Lo Turco, R. G. Cooks, *Rapid Communications in Mass Spectrometry* **2017**, *31*, 1462–1470.
- [22] J. Dhillon, C. R. Ferreira, T. J. P. Sobreira, R. D. Mattes, *Current Developments in Nutrition* **2017**, *1*, e001545.
- [23] T. Casey, K. Harlow, C. R. Ferreira, T. J. P. Sobreira, A. Schinckel, K. Stewart, *Journal of Applied Animal Research* **2018**, *46*, 667–676.
- [24] K. E. Yannell, C. R. Ferreira, S. E. Tichy, R. G. Cooks, *Analyst* **2018**, *143*, 5014–5022.
- [25] J. Franco, C. Ferreira, T. J. Paschoal Sobreira, J. P. Sundberg, H. HogenEsch, *PLOS ONE* **2018**, *13*, (Ed.: S. N. Witt), e0196595.
- [26] C. B. de Lima, C. R. Ferreira, M. P. Milazzotto, T. J. P. Sobreira, A. A. Vireque, R. G. Cooks, *Journal of Mass Spectrometry* **2018**, *53*, 1247–1252.
- [27] Z. Xie, L. E. Gonzalez, C. R. Ferreira, A. Vorsilak, D. Frabutt, T. J. T. Sobreira, M. Pugia, R. G. Cooks, *Analytical Chemistry* **2019**, *91*, 11349–11354.

CHAPTER 4. MRM-PROFILING OF LIPIDS TO DISTINGUISH STRAIN-LEVEL DIFFERENCES IN MICROBIAL RESISTANCE IN *ESCHERICHIA COLI*

4.1 Abstract

The worldwide increase in antimicrobial resistance is due to antibiotic over-use in agriculture and over-prescription in medicine. For appropriate and timely patient support, faster diagnosis of antimicrobial resistance is required. Current methods for bacterial identification rely on genomics and proteomics and use comparisons with databases of known strains, but the diagnostic value of metabolites and lipids has not been explored significantly. Standard mass spectrometry/chromatography methods involve multiple dilutions during sample preparation and separation. To increase the amount of chemical information acquired and the speed of analysis of lipids, MRM-profiling has been applied. The MRM-profiling workflow includes a discovery stage and a screening stage. The discovery stage employs precursor ion (PREC) and neutral loss (NL) scans to screen representative pooled samples for functional groups associated with particular lipid classes. The information from the first stage is organized in precursor/product ion pairs, or MRMs, and the screening stage rapidly interrogates individual samples for these MRMs. In this study, we performed MRM-profiling of lipid extracts from four different strains of *Escherichia coli* cultured with amoxicillin or amoxicillin/clavulanate, a β -lactam and β -lactamase inhibitor, respectively. Statistical analyses, including t tests, analysis of variance (ANOVA) and receiver operating characteristic (ROC) curves, were used to determine the significance of each MRM. Principal component analysis (PCA) was applied to distinguish different

strains cultured under conditions that allowed or disallowed development of bacterial resistance. The results demonstrate that MRM-profiling distinguishes the lipid profiles of resistant and non-resistant *E. coli* strains.

4.2 Introduction

4.2.1 Antimicrobial Resistance

Annually there are over 1,200,000,000 health care visits in the United States of which 12.6% result in ~154,000,000 antibiotic prescriptions for bacterial infections.^[1] Urinary, respiratory and skin infections are most common.^[2] The top pathogens responsible for 80% to 90% of infections are *Escherichia coli*, *Staphylococcus aureus*, and *Klebsiella pneumoniae*, the latter two of which are part of the ESKAPE group of pathogens which also include *Enterococcus faecium*, *Acinetobacter baumannii*, *Pseudomonas aeruginosa*, and *Enterobacter* species.^[3-5] Infections are especially common in certain care settings and patient populations where they cause high recurrence rates and great severity of infections.^[6-8] Potential infections are frequently treated prior to confirmation of the presence of pathogens, leading to over-prescription which is strongly associated with the development of antibiotic-resistance and may eradicate potentially commensal microbiome populations, resulting in dysfunction against future pathogens.^[9-12] High rates of infection recurrence and the emergence of pathogens with antimicrobial resistance are found among patients with frequent antibiotic dosing.^[11,13,14] There therefore remains a need for rapid bacterial identification to help suppress this process.

4.2.2 Clinical Identification and Diagnosis

In current clinical settings, the identification of bacteria is usually determined based on phenotype and/or genotype. Culture-based phenotyping methods are commonly used in clinical laboratories.^[15] Molecular diagnosis, including sequencing of riboso-

mal genes,^[16] whole genome sequencing,^[17,18] and amplification methods,^[19] represents an alternative strategy for bacterial typing. Current MS-based typing methods are largely focused on the protein profile with an emphasis on ribosomal proteins.¹⁶ In the last decade, matrix assisted laser desorption/ionization coupled with time-of-flight mass spectrometry (MALDI-TOF MS) has been applied successfully using relatively simple sample preparations to acquire fingerprint mass spectra and accomplish identification by database searches.^[20-22] Several commercial platforms have emerged and profoundly changed the state of clinical testing. In addition, tandem MS with or without liquid chromatography has also been used with great success.^[23-25]

4.2.3 Lipid Analysis

Metabolomics, which covers a wide range of small molecules but is not widely applied to bacterial identification, is an appealing and emerging field of omics in biomarker discovery by MS.^[26-29] Lipids are believed to play an indispensable metabolic role in many essential biological processes. In microorganisms, the diversity in structures and the complexity of biosynthesis pathways of bacterial lipids enable bacterial cells to adjust their lipid profiles in response to environmental changes, including antibiotic treatment.^[30-32] Conventional lipid pathway analysis involves extensive sample preparation and complex protocols for the characterization of potential lipid biomarkers.^[33,34] The unclear relationship between lipids and molecular function further slows down the pace of development of analytical methods. To accelerate exploratory lipidomic discovery, a novel two-stage methodology, MRM-profiling, has been developed as a diagnostic/distinguishing factor. It has previously been tested on several model systems, including Parkinson's disease,^[35] polycystic ovarian syndrome,^[36] diet compliance,^[37] colostrum uptake,^[38] atopic dermatitis,^[39] and embryo metabolism.^[40] The results of MRM-profiling have proven to be broadly consistent with those from pathological or clinical analysis.

Here we report a study on the feasibility of using MRM-profiling to differentiate lipid profile differences among bacterial strains with different antimicrobial resistance. Lipid extracts of bacteria were analyzed using electrospray ionization MS (ESI-MS), screened by precursor ion and neutral loss scans and discriminated using PCA. The experiments focused on glycerophospholipids and sphingolipids. Statistical analytical methods, specifically the t test and ROC curves, provided details as to which of the MRMs were most informative. Additionally, lipid differences observed among bacteria treated using various concentrations of amoxicillin and amoxicillin/clavulanate indicated that lipid profiles are modulated by environmental changes. The lipid composition of bacterial lysates was found to allow discrimination between resistant and non-resistant *E. coli* strains.

4.3 Experimental Section

4.3.1 Chemicals

All chemicals were all purchased from Sigma-Aldrich Co. LLC (St. Louis, MO) except that clavulanate was purchased from Crescent Chemical (Bangladesh).

4.3.2 Bacterial Culture

Non-resistant *E. coli* strains (ATCC[®] 25922[™], CDC AR-bank #0077, and ATCC[®] 4157[™]) and resistant strains with β -lactam resistance gene CTX-M-14 or 15 (CDC AR-bank #0086, CDC AR-bank #0162, CDC AR-bank #0151) were obtained from the ATCC or the CDC and FDA antibiotic resistance isolate bank. Bacterial stocks, stored at -80°C until usage, were generated from tryptic soy broth (TSB) (Becton Dickinson, Franklin Lakes, NJ) cultures inoculated with a single colony taken from streak plate isolates from the supplier's stock on tryptic soy agar (TSA) (Becton Dickinson, Franklin Lakes, NJ). Fresh bacteria were cultured from stock by gentle scraping with a sterile implement off the top of the stock and by streaking onto a

fresh TSA plate for single colony growth, which was incubated for 15 hours at 37 °C. A single colony was then re-streaked onto a fresh TSA plate and was incubated for 15 hours at 37 °C. Bacterial titer was estimated by resuspending morphologically similar colonies into 20 mL of fresh TSB and by measuring optical density at 600 nm (OD_{600}) absorbance readings using a BioTek Synergy HTX multi-mode plate reader (BioTek, Winooski, VT) with McFarland standards (Scientific Device Laboratory, Inc., Des Plaines, IL). Verification of culture concentrations was performed with a ten-fold serial dilution in TSB; a 1.0 μ L loopful from each dilution was streaked onto BD BBL™ Trypticase™ Soy Agar plates (Becton, Dickinson and Co., Franklin Lakes, NJ), and colonies were counted after incubation at 37 °C for 16 hours.

4.3.3 Minimum Inhibitory Concentration Test

A standard 96-well plate-based minimum inhibitory concentration (MIC) test was used to measure antibiotic efficiency of amoxicillin and amoxicillin/clavulanate combination against bacteria in mono-culture. After overnight growth on the corresponding culture medium and OD_{600} measurement, MIC testing was performed with cation-adjusted Mueller-Hinton broth. In a row of the plate, 11 wells contained a starting culture at 5×10^5 cfu/mL challenged with decreasing antibiotic concentrations delivered by serial dilution (e.g. 128, 64, 32, 16, 8, 4, 2, 1, 0.5, 0.25, 0 μ g/mL); the last well contained blank medium as a sterility control. The lowest antibiotic concentration at which no cell number increase was measured via OD_{600} after a 24-hour incubation was the MIC of the antibiotic for that bacterial strain. All MIC tests were conducted in compliance with Clinical Laboratory Standards Institute (CLSI) procedures of clinical testing. The determined values of MIC for each strain appear in Table 4.1.

Table 4.1. MIC results of each strain

Strain	MIC of Amoxicillin ($\mu\text{g}/\text{mL}$)	MIC of Amoxicillin/Clavulanate Combination	
		Amoxicillin ($\mu\text{g}/\text{mL}$)	Clavulanate ($\mu\text{g}/\text{mL}$)
ATCC 25922	8	16	8
ATCC 4157	4	4	2
CDC 0162	N/A ^a	>128 ^b	>64 ^b
CDC 0151	N/A ^a	>128 ^b	>64 ^b

^aMIC not applicable for resistant strains.

^bBecause the concentration of antibiotics needed for inhibition was too high for feasibility, the half MIC condition of Amoxicillin/Clavulanate combination was chosen as 128 $\mu\text{g}/\text{mL}$ for Amoxicillin and 64 $\mu\text{g}/\text{mL}$ for Clavulanate.

4.3.4 Sample Preparation

Samples of specific types of bacteria and MIC concentrations were taken from culture medium, normalized to 1×10^7 cells/mL by OD_{600} , and were lysed with sonication. Lysate of bacteria was collected and stored at -80°C . Lipid extraction was accomplished using the Bligh-Dyer^[41] strategy. After drying, lipid extracts were re-dissolved in ACN/MeOH/300 mM $\text{NH}_4\text{CH}_3\text{CO}_2$ (in H_2O) (3 : 6.65 : 0.35, $v/v/v$) and transferred into autosampler vials ready for analysis. The extract solution was diluted to 2.5×10^5 cells/ μL in vial, which is equivalent to lipid extracts of 2×10^6 cells in each injection of 8 μL solution.

4.3.5 Multiple Reaction Monitoring Profiling

MRM-profiling is a two-stage MS methodology that benefits from various scan modes in tandem mass spectrometry—especially PREC and NL. In the discovery stage, PREC, NL, and MRM methods are applied to representative samples, mostly focusing on recognition of functional groups present in glycerophospholipids, acyl-carnitines, ceramides, and acyl residues containing different number of carbons with various degree of unsaturation. Specifically, glycerophospholipids contain glycerophosphate (PA), glycerophosphocholine (PC), glycerophosphoethanolamine (PE), glycerophos-

phoglycerol (PG), glycerophosphoinositol (PI), and glycerophosphoserine (PS). The PREC and NL scans were used as sources of MRM transitions and this experimental data was supplemented by MRM transitions deduced from data in the online lipid database, LipidMaps. Altogether 32 NL scan methods, 33 PREC scan methods, and 13 MRM methods, as listed in Table 2.1 and Table 2.3, were used to survey representative samples from *E. coli* strains CDC 0077 and CDC 0086 cultured without amoxicillin. Experiments were carried out using a triple quadrupole mass spectrometer, Agilent QQQ 6410 (Santa Clara, CA), equipped with Agilent G1367A 1100 series autosampler (Santa Clara, CA). Samples were introduced into the mass spectrometer by direct flow injection ESI, i.e. without chromatographic separation. The ESI voltage was -3.5 kV. Dwell time was 25 ms. Collision energy (in manufacturer's unit) and other scan method details are in Table 2.1 and Table 2.3. For each scan method, 8 μ L of sample was injected at a flow rate of 20 μ L/min. After data acquisition, transitions that were at least 30% higher in ion counts than blank samples were selected. Other values of threshold or data filtering concepts could have been employed but the tradeoff between chemical information and total instrument time required had an effect on the next stage, therefore we chose to be conservative to avoid losing chemical information. In addition, since representative samples were used, which could not reflect the scope of lipid profiles of all strains, keeping more transitions is beneficial to retaining as much chemical information as possible. In total, 2329 transitions, of which 1900 were in the positive ion mode and 429 in the negative ion mode, resulted from the discovery stage. The distribution of MRMs among different classes of lipids or functional groups are shown in Figure 4.1 and Figure 4.2 for positive and negative ion modes, respectively. This list served as a pool of candidates for building up MRM methods for the next Screening stage. Selected transitions were then arranged into 9 MRM methods (7 in positive ion mode, 2 in negative ion mode) to investigate individual samples using the same instrument parameters as used in the Discovery stage. Given that the screening time for each method is 3 min, this results in a total analysis time of 30 min to screen each sample.

4.3.6 Statistical Analysis

Raw data were processed using Proteo-Wizard to extract the ion signals of each transition. The lowest ion count was regarded as the noise level of instrument. The cutoff for the screening stage data was chosen as $3 \times$ noise intensity to remove uninformative transitions with low ion intensities. The resulting data was represented as a table of ion counts, in which columns were samples and rows were features (MRMs in this case). All statistical analysis, including t test, analysis of variance (ANOVA), PCA, and ROC curves, were calculated and plotted using MetaboAnalyst. For PCA, ANOVA, and t test, the original data were scaled by mean-centering and dividing the

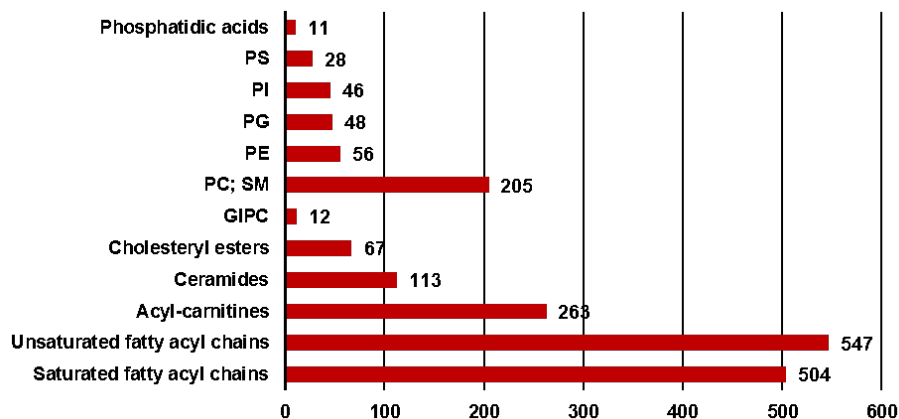


Figure 4.1. Distribution of MRMs selected for screening stage in positive mode. Altogether 1,900 transitions were reorganized into 9 MRM methods.

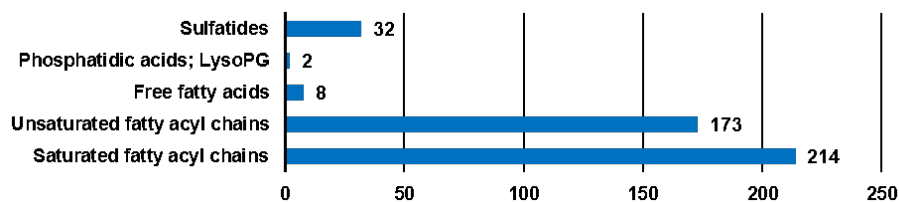


Figure 4.2. Distribution of MRMs selected for screening stage in negative mode. Altogether 429 transitions were reorganized into 2 MRM methods.

individual intensities by the standard deviation of each MRM. For the ROC curve, no scaling was applied and the area under the curve (AUC) was calculated for each MRM. The cutoff applied to the t test and ANOVA was a false discovery rate (FDR) adjusted p value (or q value) of 0.05 throughout the data processing.

4.4 Results and Discussion

4.4.1 Lipid Analysis of Non-Resistant Strains

Lipid analysis was carried out for non-resistant strains (ATCC 25922 and ATCC 4157) to investigate the effect of antibiotic application. Both strains were cultured under five conditions: no amoxicillin or amoxicillin/clavulanate, amoxicillin at half MIC, amoxicillin at MIC, amoxicillin/clavulanate at half MIC, and amoxicillin/clavulanate at MIC. MRMs were filtered by ion counts and FDR adjusted p value in ANOVA, and then analyzed by PCA. Figure 4.3 shows the PCA scores plots of both strains. In the PCA scores plot, each point represents an individual lipid extract sample from the cultured bacteria and the elliptical shaded area is the calculated 95% confidence region for each group. In the case of ATCC 25922 as shown in Figure 4.3(a) where 197 MRMs were used, bacteria treated with amoxicillin or amoxicillin/clavulanate at MIC are well separated along principal component (PC) 1 from bacteria cultured at half MIC or without amoxicillin. PC1 and PC2 contribute 76% to the total variance. This separation can be attributed to the nature and the amount of the antibiotic, which leads to bacterial growth inhibition and hence the observed changes in lipid profiles.

Similar separation due to treatment differences are observed in the non-resistant strain ATCC 4157 in Figure 4.3(b). With the same data filters, 157 MRMs were selected. PC1 and PC2 cover 74% of the entire variance observed. Different from ATCC 25922, the group grown with amoxicillin at MIC clusters away from the other groups on the PC1 dimension in the score plot. Groups treated with amoxicillin/clavulanate

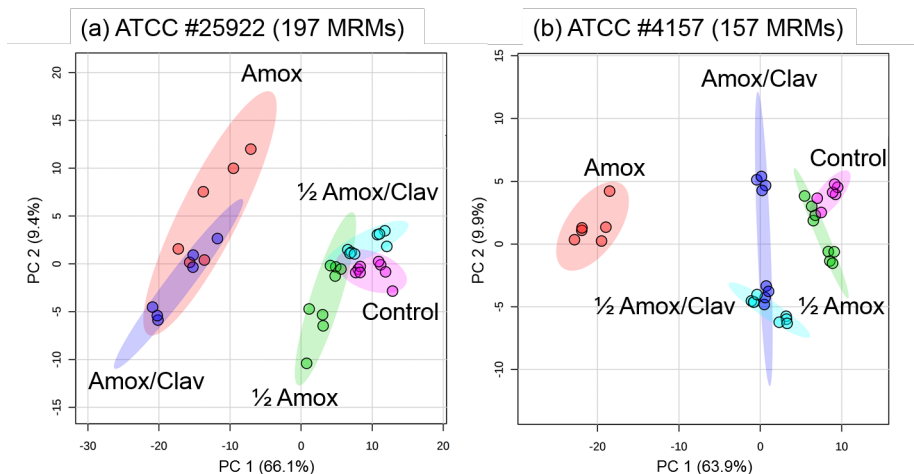


Figure 4.3. PCA scores plots of non-resistant bacterial strains (a) ATCC 25922 and (b) ATCC 4157 after various antibiotic treatments. The color-shaded areas are the calculated range with 95% confidence. Amoxicillin and clavulanate are abbreviated as Amox and Clav, respectively.

tend to overlap on PC1, while control and half MIC amoxicillin are closer. The MIC amoxicillin/clavulanate group is differentiated by PC1 to be closer to groups treated with low concentration of amoxicillin, instead of merging with the MIC amoxicillin group as in ATCC 25922.

4.4.2 Lipid Profile Differences Between Non-Resistant and Resistant Bacterial Strains

The results of attempts to distinguish non-resistant and resistant strains are promising. The purpose of carrying out statistical analysis of different strains exposed to the same treatment is to identify transitions that are responsible for the separation between strains. Two non-resistant strains (ATCC 25922 and ATCC 4157) and two resistant strains (CDC 0162 and CDC 0151) were cultured without amoxicillin or amoxicillin/clavulanate as controls or with amoxicillin/clavulanate at half MIC. Transitions related to acyl-carnitines were found to be inconsistent (data not shown) and

were removed from the statistics to better concentrate on the pattern of significant phospholipid transitions. Initially, for the control group, 86 MRMs were used for the statistical analysis, from which 38 MRMs were then selected using the FDR adjusted p value in ANOVA. From the PCA scores plot of these transitions shown in Figure 4.4(a), PC1 and PC2 contribute 57% to the total variance. The major separation occurs along PC1. Statistical analysis was also carried out in terms of distinguishing non-resistant and resistant strains by regrouping samples into two sets. Because PCA is an unsupervised method, the PCA scores plot remains the same regardless of the labels of each sample if the same set of data is used. We note that, in cases where no antibiotic stress was applied, resistant and non-resistant strains can be well differentiated by PCA. Outcomes by t tests and ROC curves can provide more insight into the differences between strains. The t test results in Figure 4.4(b) imply that 20 transitions, all of which show up in the 35 MRMs in the previous analysis, are significant for the differentiation. PC1 and PC2 take up 67% of the variance. ROC curves can be used to determine important transitions that are potentially characteristic for each set. As shown in Figure 4.5, there are seven transitions with AUC above 0.9, including three from saturated fatty acyl chain residues, two from PS, one from PE, and one from PG. Transitions selected from each analysis and their corresponding functional group or lipid class are tabulated in Table 4.2.

Turning to antibiotic treated bacteria, after elimination of transitions from acyl-carnitines and using the same data filter, 86 MRMs were left. ANOVA and t tests produced sets of 34 and 12 transitions with the same cutoff applied, respectively. From the PCA results in Figure 4.6, transitions selected from ANOVA do not provide perfect separation between ATCC 25922 and CDC 0162. Transitions from t tests offer similar separation along PC1 and its first two PCs explain 82% of the total variance. However, the number of features is fewer than in the control set. Among the 12 significant MRMs, three MRMs are found to have AUC above 0.9 from ROC curve, including one from PE, one from 26:0 fatty acyl chain residue, and one from

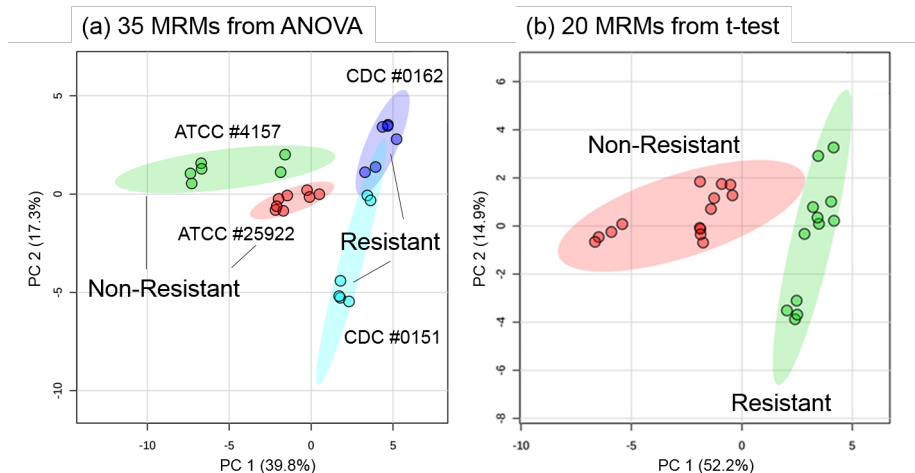


Figure 4.4. PCA scores plots of control samples (no amoxicillin or amoxicillin/clavulanate applied) using transitions selected from (a) ANOVA and (b) *t* test. Color-shaded areas are the calculated range with 95% confidence.

Table 4.2. Significant MRM transitions from different statistical analysis of control set

Transition	Class ^a	Transition	Class	Transition	Class
681.4 → 436.4	14:0	627.2 → 382.2	14:0	864.3 → 227.1	14:0
483.5 → 283.1	18:0	497.4 → 283.1	18:0	529.9 → 228.9	18:0
920.5 → 283.1	18:0	919.0 → 283.1	18:0	576.0 → 251.0	20:2
732.4 → 591.4	PE	966.2 → 637.2	20:0	716.1 → 397.1	20:5
780.5 → 591.5	PG	701.9 → 382.9	20:5	913.6 → 594.6	20:5
512.3 → 327.3	PS	526.0 → 177.0	22:4	588.2 → 235.2	22:2
600.2 → 415.2	PS	846.6 → 184.1	PC	504.1 → 119.1	24:0
ROC (7 MRMs)		794.6 → 605.6	PG	532.0 → 119.0	26:0
		820.6 → 631.6	PG	590.1 → 177.1	26:0
		644.0 → 459.0	PS	900.7 → 264.1	Cer
		688.4 → 503.4	PS	650.5 → 509.5	PE
		732.4 → 547.4	PS	689.9 → 548.9	PE
		776.5 → 591.5	PS	704.3 → 563.3	PE
<i>t</i> test (20 MRMs)				806.5 → 617.5	PG
				638.0 → 453.0	PS
ANOVA (35 MRMs)					

^aThese are tentative assignment. The classes of fatty acyl chain residues are abbreviated as “number of carbons : number of carbon-carbon double bonds”. For example, “20:2” means a fatty acyl chain residue with 20 carbon atoms and 2 carbon-carbon double bonds.

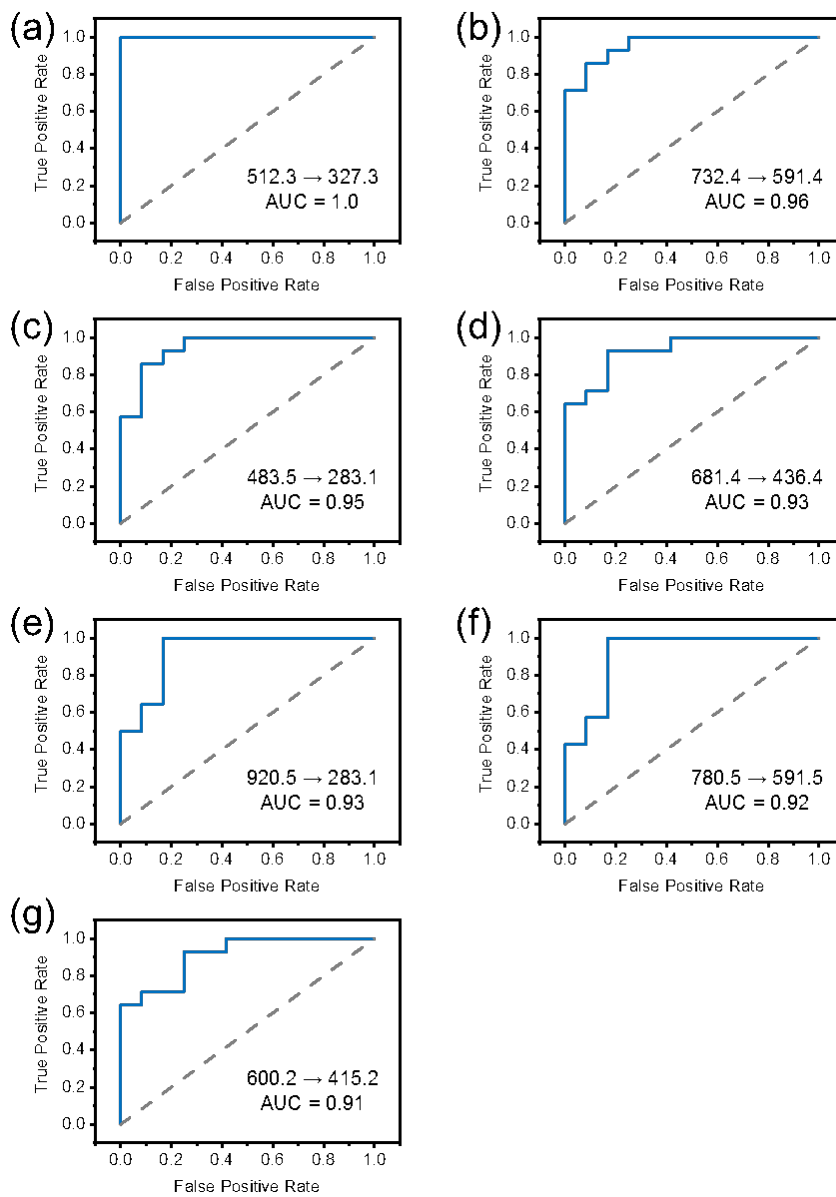


Figure 4.5. ROC curves significant transitions (AUC > 0.9) from control set.

PG, as shown in Figure 4.7. Details of transitions from each analysis are listed in Table 4.6. Bacteria treated with amoxicillin/clavulanate at half MIC and the controls have similar lipid transitions determined to be responsible for the separation.

Lipids associated with each MRM are postulated from the characteristic PREC and NL scans, as tabulated in Table 4.4. Although the exact structure of the lipids associated with each transition could not be decided merely by the MS/MS experiment, it is the pattern of the entire set of selected transitions spread over nine methods that provides reliable differentiation between strains from multiple classes of lipids. The distribution among the lipid classes of the transitions selected from t tests is shown in Figure 4.8. Application of amoxicillin/clavulanate resulted in an increase in the number of informative transitions in unsaturated fatty acyl chain residues and a decrease in those in saturated fatty acyl chain residues. The number of informative transitions from PS dropped significantly after antibiotic treatment. Additionally, the total number of significant transitions from glycerophospholipids is larger when no amoxicillin or amoxicillin/clavulanate are applied, implying that more glycerophospholipids are detected. This is consistent with previous research.^[42] In spite of these successes at differentiation, samples containing both resistant and non-resistant *E. coli* may be more difficult to distinguish.

Different from exact mass searches in the database as is done in proteomics, MRM-profiling offers opportunity to investigate changes in functional groups with more confidence. The low resolution of the instrument and the use of direct analysis with MRM methods means that it is still possible that isomeric ion pairs exist. For example, PG (35:1) and PGo (36:1) have monoisotopic masses with close values at 762.5411 ($C_{41}H_{79}O_{10}P$) and 762.5775 ($C_{42}H_{83}O_9P$), respectively. In the MRM method, with NH_4Ac introduced into the spray, the ammonium adducts are predominant for PG, making the corresponding transitions appear as m/z 780.5 \rightarrow 591.5 for both molecules. Nevertheless, when analyzing a lipid extract, the neutral loss of 189 from the head group in PG is what one should focus on because both candidate ion

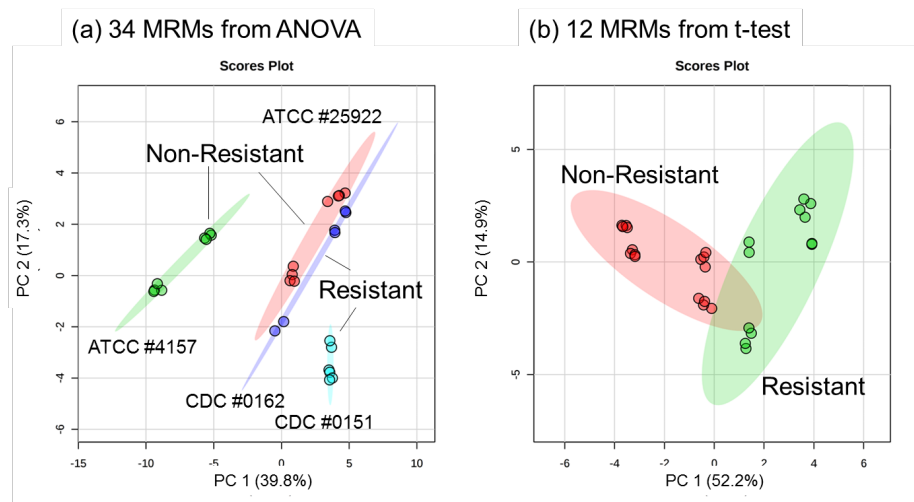


Figure 4.6. PCA score plots of samples treated with amoxicillin/-clavulanate at half MIC using transitions selected from (a) ANOVA and (b) t test. The color-shaded areas are the calculated range with 95% confidence.

Table 4.3. Significant MRM transitions from different statistical analysis of samples treated with amoxicillin/clavulanate at half MIC

Transition	Class ^a	Transition	Class	Transition	Class	Transition	Class
642.3 → 229.3	26:0	681.4 → 436.4	14:0	505.9 → 260.9	14:0	586.1 → 229.1	22:0
650.5 → 509.5	PE	548.0 → 229.0	20:5	627.2 → 382.2	14:0	576.0 → 223.0	22:2
820.6 → 631.6	PG	703.2 → 384.2	20:5	864.3 → 227.1	14:0	588.2 → 235.2	22:2
ROC (3 MRMs)		913.6 → 594.6	20:5	506.1 → 235.1	16:1	621.0 → 236.0	24:0
		614.1 → 229.1	24:0	529.9 → 228.9	18:0	900.7 → 264.1	Cer
		704.3 → 563.3	PE	919.0 → 283.1	18:0	281.3 → 281.3	FFA
		732.4 → 591.4	PE	558.2 → 263.2	18:3	846.6 → 184.1	PC
		780.5 → 591.5	PG	576.0 → 251.0	20:2	689.9 → 548.9	PE
		794.6 → 605.6	PG, PE	551.9 → 228.9	20:3	806.5 → 617.5	PG
	t test (12 MRMs)			701.9 → 382.9	20:5	512.3 → 327.3	PS
				716.1 → 397.1	20:5	688.4 → 503.4	PS
ANOVA (34 MRMs)							

^aAbbreviations have the same meanings as elaborated in Table 4.2

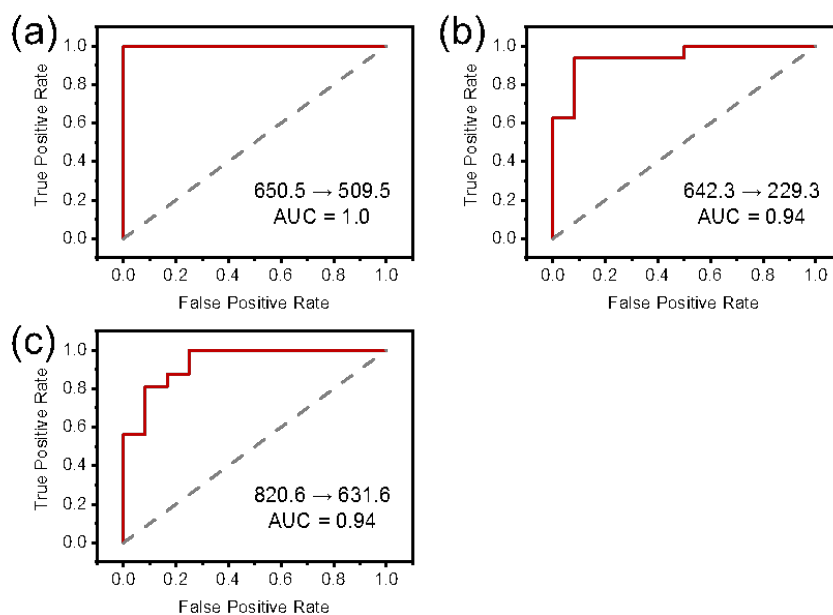


Figure 4.7. ROC curves significant transitions ($AUC > 0.9$) from samples treated with amoxicillin/clavulanate at half MIC.

Table 4.4. Postulated classification of transitions selected from t test and ROC curve

No Antibiotic Treatment		Amox/Clav at $\frac{1}{2}$ MIC	
Transition	Possible Formula ^a	Transition	Possible Formula ^a
732.4 → 591.4	PE(35:1)	650.5 → 509.5	PE(29:0)
780.5 → 591.5	PG(35:1)	820.6 → 631.6	PGo(39:2)
512.3 → 327.3	PS(16:0)	704.3 → 563.3	PE(33:1)
600.2 → 415.2	PS(23:5)	732.4 → 591.4	PE(35:1)
846.6 → 184.1	PC(40:0)	780.5 → 591.5	PG(35:1)
794.6 → 605.6	PGo(37:1)	794.6 → 605.6	PGo(37:1), PE(40:5)
820.6 → 631.6	PGo(39:2)		
644.0 → 459.0	PS(26:0)		
688.4 → 503.4	PS(29:0)		
732.4 → 547.4	PS(32:0)		
776.5 → 591.5	PS(35:0)		

^aDue to ammonium acetate, the precursor ion m/z could be ammonium adducts of lipids, such as PG. One possible formula of each class of individual transition is listed.

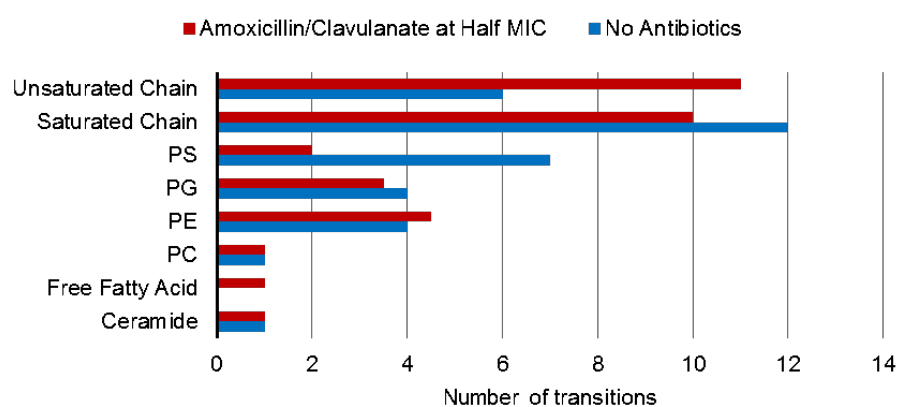


Figure 4.8. Distribution of transitions selected from *t* test between controls and sample treated with amoxicillin/clavulanate at half MIC. “Saturated Chain” refers to the saturated fatty acyl chain residues. “Unsaturated Chain” refers to fatty acyl chain residues with degree of unsaturation ranging from 1 to 5.

pairs are PG. Although the number of antibiotics types is limited in current study, MRM-profiling might be more sensitive and efficient than existing methods as there are more lipid molecules per cell and analysis of small molecules has advantages in ion transmission and ionization efficiency. This preliminary study has demonstrated the feasibility of distinguishing bacterial strains by carrying out MRM-profiling to characterize lipid patterns.

4.5 Conclusions

We have demonstrated that MRM-profiling can be applied to distinguish four different strains of *E. coli*, including two non-resistant and two resistant strains. Different strains are well differentiated by PCA using significant MRMs acquired from *t* test. This indicates that the lipid profiles not only serve to characterize bacterial species, but they also change in resistant strains compared to non-resistant strains and they are sensitive to antibiotic challenge. Lipid biomarker candidates are also determined, and this tool can help zeroing in on the biomarkers most significant for the separation. Based on previous studies in other complex biological systems, MRM-profiling could expedite and improve the identification of lipids related with resistance, virulence, and viability. As such it will help benchmark the gene pathway involved in the phenotypes as a novel approach to identify unique resistance genes.

4.6 References

- [1] K. E. Fleming-Dutra, A. L. Hersh, D. J. Shapiro, M. Bartoces, E. A. Enns, T. M. File, J. A. Finkelstein, J. S. Gerber, D. Y. Hyun, J. A. Linder, R. Lynfield, D. J. Margolis, L. S. May, D. Merenstein, J. P. Metlay, J. G. Newland, J. F. Piccirillo, R. M. Roberts, G. V. Sanchez, K. J. Suda, A. Thomas, T. M. Woo, R. M. Zetts, L. A. Hicks, *JAMA* **2016**, *315*, 1864.
- [2] A. M. Mohareb, A. F. Dugas, Y.-H. Hsieh, *The American Journal of Emergency Medicine* **2016**, *34*, 1059–1065.
- [3] L. M. Weiner, A. K. Webb, B. Limbago, M. A. Dudeck, J. Patel, A. J. Kallen, J. R. Edwards, D. M. Sievert, *Infection Control & Hospital Epidemiology* **2016**, *37*, 1288–1301.

- [4] S. Santajit, N. Indrawattana, *BioMed Research International* **2016**, *2016*, 1–8.
- [5] M. J. Pugia, R. G. Sommer, H.-H. Kuo, P. F. Corey, D. L. Gopual, J. A. Lott, *Clinical Chemistry and Laboratory Medicine (CCLM)* **2004**, *42*, 340–346.
- [6] B. Foxman, *Infectious Disease Clinics of North America* **2014**, *28*, 1–13.
- [7] S. Salvatore, S. Salvatore, E. Cattoni, G. Siesto, M. Serati, P. Sorice, M. Torella, *European Journal of Obstetrics & Gynecology and Reproductive Biology* **2011**, *156*, 131–136.
- [8] C. A. Gidengil, A. Mehrotra, S. Beach, C. Setodji, G. Hunter, J. A. Linder, *Journal of General Internal Medicine* **2016**, *31*, 918–924.
- [9] T. F. Barlam, R. Soria-Saucedo, H. J. Cabral, L. E. Kazis, *Open Forum Infectious Diseases* **2016**, *3*, 1–7.
- [10] G. V. Sanchez, R. N. Master, J. A. Karlowsky, J. M. Bordon, *Antimicrobial Agents and Chemotherapy* **2012**, *56*, 2181–2183.
- [11] A. Aroutcheva, D. Gariti, M. Simon, S. Shott, J. Faro, J. A. Simoes, A. Gurguis, S. Faro, *American Journal of Obstetrics and Gynecology* **2001**, *185*, 375–379.
- [12] H. M. Zowawi, P. N. A. Harris, M. J. Roberts, P. A. Tambyah, M. A. Schembri, M. D. Pezzani, D. A. Williamson, D. L. Paterson, *Nature Reviews Urology* **2015**, *12*, 570–584.
- [13] M. E. Hibbing, C. Fuqua, M. R. Parsek, S. B. Peterson, *Nature Reviews Microbiology* **2010**, *8*, 15–25.
- [14] T. Conway, P. S. Cohen, *Microbiology Spectrum* **2015**, *3*, MBP–006–2014.
- [15] L. Váradi, J. L. Luo, D. E. Hibbs, J. D. Perry, R. J. Anderson, S. Orenga, P. W. Groundwater, *Chemical Society Reviews* **2017**, *46*, 4818–4832.
- [16] J. M. Janda, S. L. Abbott, *Journal of Clinical Microbiology* **2007**, *45*, 2761–2764.
- [17] C. U. Köser, M. J. Ellington, E. J. P. Cartwright, S. H. Gillespie, N. M. Brown, M. Farrington, M. T. G. Holden, G. Dougan, S. D. Bentley, J. Parkhill, S. J. Peacock, *PLoS Pathogens* **2012**, *8*, (Ed.: G. F. Rall), e1002824.
- [18] M. V. Larsen, S. Cosentino, S. Rasmussen, C. Friis, H. Hasman, R. L. Marvig, L. Jelsbak, T. Sicheritz-Ponten, D. W. Ussery, F. M. Aarestrup, O. Lund, *Journal of Clinical Microbiology* **2012**, *50*, 1355–1361.
- [19] D. J. Geha, J. R. Uhl, C. A. Gustaferrero, D. H. Persing, *Journal of Clinical Microbiology* **1994**, *32*, 1768–1772.
- [20] M. Sauget, B. Valot, X. Bertrand, D. Hocquet, *Trends in Microbiology* **2017**, *25*, 447–455.
- [21] B. Rodríguez-Sánchez, E. Cercenado, A. T. Coste, G. Greub, *Eurosurveillance* **2019**, *24*, 1–12.

- [22] N. Singhal, M. Kumar, P. K. Kanaujia, J. S. Viridi, *Frontiers in Microbiology* **2015**, *6*, 1–16.
- [23] K. Cheng, M. Drebot, J. McCrea, L. Peterson, D. Lee, S. McCorrister, R. Nickel, A. Gerbasi, A. Sloan, D. Janella, G. Van Domselaar, D. Beniac, T. Booth, L. Chui, H. Tabor, G. Westmacott, M. Gilmour, G. Wang, *PLoS ONE* **2013**, *8*, (Ed.: M. Desvaux), e57339.
- [24] Y. Charretier, O. Dauwalder, C. Franceschi, E. Degout-Charmette, G. Zambardi, T. Cecchini, C. Bardet, X. Lacoux, P. Dufour, L. Veron, H. Rostaing, V. Lanet, T. Fortin, C. Beaulieu, N. Perrot, D. Dechaume, S. Pons, V. Girard, A. Salvador, G. Durand, F. Mallard, A. Theretz, P. Broyer, S. Chatellier, G. Gervasi, M. Van Nuenen, C. Ann Roitsch, A. Van Belkum, J. Lemoine, F. Vandenesch, J.-P. Charrier, *Scientific Reports* **2015**, *5*, 13944.
- [25] J. C. Rees, C. L. Pierce, D. M. Schieltz, J. R. Barr, *Analytical Chemistry* **2015**, *87*, 6769–6777.
- [26] C. Guijas, J. R. Montenegro-Burke, B. Warth, M. E. Spilker, G. Siuzdak, *Nature Biotechnology* **2018**, *36*, 316–320.
- [27] C. H. Johnson, J. Ivanisevic, G. Siuzdak, *Nature Reviews Molecular Cell Biology* **2016**, *17*, 451–459.
- [28] H. Li, P. Balan, A. Vertes, *Angewandte Chemie - International Edition* **2016**, *55*, 15035–15039.
- [29] H. Muhamadali, D. Weaver, A. Subaihi, N. Almasoud, D. K. Trivedi, D. I. Ellis, D. Linton, R. Goodacre, *Analyst* **2016**, *141*, 111–122.
- [30] C. Sohlenkamp, O. Geiger, *FEMS Microbiology Reviews* **2016**, *40*, (Ed.: F. Narberhaus), 133–159.
- [31] W. Hewelt-Belka, J. Nakonieczna, M. Belka, T. Baczek, J. Namieśnik, A. Kot-Wasik, *Journal of Proteome Research* **2016**, *15*, 914–922.
- [32] H. Strahl, J. Errington, *Annual Review of Microbiology* **2017**, *71*, 519–538.
- [33] A. D. Watson, *Journal of Lipid Research* **2006**, *47*, 2101–2111.
- [34] M. Li, E. Zeringer, T. Barta, J. Schageman, A. Cheng, A. V. Vlassov, *Philosophical Transactions of the Royal Society B: Biological Sciences* **2014**, *369*, 20130502.
- [35] C. R. Ferreira, K. E. Yannell, B. Mollenhauer, R. D. Espy, F. B. Cordeiro, Z. Ouyang, R. G. Cooks, *Analyst* **2016**, *141*, 5252–5255.
- [36] F. B. Cordeiro, C. R. Ferreira, T. J. P. Sobreira, K. E. Yannell, A. K. Jarmusch, A. P. Cedenho, E. G. Lo Turco, R. G. Cooks, *Rapid Communications in Mass Spectrometry* **2017**, *31*, 1462–1470.
- [37] J. Dhillon, C. R. Ferreira, T. J. P. Sobreira, R. D. Mattes, *Current Developments in Nutrition* **2017**, *1*, e001545.

- [38] T. Casey, K. Harlow, C. R. Ferreira, T. J. P. Sobreira, A. Schinckel, K. Stewart, *Journal of Applied Animal Research* **2018**, *46*, 667–676.
- [39] J. Franco, C. Ferreira, T. J. Paschoal Sobreira, J. P. Sundberg, H. HogenEsch, *PLOS ONE* **2018**, *13*, (Ed.: S. N. Witt), e0196595.
- [40] C. B. de Lima, C. R. Ferreira, M. P. Milazzotto, T. J. P. Sobreira, A. A. Vireque, R. G. Cooks, *Journal of Mass Spectrometry* **2018**, *53*, 1247–1252.
- [41] E. G. Bligh, W. J. Dyer, *Canadian Journal of Biochemistry and Physiology* **1959**, *37*, 911–917.
- [42] E. R. Schenk, F. Nau, C. J. Thompson, Y.-C. Tse-Dinh, F. Fernandez-Lima, *Journal of Mass Spectrometry* **2015**, *50*, 88–94.

CHAPTER 5. HIGH-THROUGHPUT BIOASSAYS USING "DIP-AND-GO" MULTIPLEXED ELECTROSPRAY MASS SPECTROMETRY

5.1 Abstract

A multiplexed system based on inductive nanoelectrospray ionization mass spectrometry (nESI-MS) has been developed for high-throughput screening (HTS) bioassays. This system combines inductive nESI and field amplification micro-electrophoresis to achieve a "dip-and-go" sample loading and purification strategy that enables nESI-MS based HTS assays in 96-well microtiter plates. The combination of inductive nESI and micro-electrophoresis makes it possible to perform efficient *in situ* separations and clean-up of biological samples. The sensitivity of the system is such that quantitative analysis of peptides from 1 to 10,000 nM can be performed in a biological matrix. A prototype of the automation system has been developed to handle 12 samples (i.e. one row of a microtiter plate) at a time. The sample loading and electrophoretic clean-up of biosamples can be done in parallel within 20s followed by MS analysis at a rate of 1.3 to 3.5 s/sample. The system was used successfully for the quantitative analysis of BACE1-catalyzed peptide hydrolysis, a prototypical high-throughput screening (HTS) assay of relevance to drug discovery. IC₅₀ values for this system were in agreement with LC-MS but recorded in times more than an order of magnitude shorter.

5.2 Introduction

High-throughput, target-based screening has become a staple of the drug discovery process.^[1,2] The introduction of robotic systems for sample preparation and plate handling enables bioassays to be run in a fully automated fashion, which allows assessment of the functional activity of small molecule compound libraries^[3] at scales in the order of millions of compounds.^[4] Optical detection formats such as absorbance, fluorescence^[5] and luminescence^[6] are well-suited to HTS due to the rapid nature of the measurement (ca. 10 to 100 ms/sample). Though effective, not all bioassays are inherently suited to optical detection due to labelling reactivity, interference of the biological matrix and the emerging demands for intact molecule bioassays.^[7] For these reasons, mass spectrometry (MS) is widely considered an attractive alternative to optical detection methods for HTS bioassays,^[2] due to its inherent selectivity, sensitivity and label-free characteristics. As a result, a number of MS platforms have been applied to screening of bioassays, including LC-MS at rates of ca. 0.5 to 8 min/sample,^[8] RapidFire-MS at rates of ca. 6 to 8 s/sample, MALDI-MS at a rate of ca. 0.3 s/sample^[9-11] and, acoustic droplet ejection MS at rates of 0.5 to 1 s/sample.^[12,13] For the above techniques, the sacrifice in separation increases the HTS rate but can lead to loss of specificity and sensitivity in bioassays; methods enabling both high-throughput and efficient separation and analysis remain in high demand.

Nanoelectrospray ionization^[14] (nESI) is highly sensitive^[15,16] and one of the most robust^[17] sample introduction methods used for MS-based analysis of biological samples. The common implementation of nESI uses tapered emitters pulled from glass tubes.^[14] Nevertheless, the outstanding analytical performance of nESI has not been exploited for HTS analysis because the sample introduction step in nESI has only been done manually. In recent years, our group has developed inductive nESI which enables the ionization of liquid samples using a remote electrode.^[18-20] Inductive nESI, better termed inductive picoelectrospray (pL/min flowrate spray, pESI) can perform reliable analysis from small confined volumes including droplets^[21] and single cells^[20]

with sensitivity down to the zeptomole level.^[19] When either a static^[20,22] or alternating electrical field^[19] is applied to initiate inductive nESI, the polarization of the liquid causes the spatial separation of ions,^[20,23–27] allowing *in situ* micro-electrophoresis. This effect becomes particularly significant when: a) sample amounts are at the nanoliter level and b) the electrical field applied to initiate inductive nESI is also used to effect micro-electrophoresis. We hypothesize that the combination of inductive nESI with high performance micro-electrophoresis could constitute a promising approach for HTS bioassays.

Herein, we establish the performance of a dip-and-go multiplex system (5.1) for HTS bioassays based on a combination of inductive nESI with field amplified micro-electrophoretic cleaning. Inductive nESI enables the "dip" method of sample introduction for samples of approximately 100 nL volume from a 96-well microtiter plate. The samples are introduced into the emitters by simply immersing the emitter tips into the sample solution, significantly decreasing the time compared to traditional nESI techniques. To fit the format of a 96-well microtiter plate, a 3D printed emitter holder was used for simultaneous introduction of samples from one row of the microtiter plate. We used a DC electrical field to initiate inductive nESI and to perform micro-Electrophoresis by simply modulating the electrical field strength. During the "dip" event we load three separate bands of solutions with different electrical conductivity into the emitter. This allows field amplification,^[28] a method that can dramatically increase the performance of micro-electrophoresis. The high-performance cleaning process takes just 10 s and is applied to the emitters in parallel, resulting in a significantly improved and rapid sample clean-up process. Subsequently, the emitters are subjected to inductive nESI analysis. The emitter holder is moved in front of the mass spectrometer to allow screening at a rate of 1.3 to 3.5 s/sample. The total analysis time of one row of a 96-well microtiter plate is ca. 2 min, comprised of ca. 10 s for sample loading, 10 s for field amplification micro-electrophoretic cleaning, ca. 40 s for inductive nESI analysis and 50 s for homing the device for measurement of

the next row. In order to evaluate the performance of our multiplexed nESI system for application to HTS bioassays we selected BACE1 as a prototypical enzyme of relevance for HTS since it has been successfully screened by mass spectrometry in the past.^[29]

5.3 Experimental Section

5.3.1 Chemicals

6-Hydroxyindanone, substituted benzaldehydes, sodium acetate, glycerol, Brij-27 ($\text{CH}_3(\text{CH}_2)_{12}(\text{OCH}_2\text{CH}_2)_n\text{OH}$), DMSO, formic acid and OM99-2 were all purchased from Sigma-Aldrich and used as received. BACE1 protein was provided by Merck & Co., Inc., Kenilworth, NJ, USA. The substrate KTEEISEVNLDAEFRHDK, product KTEEISEVNL and internal standard 20 mM were purchased from CPC Scientific (Sunnyvale, CA) with purity of >95%; all peptides were N-terminal amines and C-terminal free acids. Human serum was purchased from BioIVT (Westbury, NY).

5.3.2 Reactions

Claisen-Schmidt Reaction Reactions are performed at 100 mM with equivalent reactants and 1.8 M KOH. Reactions were quenched by 10× dilution with methanol in 96-well microtiter plate.

BACE1 Reaction 2.5 μL of diluted OM99-2 (in DMSO) was added to 4 nM BACE1 enzyme in 300 μL of assay buffer consisting of 20 mM NaOAc, pH 4.5, 5% glycerol, 0.001% Brij-27. The mixtures were subsequently incubated for 30 min at ambient temperature. Afterwards, the reaction was initiated by addition of 200 μL of 25 μM peptide substrate (KTEEISEVNLDAEFRHDK; 10 μM final concentration) and incubated for 210 min at ambient temperature. The reaction was quenched with 500 μL of

“Dip and Go” multiplexed system for HTS bioassay

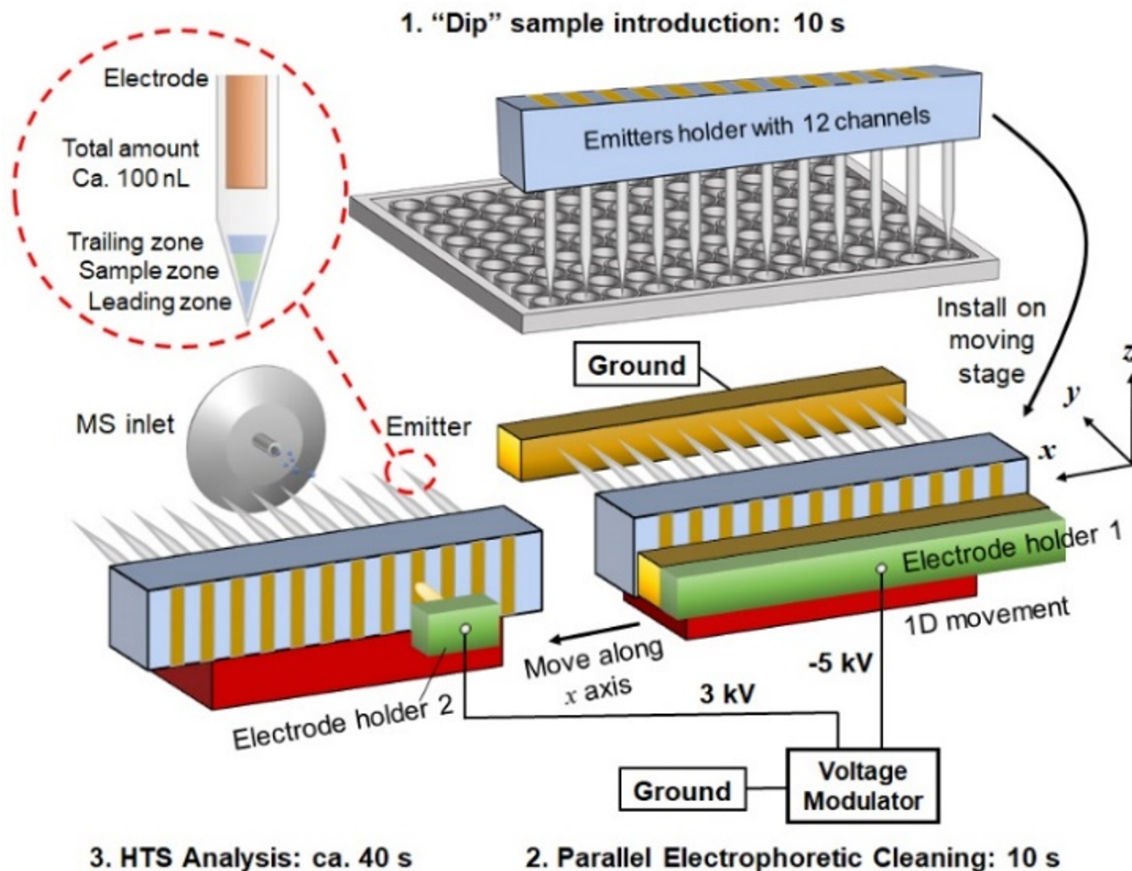


Figure 5.1. Instrumentation for dip-and-go multiplexed HTS bioassay. The emitter holder has 12 channels which can hold 12 emitters designed to fit the 96-well plate format. Step 1 is the "dip" step used for sample introduction. The emitters are immersed into water, sample solution and water in turn (the figure only shows dip into sample solution) to load the leading and trailing zones with pure water and the mid zone with sample solution. In Step 2 the holder is installed on a 1D moving stage and subjected to 10 s electrophoretic cleaning. In Step 3, the emitters are moved into position for inductive nESI-MS analysis.

quench solution containing 2% formic acid and 300 nM KTEEISEVN[L-¹³C₇] internal standard.

5.3.3 Dip-and-Go System

For sample introduction, the emitters (attached to a holder) were 1) immersed into water in a reservoir for 2 s; 2) immersed into sample solution for 5 s and 3) immersed into water again for 3 ss. The immersion depths in steps 1 and 2 were 3 mm and 5 mm in step 3. The above operations have two aims: 1) to wash the remaining sample solution from the outside of the emitter and so make the emitter reusable; 2) to load the leading and trailing zones with pure water for field amplification micro-CZE. After sample introduction, the holder with emitters inserted was placed at the start position of the 1D moving stage. Electrophoretic clean-up of samples was then carried out by applying -5 kV to the set of electrodes for 10 s. Then the holder was translated and the samples in the individual emitters were subjected to inductive nESI analysis in turn with 3.2 kV being automatically applied to each electrode when (and only when) the emitter transited in front of the MS inlet. Since the holder only has 12 channels (spanning one row of the 96-well microtiter plate), this procedure was repeated 8 times to analyze a single microtiter plate. Emitters are reusable and therefore do not need to be changed between analysis of different rows.

5.3.4 Mass Spectrometry Setup

nESI-MS Experiments were carried out using a Thermo LTQ mass spectrometer (Thermo Scientific, San Jose, CA). The instrumental parameters were as follows: capillary temperature = 250 °C; max injection time = 100 ms; microscan = 1; spray voltage = 3.2 kV. All nESI emitters were pulled from borosilicate tubing (B150-86-10, Sutter) using a micropipette puller (P-97, Sutter Instrument, Novato, CA). The emitter orifice was 25 μ m. For quantification, peak heights were used.

LC-MS Reaction mixtures were analyzed by liquid chromatography-mass spectrometry using an Agilent 1260 UPLC coupled to an Agilent 6224A time-of-flight mass spectrometer operating in positive ion electrospray mode. Two microliters of the quenched reaction mixture were injected onto a Waters Xbridge BEH-C18 column (4.6×50 mm, $2.5 \mu\text{m}$) held at ambient temperature. Analytes were eluted using a binary solvent system composed of 0.1% formic acid in water (mobile phase A) and 0.1% formic acid in 90% acetonitrile (aq, mobile phase B), run at a constant flow rate of $750 \mu\text{L}/\text{min}$. The column was initially equilibrated with 99% A/1% B and held for 2 min after injection. The solvent composition was then linearly ramped to 70% B/30% A over a period of 2 min and then ramped again to 99% B/1% A over an additional 0.5 min. The composition was held at 99% B for 2.5 min and then immediately returned to 99% A and held for additional 1 min prior to the next injection. The first 1.5 min of the gradient were diverted to waste. The mass spectrometer settings were as follows: gas temperature was 335°C , gas flow was $12 \text{ L}/\text{min}$, nebulizer was 60 psi, capillary voltage was 4 kV, fragmentor voltage was 135 V, skimmer voltage was 65 V and data were acquired from m/z 100 to 950 at a rate of 5 spectra/s.

5.4 Performance of System

5.4.1 Reaction Screening

First, we used the multiplexed system to perform chemical reaction screening in a 96-well to test the basic analytical performance. As a test case, we investigated substituent effects on the Claisen-Schmidt reaction, screening multiple reactions to generate a Hammett plot. Reactions between 6-hydroxyindanone and five benzaldehydes with different substitutes were examined in a 96-well plate in a period of 30 min. The reactions are quenched using $10\times$ methanol and, without chemical pretreatment, split into 5 rows for MS analysis. In Figure 5.2, we dipped the emitters into the sample wells for 5 seconds and then performed inductive nESI-MS analysis at rate of $1.3\text{s}/\text{sample}$. The high linearity of Hammett plot indicates the good performance

of the dip-and-go system in chemical reaction screening. We have also investigated the difference between normal nESI and inductive nESI considering the concern that the reaction could be possibly accelerated out of different ionization mechanism. As shown in Figure 5.3, no obvious acceleration was observed for the model reaction. In both cases, the product-to-reactant ratio is below 3%, which is much smaller than the accelerating conditions ($> 50\%$),^[30] confirming that inductive nESI has similar result as normal nESI without reaction acceleration.

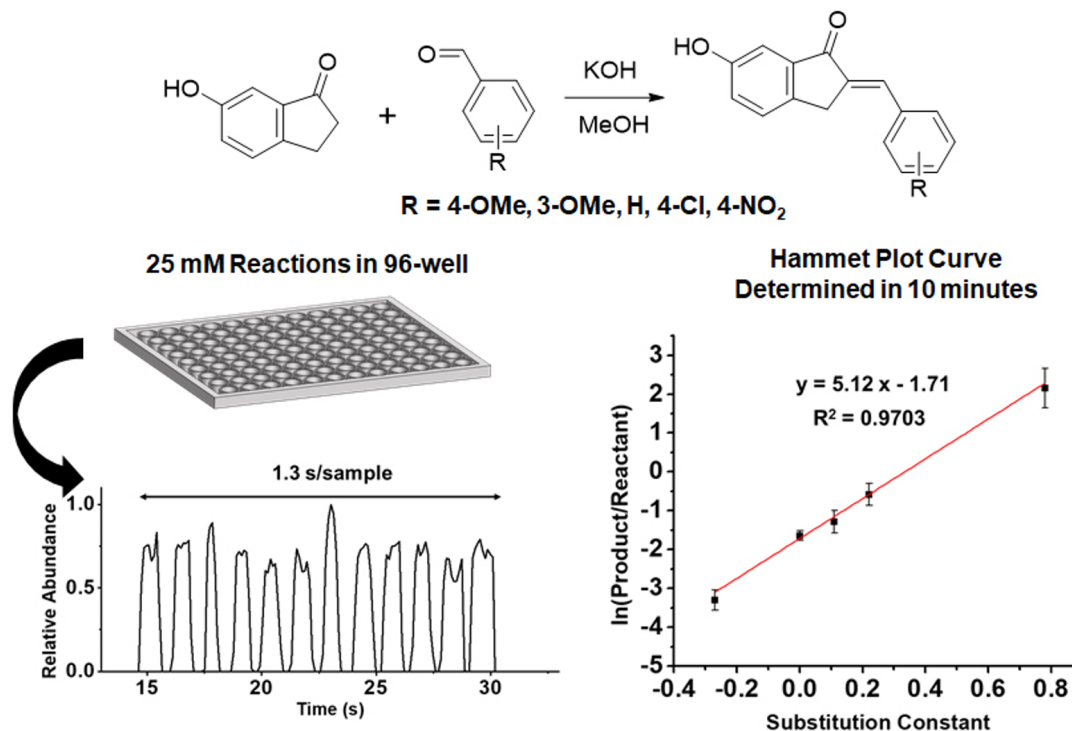


Figure 5.2. Screening of Claisen-Schmidt reactions in 96-well plate to test the analytical performance of the dip-and-go multiplexed system. Reactions between 6-hydroxyindanone and 5-substituted benzaldehydes were tested. The final reaction mixture in each well was: 25 mM 6-hydroxyindanone, 25 mM aldehyde, and 450 mM KOH. Reactions were run for 30 min and quenched with 10 \times dilution by methanol in each of the 5 rows for the subsequent inductive nESI analysis. Each point in the Hammett plot is the average of 5 measurements. The inductive nESI is performed under non-accelerating conditions (distance from emitter tip to MS inlet is 2 mm).

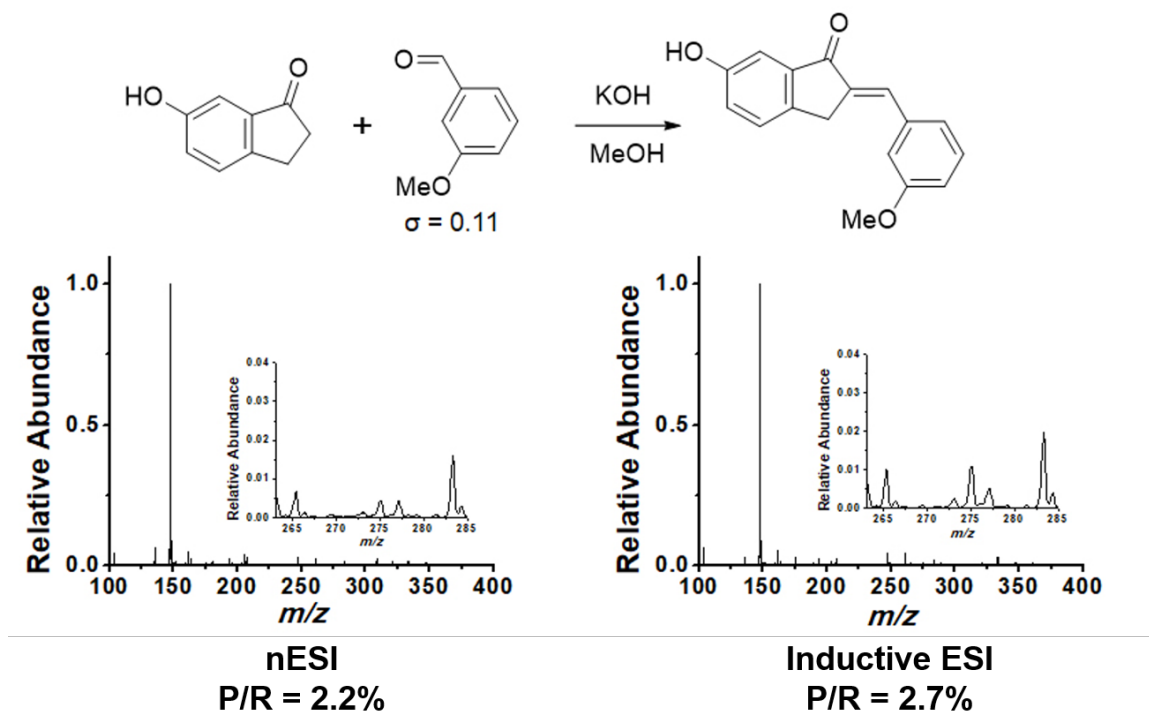


Figure 5.3. Confirmation of non-accelerating analysis conditions of inductive nESI. The reaction solution was mixed for 30 s followed by analysis of both nESI and inductive nESI; the product/reagent ratio is less than 3%.

5.4.2 Capability of Bioassays

For the bioassays, we examined the analytical performance of inductive nESI with field amplification micro-electrophoresis. Figure 5.4 compares analysis of the reaction product peptide here designated as KTEEISEVNL and its isotopically labeled internal standard (IS) KTEEISEVN(L- $^{13}\text{C}_7$) (stoichiometry is 1 : 1) in different biological matrices using full m/z scan mass spectra. Spectra obtained without electrophoretic cleaning (left column) show strong ion suppression effects leading to signal to noise ratios (SNR) below 3. This is inadequate even for qualitative analysis. The spectra obtained after 10 s of electrophoretic clean-up (right column) by contrast show SNR

of 17.7 and 5.4 in the reaction buffer and in buffer with interfering peptides, respectively. After clean-up, the ratio of KTEEISEVNL and IS remains 1 : 1 as expected, demonstrating the precision of the technique. An LoQ of 150 nM was obtained for the KTEEISEVNL using full scan MS at SNR > 10 as shown in Figure 5.5. Plots of the calibration curve acquired by full scan MS after clean-up MS in Figure 5.6 demonstrate a linear dynamic range from 150 nM to 4000 nM ($R^2 = 0.9950$).

The results of analyzing 1000 nM KTEEISEVNL in diluted human serum are also encouraging. As shown in full scan spectra in Figure 5.4, electrophoretic clean-up of human serum sample shows SNR of 14.5 for the target peptide while the peptides peaks are submerged under baseline without cleaning. Ion isolation followed by a mass scan increased the SNR from below 3 to 20 – 40 and also increased the signal intensity 13.2 to 130-fold as included in Figure 5.7 and Table 5.1.

Table 5.1. Comparison of inductive nESI with and without field amplification micro-CZE of serum sample in isolation scan mode from Figure 5.7.

Dilution Factor	Without micro-CZE		With micro-CZE		Signal
	m/z 585.0	SNR	m/z 585.0	SNR	Enhance
33×	2.97×10^1	< 3	3.85×10^3	21.4	130
17×	3.26×10^1	< 3	1.76×10^3	43.3	54.0
7×	1.57×10^1	< 3	2.08×10^2	21.9	13.2

The performance in HT bioscreening was also evaluated using the multiplexed system that integrates inductive nESI with field amplification micro-electrophoresis. Twelve emitters were loaded on a 3D printed holder to perform analysis for one row of a 96-well microtiter plate. As shown in Figure 5.8, the average deviation of the experimentally observed ratio from the expected ratio was 11.0% and 6.1% for rows A and B, respectively. The results shown in Figure 5.8 are for a screening rate of 4s/sample recorded at ca. 20 spectra per sample. Since appropriate precision can

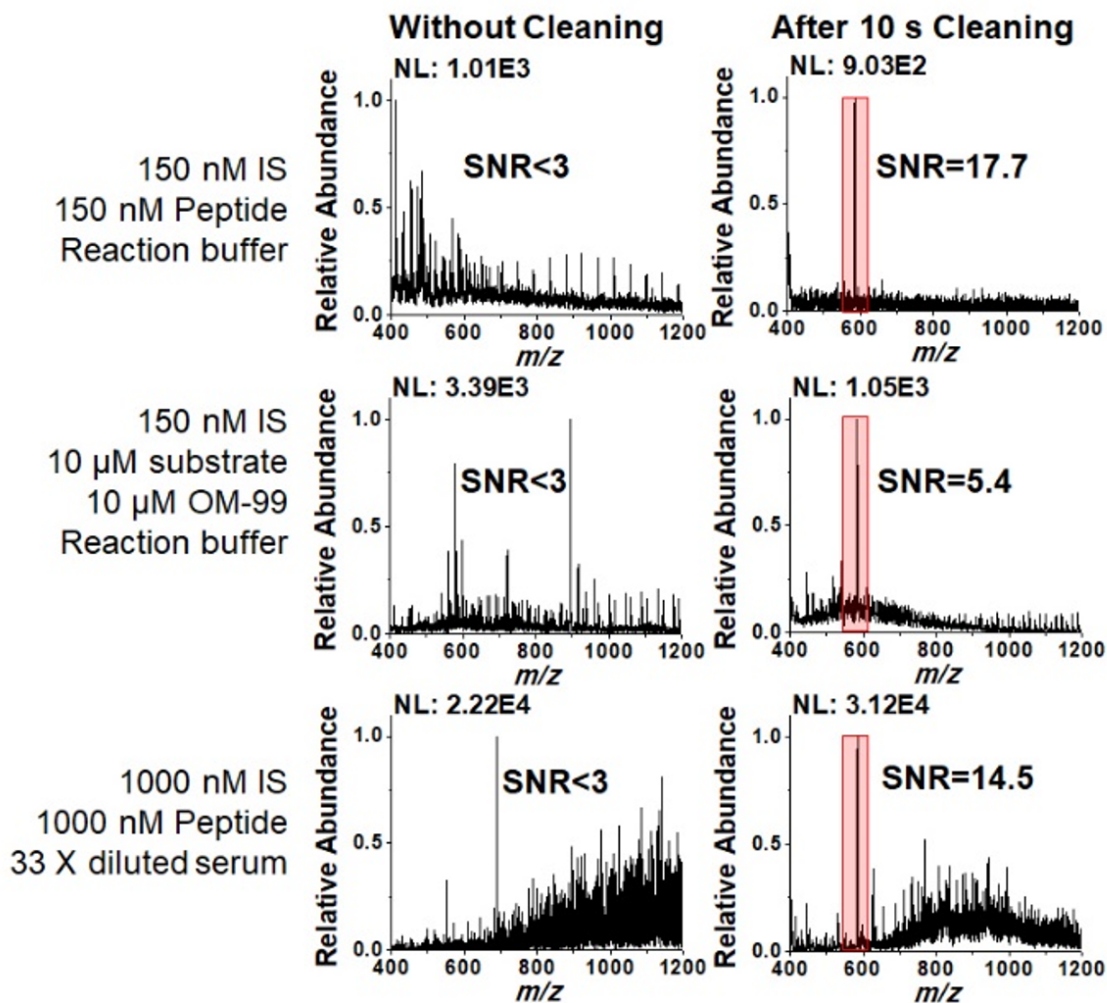


Figure 5.4. Full scan mass spectra using inductive nESI analysis of KTEEISEVNL (m/z 581.5) with internal standard KTEEISEVN(L- $^{13}\text{C}_7$) (m/z 585.0) in different biological matrices with and without field amplification micro-electrophoretic clean-up. Reaction buffer is 2 nM BACE1 enzyme, 6 mM sodium acetate, 1.5% glycerol, 0.25% DMSO, 3 ppm Brij-27 and 1% formic acid.

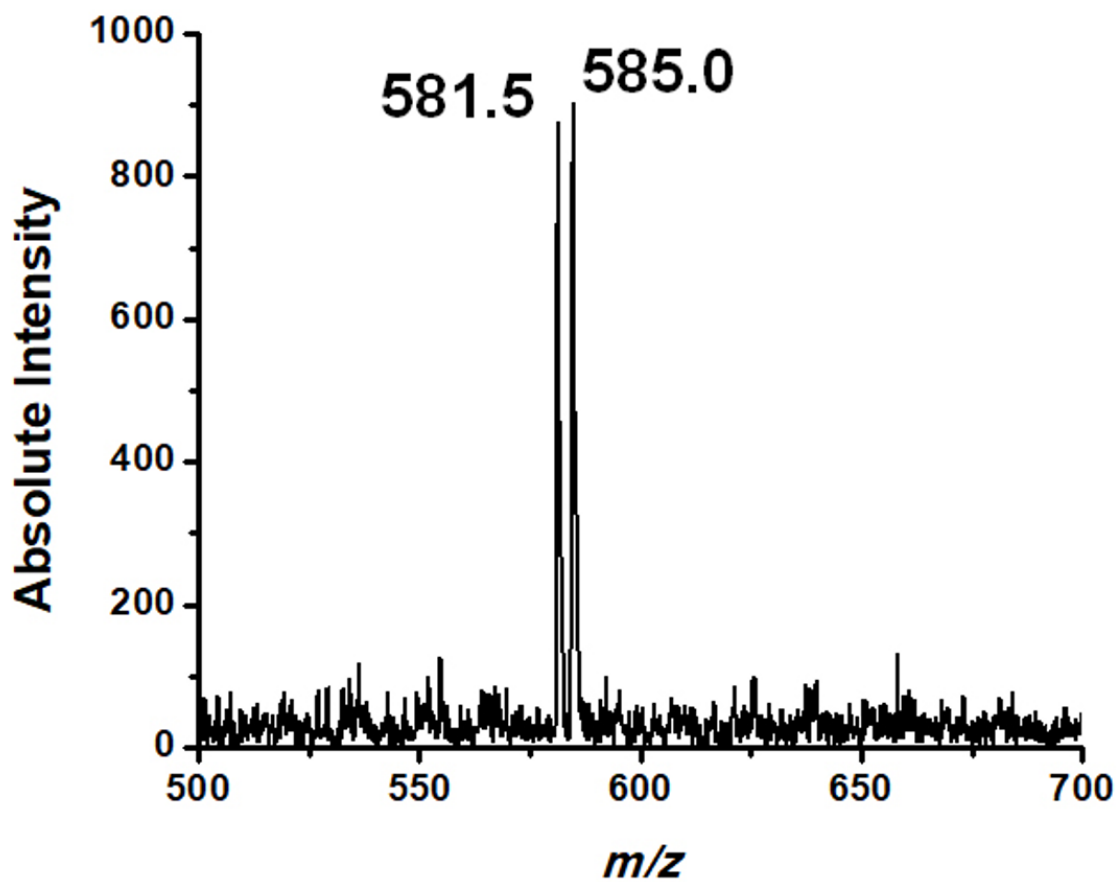


Figure 5.5. Test of LoQ of KTEEISEVNL (*m/z* 581.5) with its internal standard KTEEISEVN(L-¹³C₇) (*m/z* 585.0) using inductive nESI with field amplification micro-CZE. The concentration of each peptide is 150 nM in reaction buffer of 2 nM BACE1 enzyme, 6 mM sodium acetate, 1.5% glycerol, 0.25% DMSO, 3 ppm Brij-27 and 1% formic acid.

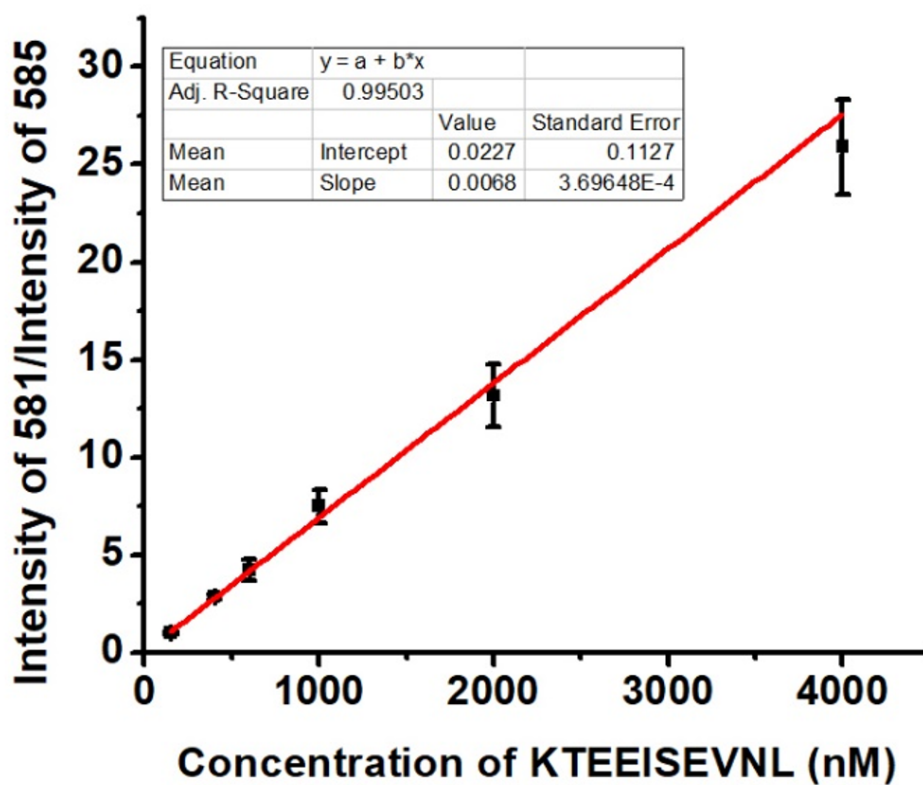


Figure 5.6. Calibration curve of the dip-and-go analysis for KTEEI-SEVNL (m/z 581.5) with 150 nM KTEEISEVN(L - $^{13}C_7$) (m/z 585.0) as internal standard in reaction buffer system (2 nM BACE1 enzyme, 6 mM sodium acetate, 1.5% glycerol, 0.25% DMSO, 3 ppm Brij-27 and 1% formic acid). The intensity of ions at m/z 581.5 and m/z 585.0 are directly read from full scan mass spectra. The curve shows a good linear dynamic range from 150 nM to 4000 nM.

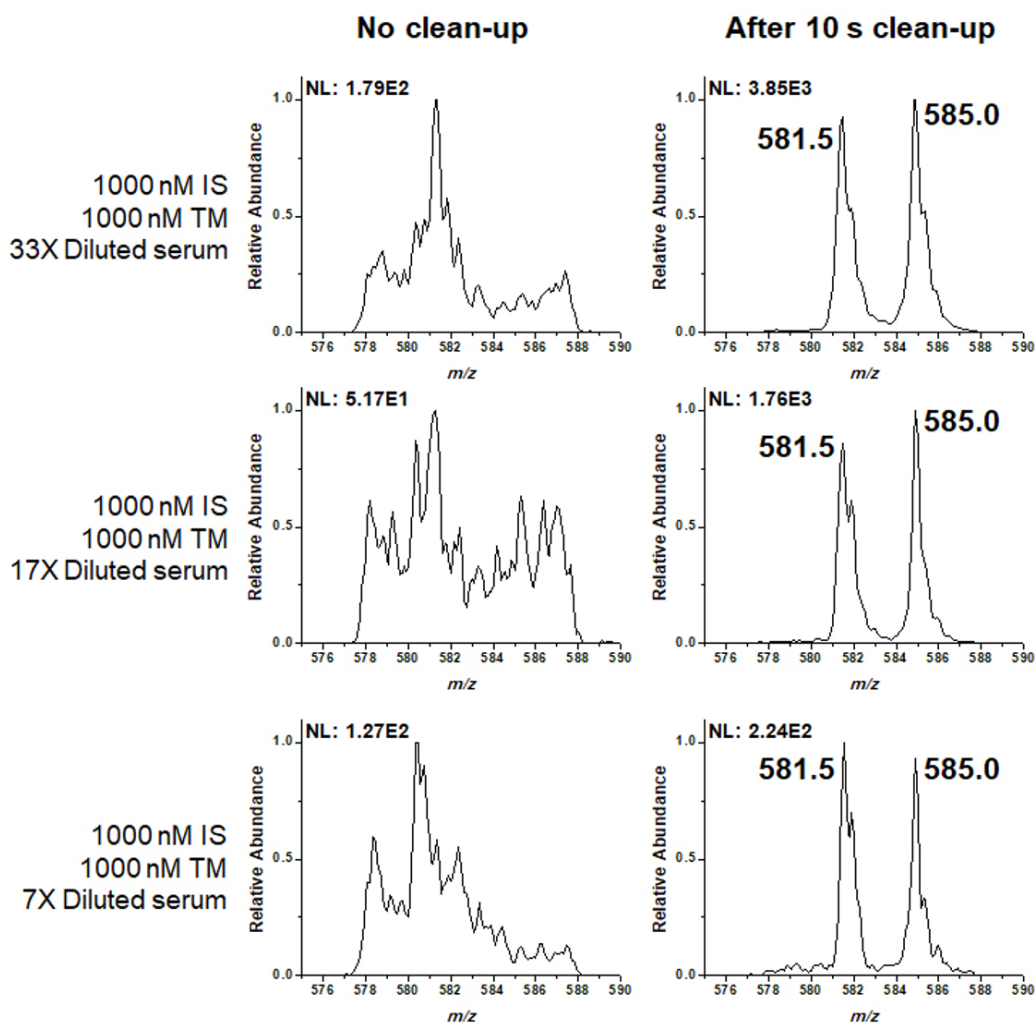


Figure 5.7. Comparison of inductive nESI with and without field amplification micro-CZE in isolation scan mode. In this mode, we isolated ions in range of m/z 578 - 588, which covers the target and internal standard peptide. The spectra and results of peptides in different human serum matrix system after analysis are shown for comparison.

be achieved by averaging 7 scans for reliable quantification, the screening rate can be further decreased but not to less than 2s/sample. We also tested the carryover using one emitter for multiple dip-and-go measurements to evaluate the feasibility of using the emitters multiple times for analysis of a full microtiter plate. As shown in Figure 5.9, we used a single emitter for "dip and go" analysis of 10 samples. Any two consecutive samples were spiked to show 16-fold differences in KTEEISEVNL to IS ratio. The results show an average deviation of 2.5% for these ten measurements, indicating very small carryover when using a single emitter multiple times. Briefly, the relative standard deviation was less than 15% at a scan rate of 2s/sample to 4s/sample with little carryover. The above results demonstrate the power of the dip-and-go multiplexed system in bioassays.

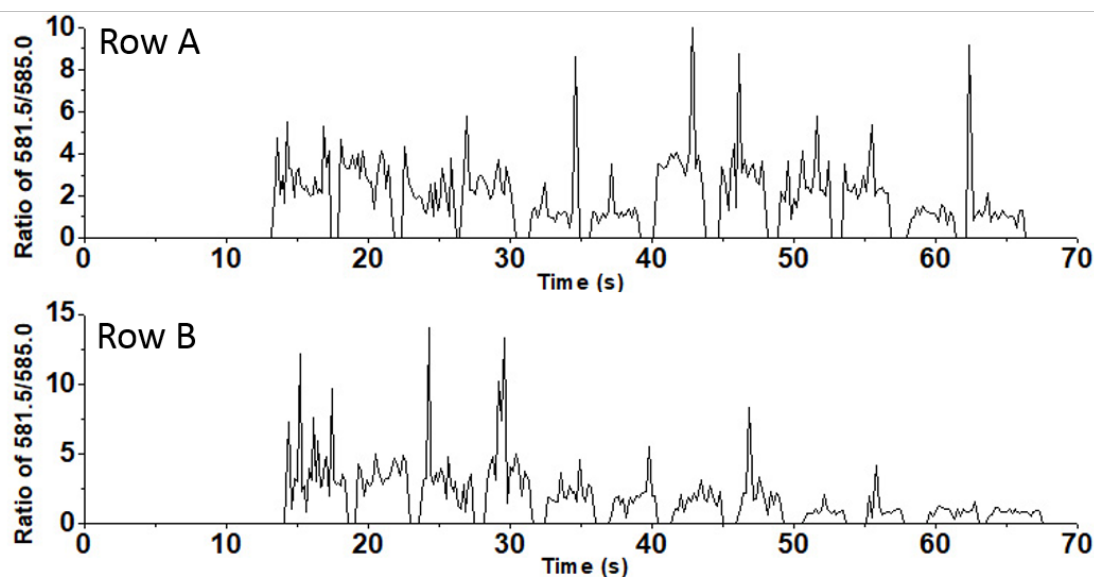


Figure 5.8. HTS bioassays of KTEEISEVNL (m/z 581.5) with 250 nM KTEEISEVNL(L - $^{13}C_7$) (m/z 585.0) as internal standard in reaction buffer (2 nM BACE1 enzyme, 6 mM sodium acetate, 1.5% glycerol, 0.25% DMSO, 3 ppm Brij-27 and 1% formic acid) using the dip-and-go multiplexed system. The intensity of KTEEISEVNL and IS are from the full scan MS. The screening rate is 4s/sample and the total analysis time for one row is ca. 50 s. The average deviation for row A is 11.0% and for row B is 6.1%

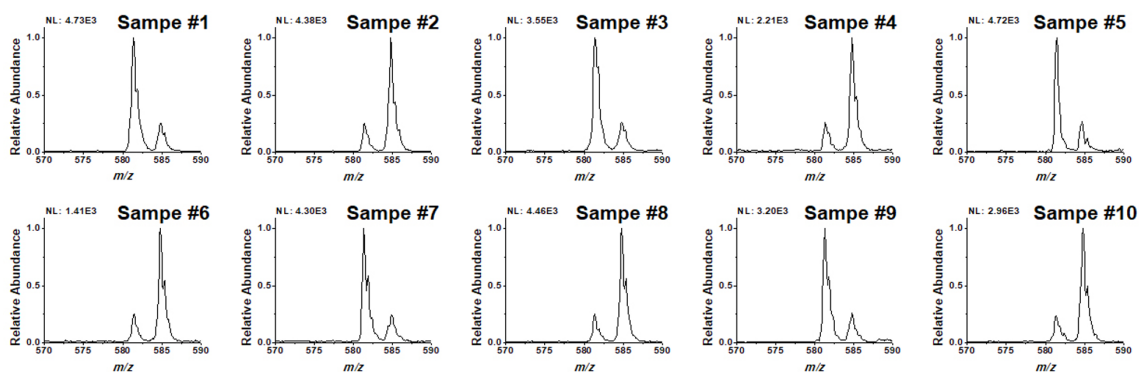


Figure 5.9. Test of carryover using one emitter for multiple measurements. For all the samples with odd numbers, we spiked the target molecule (TM) KTEEISEVNL and internal standard (IS) in a ratio of 4:1 (1000 nM and 250 nM) in reaction buffer (2 nM BACE1 enzyme, 6 mM sodium acetate, 1.5% glycerol, 0.25% DMSO, 3 ppm Brij-27 and 1% formic acid). For all the samples with even numbers, the ratio of TM to IS is 1:4 (250 nM and 1000 nM). We used the same emitter for dip-and-go measurements of Samples 1 to 10. The spectra are shown. The average deviation of experimental ratio from expected ratio is 2.5%, indicating very small carryover when reusing one emitter multiple times.

Figure 5.10 shows the operating mode of field amplification micro-electrophoresis. Figure 5.10(a) shows the formation of three distinct sample and solvent zones before electrophoresis: the highly conductive sample solution with its complex matrix (Zone 2) and the surrounding low conductivity leading (Zone 1) and trailing (Zone 3) zones of pure water. Electrophoresis (on at 3 s, off at 12 s) in Figure 5.10(b) was performed by simply changing the electrode voltage from zero to -5 kV and maintaining this value for ca. 10 s. After electrophoresis (12 s to 45 s) in Figure 5.10(b), the electrode voltage was changed to 3 kV for inductive nESI analysis. The total ion chromatogram (TIC) in Figure 5.10(c) after cleaning is stable while the ion map in Figure 5.10(d) shows multiple extracted ion chromatograms. Three typical zones appear after clean-up as observed in Figure 5.10(e). Typical mass spectra of Zone 1 are very noisy; the spectrum of Zone 2 is very clean with the analyte peptides displaying very high SNR and enhanced signal intensity, while the spectrum of Zone 3 shows matrix peaks. These results are consistent with the following proposed mechanism, based on our prior study of this effect:^[20,24,26] during electrophoresis (-5 kV voltage applied to the electrode) a strong static electrical field in the solution pulls cations and positively charged complexes into Zone 3 (they show up later as the interference peaks in the MS of Zone 3); the initial negative potential also pushes anions into Zone 1 so cleaning the analyte in Zone 2 of negatively charged ions. By removal of the high mobility ions from Zone 2, a commensurate narrowing of the bandwidth and preconcentration of weak electrolytes (e.g. peptides) within Zone 2 will occur to compensate for the decrease in conductivity. Since electrical field strength is inversely proportional to conductivity,^[28] an amplified electrical field is created inside zones 1 and 3 which accelerates the separation (additional discussion of the clean-up process is available in Supporting Information). This special field amplification operating mode for micro-electrophoresis is quite different from traditional field amplification capillary zone electrophoresis,^[31-33] in which the sample zone has much lower conductivity than the surrounding buffer used for electrophoresis. Indeed, this operating mode is generally not achievable in traditional capillary zone electrophoresis because

buffer solution with good conductivity is needed to control the Joule heating that limits performance in electrophoresis.^[34] In the micro-electrophoresis driven by the inductive static electrical field, the current is much lower.^[20,35] Since the sample volume introduced by our dip-and-go strategy is on the order of 100 nL, a low current generates sufficient electrophoretic separation without excessive Joule heating.

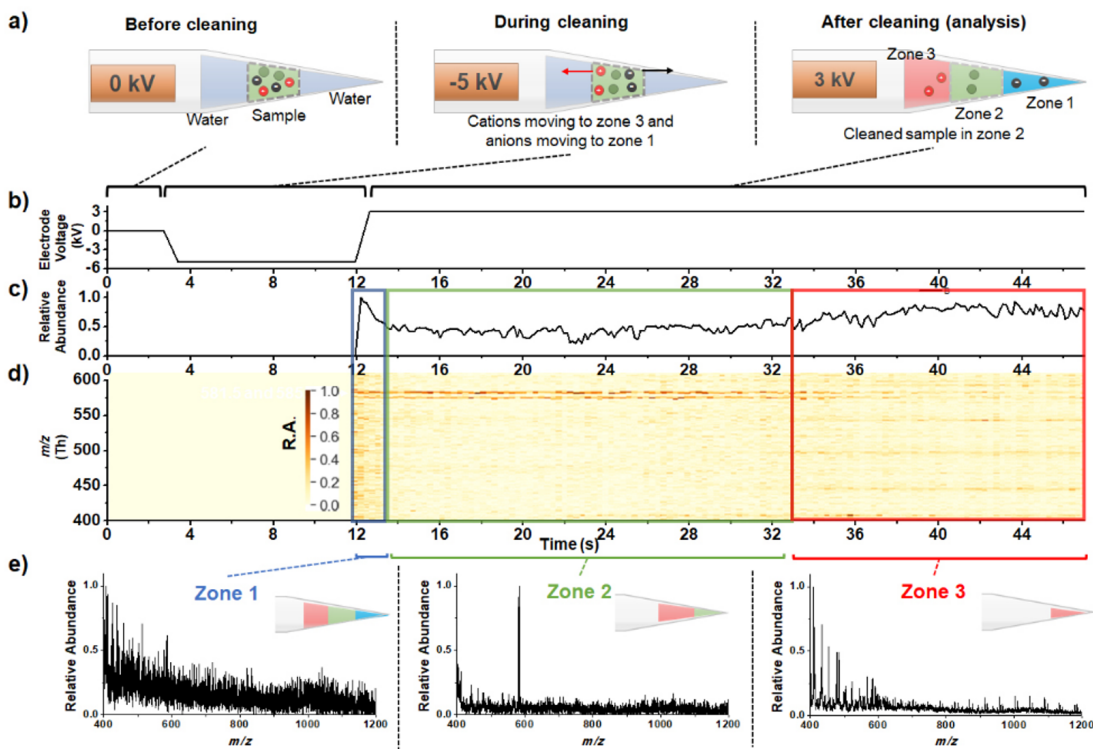


Figure 5.10. Process of field amplification micro-electrophoresis. (a) Ion migration in each step (note that electroneutrality will be maintained over the whole solution volume including Zones 1, 2, and 3 while each individual zone can have a net charge). (b) Electrode voltage vs. time in the process. (c) TIC over course of the process. (d) Ion map of the process. (e) Typical mass spectra from the three zone.)

5.4.3 High-Throughput Bioassays

As an example of a prototypical HTS application, we used our dip-and-go multiplexed system to determine the IC_{50} of the well-characterized BACE1 inhibitor OM99-2 by following BACE1 catalyzed hydrolysis of KTEEISEVNLDAEFRHDK to KTEEISEVNL. We spiked 150 nM KTEEISEVN(L- $^{13}C_7$) into the final assay as internal standard. Since the concentration of the peptide product can be very low in highly inhibited reactions, we used the MS/MS scan mode for quantification and determination of IC_{50} . As shown in Figure 5.11(a), for an artificial solution with 1 : 1 ratio of KTEEISEVNL:IS, we isolated ions from m/z 578 to 588 and fragmented them before recording product ion spectra. Two pairs of product ions showing a 1 : 1 intensity ratio for the 7 Da (singly charged) mass difference appear: the pair of m/z 246.2 to 253.2 and the pair of m/z 561.3 and 568.3. As the ion pair m/z 246.2 and 253.2 shows a very low baseline and the very high SNR of 110, this pair was used for quantification. (The advantages of the product ion spectrum vs. simple ion isolation are shown in Figure 5.12.) Twelve samples were prepared spanning 5 orders of magnitude range of OM99-2 concentrations in order to determine the IC_{50} against BACE1. These samples were placed in 7 rows (7 replicates, 84 samples in total) of a microtiter plate and analyzed by dip-and-go analysis. Figure 5.11(b) shows a typical TIC as well as EIC for the IS and target peptide from analysis of one row of samples at a scan rate of 3.5 s/sample. From left to right the inhibition is 100 % to 0 %. These seven measurements were normalized to plot the IC_{50} curve shown in Figure 5.11(c).

The IC_{50} curve determined by our dip-and-go multiplexed system is consistent with that determined by an LC-MS experiment performed specifically to allow this comparison in Figure 5.13. The total measurement time of these 84 samples by the dip-and-go method was only ca. 14 min while that for LC-MS was 11 h (8 min/sample).

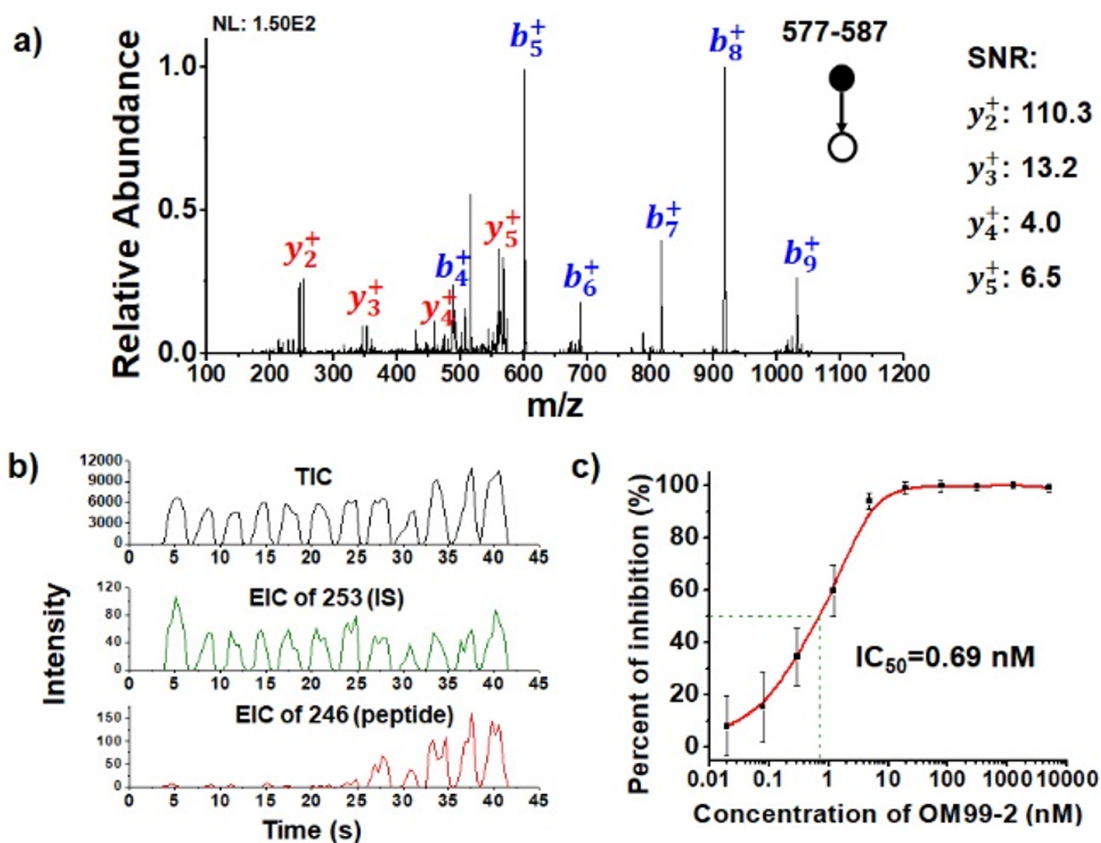


Figure 5.11. (a) MS/MS spectrum of precursor ions in range of m/z 578 to m/z 588. The collision energy used is 30 (nominal value). This range covers the doubly charged precursor ions of KTEEISEVNL (m/z 581.5) and IS (m/z 585.0). The spiked ratio of the KTEEISEVNL and IS is 1 : 1. (b) Typical TIC and EIC of dip-and-go analysis of one row of samples. (c) IC_{50} of inhibitor OM99-2 to BACE1 determined using the dip-and-go system.

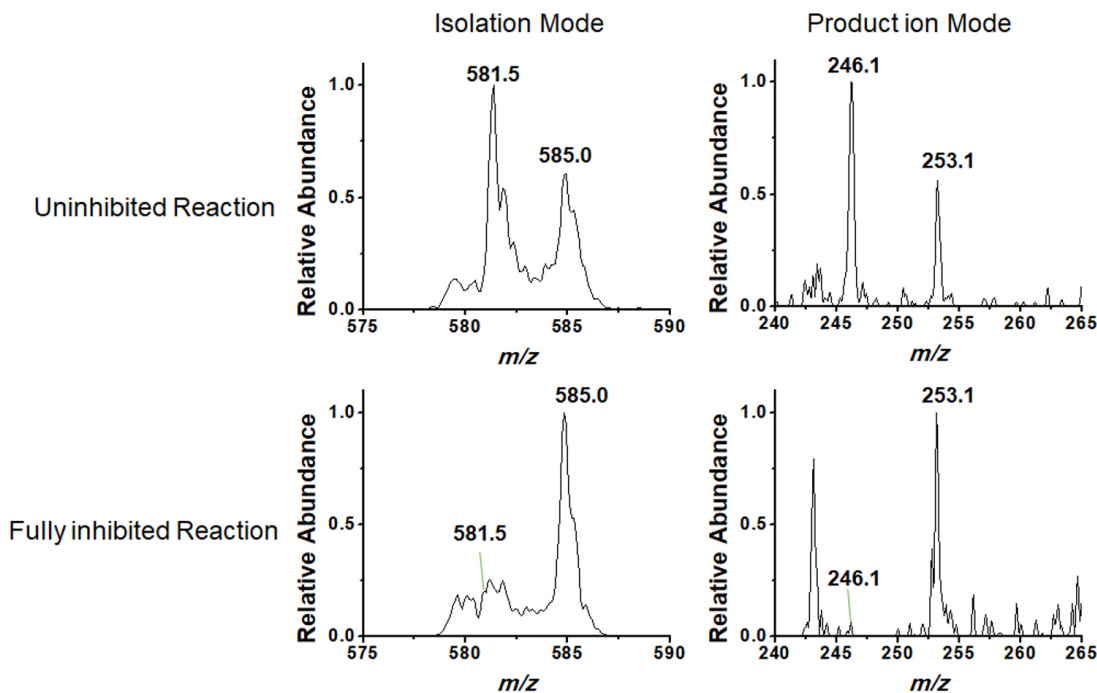


Figure 5.12. Inductive nESI spectra with field amplification micro-CZE for analysis of KTEEISEVNL (m/z 581.5 in full scan, m/z 246.1 in product ion scan) after uninhibited and fully inhibited reaction with 150 nM KTEEISEVN(L- $^{13}\text{C}_7$) (m/z 585.0 in full scan, m/z 253.1 in product ion scan) as internal standard. The left column shows the spectra in isolation scan mode and the right shows product ion scan spectra. The SNRs in product ion spectra are much better than isolation scan spectra, so can be used for quantification. The determined concentration of KTEEISEVNL after uninhibited reaction is 272 nM after fully inhibited reaction is 3.0 nM.

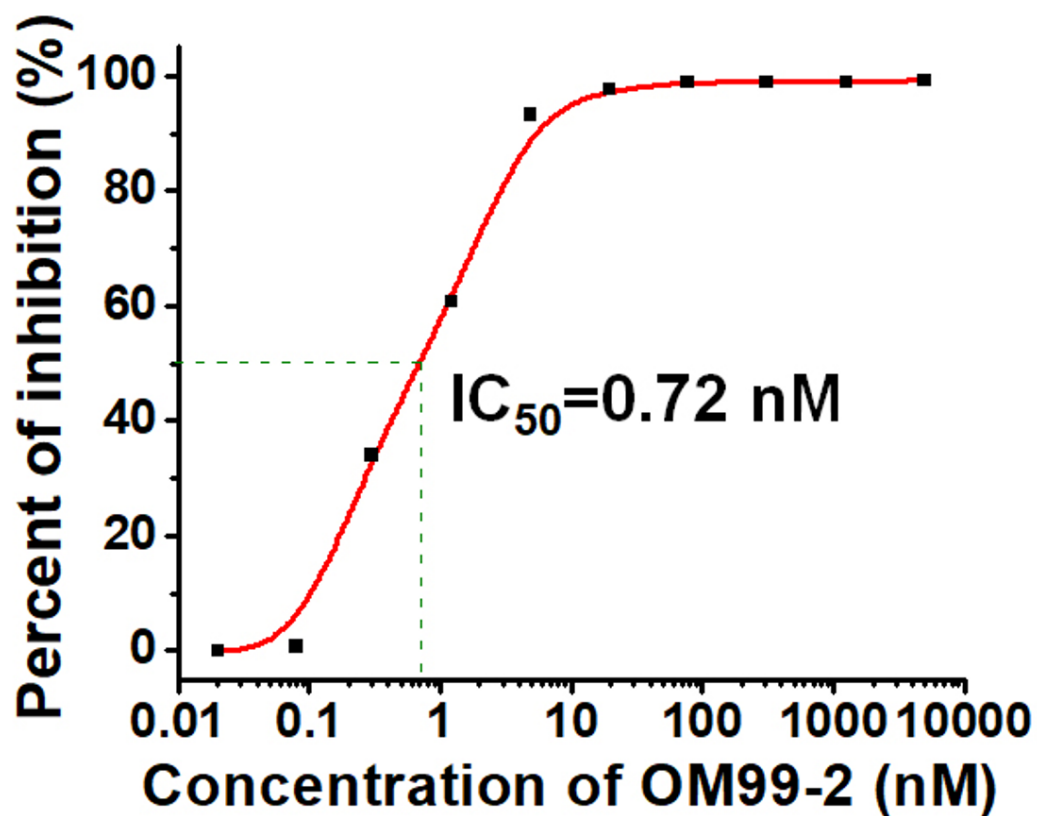


Figure 5.13. IC_{50} of OM99-2 to BACE1 determined by LC-TOF-MS. This figure is from one measurement (12 samples). Each sample took ca. 8 min for analysis. The total analysis time is ca. 1.5 h.

5.5 Discussions on Electrophoretic Cleaning and Ion Stacking

It is notable that the electrophoresis discussed in this study is different from traditional electrophoresis with electrolyte bath solutions to balance the potential in the capillary. Micro-electrophoresis in the small volume of nESI emitter tip is produced by enhanced ion migration at high electric field that still follows the mechanism of electrospray.^[24] Since there is no electrolyte bath solution to balance the electroneutrality of the solution, the solution will be polarized by the external electric field. Electroneutrality need not to be maintained everywhere in the solution, however, electroneutrality of the whole solution must obtain due to Gaussian's law and the law of conservation of charge.^[20] As a result, ions with opposite polarity will stack near one of the two ends of the solution (capacity charge). Electrochemical reactions will occur at the interfaces at both ends of the solution^[36,37] to transfer aggregated charges to the air (capacitance discharge or equivalent chemical reaction) to make this procedure continuous.

Except for the above major difference, the special micro-electrophoresis discussed here is analogous to traditional capillary electrophoresis that they are both accompanied by electroosmotic flow if the walls are not silanized. In this study, we have introduced a field amplification operating mode in which the sample is loaded between two zones of pure water. This operating mode will not change the mechanism of micro-electrophoresis, but it does enhance the performance due to the stacking effect. As silanized emitters will negatively affect the nESI-MS performance, the emitters used were not silanized so electroosmotic flow is inevitable and will cause severe loss of sample. The introduction of leading zone and stacking of target molecules in the mid zone helps overcome this problem and provides higher sensitivity.

From the typical spectrum of Zone 1, the baseline is very high however the signal intensity is very low. The reason for this is during electrophoretic clean-up, anions (e.g. formate) are stacking in Zone 1. After clean-up, there is slow relaxation (depo-

larization) of the solution so a lot of formate will still be in Zone 1. This will make the positive ion spectrum of Zone 1 very noisy. When comparing the spectrum of Zone 3 to the spectrum before clean-up, it is interesting that we observed the dissociation of Brij-27 and sodium formate clusters as shown in Figure 5.14. In the spectrum, the interfering peaks of Brij polymers have a shift of -272 Da, which is due to the loss of $(\text{HCOONa})_4$. We examined the new Brij polymer peaks and found these peaks are just $[\text{Brij-27} + \text{Na}]^+$. With the above two findings and no observation of formate salt clusters in this zone, the only plausible explanation is formate is stacking in the leading zone while electrophoretic clean-up occurs. Following the same logic, we can deduce that sodium is stacking in the trailing zone and binding to Brij during solution relaxation just after clean-up.

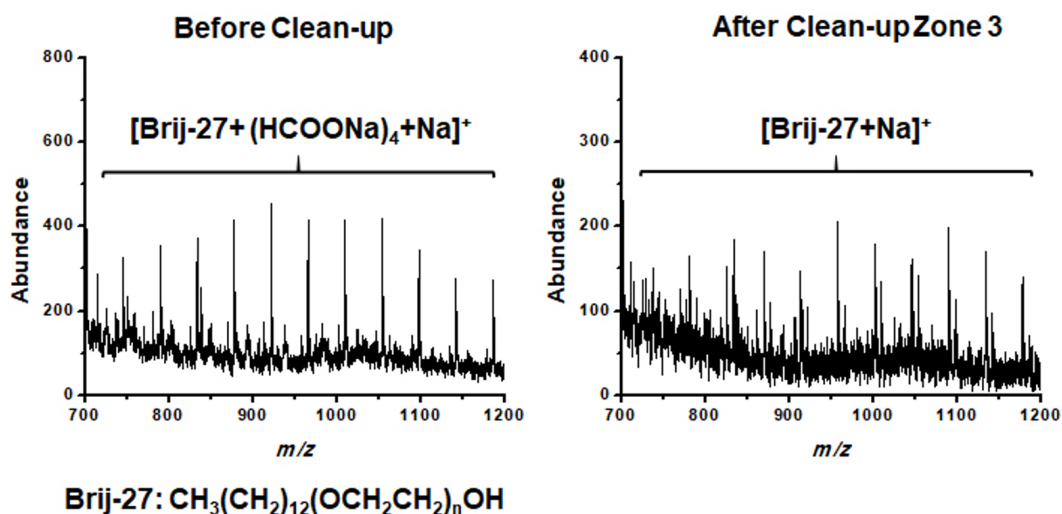


Figure 5.14. Break-up of binding of Brij-27 and sodium formate clusters before and after clean-up indicates the stacking of cations and anions in different zones after electrophoretic clean-up.

5.6 Summary

In summary, we have developed a dip-and-go multiplexed system that is suitable for HTS bioassays. This system uses a novel "dip" sample loading strategy which can be combined with inductive nESI to achieve HTS nESI analysis for the first time. We have developed a new operating mode for field amplification micro-electrophoresis in which small volumes of reaction solution are (i) purified *in situ* and (ii) preconcentrated. This method enables accelerated sample clean-up and ultra-high sensitivity HTS bioassays. The dip-and-go system shown in this manuscript is a lab prototype; the process of "dip" sample introduction is not fully automated; the voltage control system should also be improved, and data processing software needs to be developed. The screening rate of the prototype is 1.3 s/sample to 3.5 s/sample and the total analysis time for 96 samples is ca. 16 min, representing a significant improvement over the throughput of conventional LC-MS (several min per sample) and competitive with typical "catch and elute" SPE-MS systems used for current HTS bioassays such as the RapidFire platform (ca. 8 s/sample). With the aid of high-resolution MS, the performance of the "dip-and-go" system can be further improved. The current multiplexed system is quite efficient for the analysis of compounds with low electrical mobility, e.g. oligosaccharides and peptides, because they can be preconcentrated in the mid zone and separated from matrix components; the clean-up for small metabolites is still challenging since they may move together with the salts. We believe that with further optimization this system has the potential to play a significant role in accelerating chemical and pharmaceutical discovery.

5.7 References

- [1] J. Drews, *Science* **2000**, *287*, 1960–1964.
- [2] D. B. Kassel, *Chemical Reviews* **2001**, *101*, 255–267.
- [3] A. Gaulton, L. J. Bellis, A. P. Bento, J. Chambers, M. Davies, A. Hersey, Y. Light, S. McGlinchey, D. Michalovich, B. Al-Lazikani, J. P. Overington, *Nucleic Acids Research* **2012**, *40*, D1100–D1107.

- [4] M. J. Wildey, A. Haunso, M. Tudor, M. Webb, J. H. Connick in *Annual Reports in Medicinal Chemistry, Vol. 50*, Elsevier Inc., **2017**, Chapter 5, pp. 149–195.
- [5] K. H. Shaughnessy, P. Kim, J. F. Hartwig, *Journal of the American Chemical Society* **1999**, *121*, 2123–2132.
- [6] J. W. Noah, W. Severson, D. L. Noah, L. Rasmussen, E. L. White, C. B. Jonsson, *Antiviral Research* **2007**, *73*, 50–59.
- [7] J. B. Baell, J. W. M. Nissink, *ACS Chemical Biology* **2018**, *13*, 36–44.
- [8] X. S. Song, J. Zhang, X. U. Chen, O. Palyha, C. Chung, L. M. Sonatore, L. Wilsie, S. Stout, D. G. McLaren, A. Taggart, J. E. Imbriglio, S. Pinto, M. Garcia-Calvo, G. H. Addona, *Journal of Biomolecular Screening* **2016**, *21*, (Eds.: J. Wingfield, I. D. Wilson), 117–126.
- [9] C. Haslam, J. Hellicar, A. Dunn, A. Fuetterer, N. Hardy, P. Marshall, R. Paape, M. Pemberton, A. Resemannand, M. Leveridge, *Journal of Biomolecular Screening* **2016**, *21*, (Eds.: J. Wingfield, I. D. Wilson), 176–186.
- [10] M. Winter, T. Bretschneider, C. Kleiner, R. Ries, J. P. Hehn, N. Redemann, A. H. Luippold, D. Bischoff, F. H. Büttner, *SLAS Discovery* **2018**, *23*, 561–573.
- [11] M. Winter, R. Ries, C. Kleiner, D. Bischoff, A. H. Luippold, T. Bretschneider, F. H. Büttner, *SLAS Technology* **2019**, *24*, 209–221.
- [12] I. Sinclair, R. Stearns, S. Pringle, J. Wingfield, S. Datwani, E. Hall, L. Ghislain, L. Majlof, M. Bachman, *Journal of Laboratory Automation* **2016**, *21*, (Eds.: J. Olechno, C. Green, L. Rasmussen), 19–26.
- [13] G. A. Gómez-Ríos, C. Liu, M. Tascon, N. Reyes-Garcés, D. W. Arnold, T. R. Covey, J. Pawliszyn, *Analytical Chemistry* **2017**, *89*, 3805–3809.
- [14] M. Wilm, M. Mann, *Analytical Chemistry* **1996**, *68*, 1–8.
- [15] I. M. Lazar, R. S. Ramsey, S. Sundberg, J. Michael Ramsey, *Analytical Chemistry* **1999**, *71*, 3627–3631.
- [16] U. Bahr, A. Pfenninger, M. Karas, B. Stahl, *Analytical Chemistry* **1997**, *69*, 4530–4535.
- [17] X. Guo, T. L. Fillmore, Y. Gao, K. Tang, *Analytical Chemistry* **2016**, *88*, 4418–4425.
- [18] G. Huang, G. Li, J. Ducan, Z. Ouyang, R. G. Cooks, *Angewandte Chemie - International Edition* **2011**, *50*, 2503–2506.
- [19] G. Huang, G. Li, R. G. Cooks, *Angewandte Chemie - International Edition* **2011**, *50*, 9907–9910.
- [20] Z. Wei, X. Xiong, C. Guo, X. Si, Y. Zhao, M. He, C. Yang, W. Xu, F. Tang, X. Fang, S. Zhang, X. Zhang, *Analytical Chemistry* **2015**, *87*, 11242–11248.
- [21] N. Gasilova, Q. Yu, L. Qiao, H. H. Girault, *Angewandte Chemie - International Edition* **2014**, *53*, 4408–4412.

- [22] L. Qiao, R. Sartor, N. Gasilova, Y. Lu, E. Tobolkina, B. Liu, H. H. Girault, *Analytical Chemistry* **2012**, *84*, 7422–7430.
- [23] G. Li, S. Yuan, S. Zheng, Y. Liu, G. Huang, *Analytical Chemistry* **2018**, *90*, 3409–3415.
- [24] Z. Wei, S. Han, X. Gong, Y. Zhao, C. Yang, S. Zhang, X. Zhang, *Angewandte Chemie - International Edition* **2013**, *52*, 11025–11028.
- [25] X. Gong, X. Xiong, Y. Zhao, S. Ye, X. Fang, *Analytical Chemistry* **2017**, *89*, 7009–7016.
- [26] Z. Zhang, C. J. Pulliam, T. Flick, R. G. Cooks, *Analytical Chemistry* **2018**, *90*, 3856–3862.
- [27] H. Zhu, G. Zou, N. Wang, M. Zhuang, W. Xiong, G. Huang, *Proceedings of the National Academy of Sciences of the United States of America* **2017**, *114*, 2586–2591.
- [28] J. Lichtenberg, E. Verpoorte, N. F. de Rooij, *Electrophoresis* **2001**, *22*, 258–271.
- [29] G. C. Adam, J. Meng, J. M. Rizzo, A. Amoss, J. W. Lusén, A. Patel, D. Riley, R. Hunt, P. Zuck, E. N. Johnson, V. N. Uebele, J. D. Hermes, *Journal of Biomolecular Screening* **2015**, *20*, 212–222.
- [30] Z. Wei, M. Wleklinski, C. Ferreira, R. G. Cooks, *Angewandte Chemie - International Edition* **2017**, *56*, 9386–9390.
- [31] F. E. Mikkers, F. M. Everaerts, T. P. Verheggen, *Journal of Chromatography A* **1979**, *169*, 11–20.
- [32] R. L. Chien, J. C. Helmer, *Analytical Chemistry* **1991**, *63*, 1354–1361.
- [33] D. S. Burgi, R. L. Chien, *Analytical Chemistry* **1991**, *63*, 2042–2047.
- [34] G. Tang, D. Yan, C. Yang, H. Gong, J. C. Chai, Y. C. Lam, *Electrophoresis* **2006**, *27*, (Ed.: B. Gaš), 628–639.
- [35] A. Li, A. Hollerbach, Q. Luo, R. G. Cooks, *Angewandte Chemie - International Edition* **2015**, *54*, 6893–6895.
- [36] G. J. Van Berkel, F. Zhou, *Analytical Chemistry* **1995**, *67*, 2916–2923.
- [37] G. J. Van Berkel, F. Zhou, *Analytical Chemistry* **1995**, *67*, 3958–3964.

VITA

VITA

Zhuoer Xie was born in Changsha, Hunan, a central southern city in China. He lived there until 2011, when he attended Nankai University (NKU) in Tianjin, China. Zhuoer's major was Materials Chemistry in the Department of Chemistry. He carried out his first research in 2013 focusing on designing and characterizing core-shell structure catalyst for reduction of stearic acid to generate biofuel under the supervision of Prof. Naijia Guan and Prof. Landong Li. In 2014, Zhuoer started his theoretical and simulation study of critical fluid using lattice-fluid model as his undergraduate dissertation thesis with guidance from Prof. Ping Qiu. Zhuoer received his BSc. in Chemistry from NKU in 2015 and then became a graduate student in Purdue University, West Lafayette, IN, with the Ross Fellowship. Later in the fall, he officially joined Prof. R. Graham Cooks' lab for doctoral research. Zhuoer dedicated himself to analytical method development, innovation in ionization techniques, and lipid and metabolite profiling of biological samples, especially using multiple reaction monitoring profiling (MRM-profiling) workflow to expedite the exploratory research. Besides, he has also gained experiences in basic electronics, 3D modeling, statistical analysis, and bacterial culturing. In summer of 2017, he spent one month at PurSpec Inc. in Beijing, China, to master the mechanism, manipulation, and maintenance of a miniature mass spectrometer, Mini β . With this training, Zhuoer has contributed to projects regarding intraoperative diagnostic of glioma on Mini β . Zhuoer is a member of the Phi Lambda Upsilon (PLU) honor society as well as the American Society for Mass Spectrometry (ASMS) from 2016. In the meantime, Zhuoer has attended numerous conferences to present his research, including the Annual ASMS Conference, NIST Foodsafety Workshop, and AbbVie Analytical Research Symposium.

PUBLICATIONS

Multiple Reaction Monitoring Profiling (MRM-Profilng) of Lipids To Distinguish Strain-Level Differences in Microbial Resistance in *Escherichia coli*

Zhuoer Xie,[†] L. Edwin Gonzalez,[†] Christina R. Ferreira,^{†,‡} Anna Vorsilak,[§] Dylan Frabutt,[§] Tiago J. P. Sobreira,[‡] Michael Puglia,^{*,§} and R. Graham Cooks^{*,†,§}

[†]Department of Chemistry, Purdue University, West Lafayette, Indiana 47907, United States

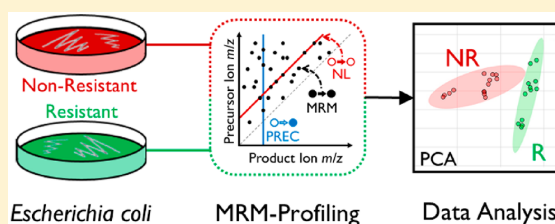
[‡]Bindley Bioscience Center, Purdue University, West Lafayette, Indiana 47907, United States

[§]Indiana Biosciences Research Institute, Indianapolis, Indiana 46202, United States

Supporting Information

ABSTRACT: The worldwide increase in antimicrobial resistance is due to antibiotic overuse in agriculture and overprescription in medicine. For appropriate and timely patient support, faster diagnosis of antimicrobial resistance is required. Current methods for bacterial identification rely on genomics and proteomics and use comparisons with databases of known strains, but the diagnostic value of metabolites and lipids has not been explored significantly. Standard mass spectrometry/chromatography methods involve multiple dilutions during sample preparation and separation. To

increase the amount of chemical information acquired and the speed of analysis of lipids, multiple reaction monitoring profiling (MRM-Profilng) has been applied. The MRM-Profilng workflow includes a discovery stage and a screening stage. The discovery stage employs precursor (PREC) ion and neutral loss (NL) scans to screen representative pooled samples for functional groups associated with particular lipid classes. The information from the first stage is organized in precursor/product ion pairs, or MRMs, and the screening stage rapidly interrogates individual samples for these MRMs. In this study, we performed MRM-Profilng of lipid extracts from four different strains of *Escherichia coli* cultured with amoxicillin or amoxicillin/clavulanate, a β -lactam and β -lactamase inhibitor, respectively. *t* tests, analysis of variance and receiver operating characteristic (ROC) curves were used to determine the significance of each MRM. Principal component analysis was applied to distinguish different strains cultured under conditions that allowed or disallowed development of bacterial resistance. The results demonstrate that MRM-Profilng distinguishes the lipid profiles of resistant and nonresistant *E. coli* strains.



Annually there are over 1.2 billion health care visits in the United States of which 12.6% result in ~154 million antibiotic prescriptions for bacterial infections.¹ Urinary, respiratory, and skin infections are most common.² The top pathogens responsible for 80% to 90% of infections are *Escherichia coli*, *Staphylococcus aureus*, and *Klebsiella pneumoniae*, the latter two of which are part of the ESKAPE group of pathogens which also include *Enterococcus faecium*, *Acinetobacter baumannii*, *Pseudomonas aeruginosa*, and *Enterobacter* species.^{3–5} Infections are especially common in certain care settings and patient populations where they cause high recurrence rates and great severity of infections.^{6–8} Potential infections are frequently treated prior to confirmation of the presence of pathogens, leading to overprescription which is strongly associated with the development of antibiotic-resistance and may eradicate potentially commensal microbiome populations, resulting in dysfunction against future pathogens.^{9–12} High rates of infection recurrence and the emergence of pathogens with antimicrobial resistance are found among patients with frequent antibiotic dosing.^{11,13,14}

There therefore remains a need for rapid bacterial identification to help suppress this process.

In current clinical settings, the identification of bacteria is usually determined based on phenotype and/or genotype. Culture-based phenotyping methods are commonly used in clinical laboratories.^{15,16} Molecular diagnosis, including sequencing of ribosomal genes,¹⁷ whole genome sequencing,^{18,19} and amplification methods,²⁰ represents an alternative strategy for bacterial typing. Current MS-based typing methods are largely focused on the protein profile with an emphasis on ribosomal proteins.¹⁶ In the past decade, matrix assisted laser desorption/ionization coupled with time-of-flight mass spectrometry (MALDI-TOF MS) has been applied successfully using relatively simple sample preparations to acquire fingerprint mass spectra and accomplish identification by database searches.^{21–23} Several commercial platforms have emerged and

Received: May 28, 2019

Accepted: August 9, 2019

Published: August 9, 2019

profoundly changed the state of clinical testing. In addition, tandem MS with or without liquid chromatography has also been used with great success.^{24–26}

Metabolomics, which covers a wide range of small molecules but is not widely applied to bacterial identification, is an appealing and emerging field of omics in biomarker discovery by MS.^{27–30} Lipids are believed to play an indispensable metabolic role in many essential biological processes. In microorganisms, the diversity in structures and the complexity of biosynthesis pathways of bacterial lipids enable bacterial cells to adjust their lipid profiles in response to environmental changes, including antibiotic treatment.^{31–33} Conventional lipid pathway analysis involves extensive sample preparation and complex protocols for the characterization of potential lipid biomarkers.^{34,35} The unclear relationship between lipids and molecular function further slows down the pace of development of analytical methods. To accelerate exploratory lipidomic discovery, a novel two-stage methodology, multiple reaction monitoring profiling (MRM-Profiling), has been developed as a diagnostic/distinguishing factor. It has previously been tested on several model systems, including Parkinson's disease,³⁶ polycystic ovarian syndrome,³⁷ diet compliance,³⁸ colostrum uptake,³⁹ atopic dermatitis,⁴⁰ and embryo metabolism.⁴¹ The results of MRM-Profiling have proven to be broadly consistent with those from pathological or clinical analysis.

Here we report a study on the feasibility of using MRM-Profiling to differentiate lipid profile differences among bacterial strains with different antimicrobial resistance. Lipid extracts of bacteria were analyzed using electrospray ionization MS (ESI-MS), screened by precursor ion and neutral loss scans and discriminated using PCA. The experiments focused on glycerophospholipids and sphingolipids. Statistical analytical methods, specifically the *t* test and ROC curves, provided details as to which of the MRMs were most informative. Additionally, lipid differences observed among bacteria treated using various concentrations of amoxicillin and amoxicillin/clavulanate indicated that lipid profiles are modulated by environmental changes. The lipid composition of bacterial lysates was found to allow discrimination between resistant and nonresistant *E. coli* strains.

EXPERIMENTAL SECTION

Chemicals. All chemicals were purchased from Sigma-Aldrich Co., LLC (St. Louis, MO) except that clavulanate was purchased from Crescent Chemical (Bangladesh).

Bacterial Culture. Nonresistant *E. coli* strains (ATCC 25922, CDC AR-bank #0077, ATCC 4157) and resistant strains with beta-lactam resistance gene CTX-M-14 or 15 (CDC AR-bank #0086, CDC AR-bank #0162, CDC AR-bank #0151) were obtained from the ATCC or the CDC and FDA antibiotic resistance isolate bank. Bacterial stocks, stored at $-80\text{ }^{\circ}\text{C}$ until usage, were generated from tryptic soy broth (TSB) (Becton Dickinson, Franklin Lakes, NJ) cultures inoculated with a single colony taken from streak plate isolates from the supplier's stock on tryptic soy agar (TSA) (Becton Dickinson, Franklin Lakes, NJ). Fresh bacteria were cultured from stock by gentle scraping with a sterile implement off the top of the stock and by streaking onto a fresh TSA plate for single colony growth, which was incubated for 15 h at $37\text{ }^{\circ}\text{C}$. A single colony was then restreaked onto a fresh TSA plate and was incubated for 15 h at $37\text{ }^{\circ}\text{C}$. Bacterial titer was estimated by resuspending morphologically similar colonies into 20 mL

of fresh TSB and by measuring optical density at 600 nm (OD_{600}) absorbance readings using a BioTek Synergy HTX multimode plate reader (BioTek, Winooski, VT) with McFarland standards (Scientific Device Laboratory, Inc., Des Plaines, IL). Verification of culture concentrations was performed with a 10-fold serial dilution in TSB; a $1.0\text{ }\mu\text{L}$ loopful from each dilution was streaked onto BD BBL Trypticase Soy Agar plates (Becton, Dickinson, and Co., Franklin Lakes, NJ), and colonies were counted after incubation at $37\text{ }^{\circ}\text{C}$ for 16 h.

Minimum Inhibitory Concentration Test. A standard 96-well plate-based minimum inhibitory concentration (MIC) test was used to measure antibiotic efficiency of amoxicillin and amoxicillin/clavulanate combination against bacteria in monoculture. After overnight growth on the corresponding culture medium and OD_{600} measurement, MIC testing was performed with cation-adjusted Mueller-Hinton broth. In a row of the plate, 11 wells contained a starting culture at 5×10^5 cfu/mL challenged with decreasing antibiotic concentrations delivered by serial dilution (e.g., 128, 64, 32, 16, 8, 4, 2, 1, 0.5, 0.25, 0 $\mu\text{g}/\text{mL}$); the last well contained blank medium as a sterility control. The lowest antibiotic concentration at which no cell number increase was measured via OD_{600} after a 24-h incubation was the MIC of the antibiotic for that bacterial strain. All MIC tests were conducted in compliance with Clinical Laboratory Standards Institute (CLSI) procedures of clinical testing. The determined values of MIC for each strain appear in Table S1 of the Supporting Information (SI).

Sample Preparation. Samples of specific types of bacteria and MIC concentrations were taken from culture medium, normalized to 10^7 cells/mL by OD_{600} , and were lysed with sonication. Lysate of bacteria was collected and stored at $-80\text{ }^{\circ}\text{C}$. Lipid extraction was accomplished using the Blish–Dyer⁴² strategy. After drying, lipid extracts were redissolved in acetonitrile/methanol/300 mM ammonium acetate (3:6.65:0.35, v/v/v) and transferred into autosampler vials ready for analysis. The extract solution was diluted to 2.5×10^5 cells/ μL in vial, which is equivalent to lipid extracts of 2×10^6 cells in each injection of $8\text{ }\mu\text{L}$ solution.

Multiple Reaction Monitoring Profiling. MRM-Profiling is a two-stage MS methodology that benefits from various scan modes in tandem mass spectrometry—especially PREC and NL. In the discovery stage, PREC, NL, and MRM methods are applied to representative samples, mostly focusing on recognition of functional groups present in glycerophospholipids, acyl-carnitines, ceramides, and acyl residues containing different number of carbons with various degree of unsaturation. Specifically, glycerophospholipids contain glycerophosphate (PA), glycerophosphocholine (PC), glycerophosphoethanolamine (PE), glycerophosphoglycerol (PG), glycerophosphoinositol (PI), and glycerophosphoserine (PS). The PREC and NL scans were used as sources of MRM transitions, and these experimental data were supplemented by MRM transitions deduced from data in the online lipid database, LipidMaps. Altogether 32 NL scan methods, 33 PREC scan methods, and 13 MRM transitions, as listed in Table S2 were used to survey representative samples from *E. coli* strains CDC 0077 and CDC 0086 cultured without amoxicillin. Experiments were carried out using a triple quadrupole mass spectrometer, Agilent QQQ 6410 (Santa Clara, CA), equipped with Agilent G1367A 1100 series autosampler (Santa Clara, CA). Samples were introduced into the mass spectrometer by direct flow injection ESI, i.e.,

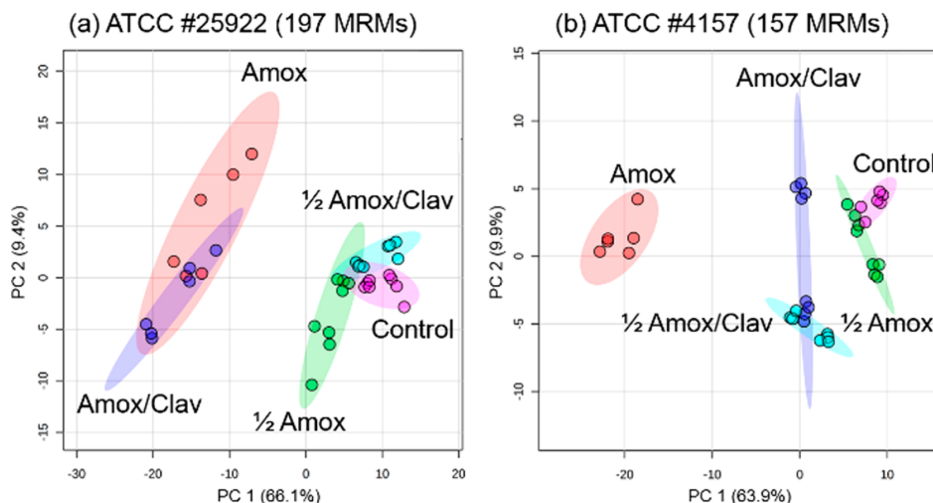


Figure 1. PCA scores plots of nonresistant bacterial strains (a) ATCC 25922 and (b) ATCC 4157 after various antibiotic treatments. The color-shaded areas are the calculated range with 95% confidence. Amoxicillin and clavulanate are abbreviated as Amox and Clav, respectively.

without chromatographic separation. The ESI voltage was -3.5 kV. Dwell time was 25 ms. Collision energy (in manufacturer's unit) and other scan method details are in Table S2. For each scan method, $8 \mu\text{L}$ of sample was injected at a flow rate of $20 \mu\text{L}/\text{min}$. After data acquisition, transitions that were at least 30% higher in ion counts than blank samples were selected. Other values of threshold or data filtering concepts could have been employed but the trade-off between chemical information and total instrument time required had an effect on the next stage, therefore we chose to be conservative to avoid losing chemical information. In addition, since representative samples were used, which could not reflect the scope of lipid profiles of all strains, keeping more transitions is beneficial to retaining as much chemical information as possible. In total, 2329 transitions, of which 1900 were in the positive ion mode and 429 in the negative ion mode, resulted from the discovery stage. The distribution of MRMs among different classes of lipids or functional groups are shown in Figures S1 and S2 for positive and negative ion modes, respectively. This list served as a pool of candidates for building up MRM methods for the next screening stage. Selected transitions were then arranged into 9 MRM methods (7 in positive ion mode, 2 in negative ion mode) to investigate individual samples using the same instrument parameters as used in the Discovery stage. Given that the screening time for each method is 3 min, this results in a total analysis time of 30 min to screen each sample.

Statistical Analysis. Raw data were processed using Proteo-Wizard to extract the ion signals of each transition. The lowest ion count was regarded as the noise level of instrument. The cutoff for the screening stage data was chosen as $3\times$ noise intensity to remove uninformative transitions with low ion intensities. The resulting data was represented as a table of ion counts, in which columns were samples and rows were features (MRMs in this case). t test, analysis of variance (ANOVA), PCA, and ROC curves were calculated and plotted using MetaboAnalyst. For PCA, ANOVA, and t test, the original data were scaled by mean-centering and dividing the individual intensities by the standard deviation of each MRM. For the ROC curve, no scaling was applied and the area under

the curve (AUC) was calculated for each MRM. The cutoff applied to the t test and ANOVA was a false discovery rate (FDR) adjusted p -value (or q -value) of 0.05 throughout the data processing.

RESULTS AND DISCUSSION

Lipid Analysis of Nonresistant Strains. Lipid analysis was carried out for nonresistant strains (ATCC 25922 and ATCC 4157) to investigate the effect of antibiotic application. Both strains were cultured under five conditions: no amoxicillin or amoxicillin/clavulanate, amoxicillin at half MIC, amoxicillin at MIC, amoxicillin/clavulanate at half MIC, and amoxicillin/clavulanate at MIC. MRMs were filtered by ion counts and FDR adjusted p -value in ANOVA, and then analyzed by PCA. Figure 1 shows the PCA scores plots of both strains. In the PCA scores plot, each point represents an individual lipid extract sample from the cultured bacteria and the elliptical shaded area is the calculated 95% confidence region for each group. In the case of ATCC 25922 as shown in Figure 1(a) where 197 MRMs were used, bacteria treated with amoxicillin or amoxicillin/clavulanate at MIC are well separated along principal component (PC) 1 from bacteria cultured at half MIC or without amoxicillin. PC1 and PC2 contribute 76% to the total variance. This separation can be attributed to the nature and the amount of the antibiotic, which leads to bacterial growth inhibition and hence the observed changes in lipid profiles.

Similar separation due to treatment differences are observed in the nonresistant strain ATCC 4157 in Figure 1(b). With the same data filters, 157 MRMs were selected. PC1 and PC2 cover 74% of the entire variance observed. Different from ATCC 25922, the group grown with amoxicillin at MIC clusters away from the other groups on the PC1 dimension in the score plot. Groups treated with amoxicillin/clavulanate tend to overlap on PC1, while control and half MIC amoxicillin are closer. The MIC amoxicillin/clavulanate group is differentiated by PC1 to be closer to groups treated with low concentration of amoxicillin, instead of merging with the MIC amoxicillin group as in ATCC 25922.

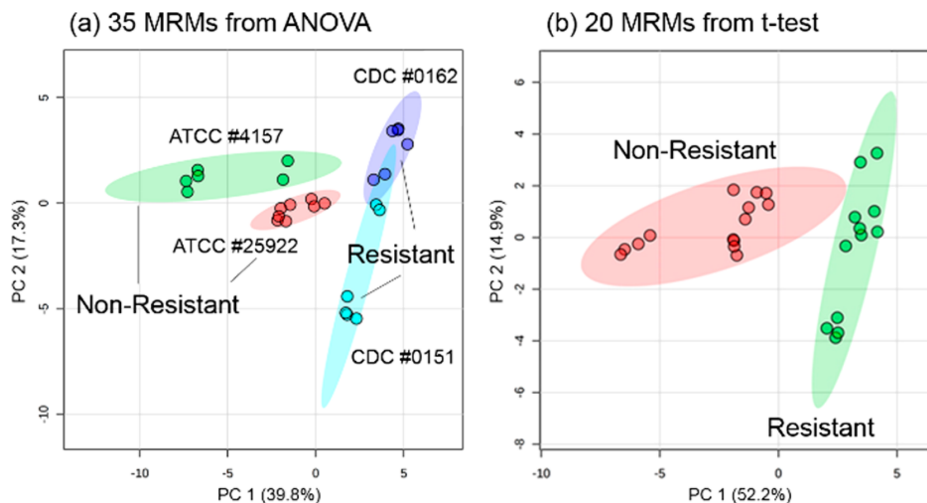


Figure 2. PCA scores plots of control samples (no amoxicillin or amoxicillin/clavulanate applied) using transitions selected from (a) ANOVA and (b) *t* test. Color-shaded areas are the calculated range with 95% confidence.

Lipid Profile Differences Between Non-Resistant and Resistant Bacterial Strains. The results of attempts to distinguish nonresistant and resistant strains are promising. The purpose of carrying out statistical analysis of different strains exposed to the same treatment is to identify transitions that are responsible for the separation between strains. Two nonresistant strains (ATCC 25922 and ATCC 4157) and two resistant strains (CDC 0162 and CDC 0151) were cultured without amoxicillin or amoxicillin/clavulanate (as controls) or with amoxicillin/clavulanate at half MIC. Transitions related to acyl-carnitines were found to be inconsistent (data not shown) and were removed from the statistics to better concentrate on the pattern of significant phospholipid transitions. Initially, for the control group, 86 MRMs were used for the statistical analysis, from which 38 MRMs were then selected using the FDR adjusted *p*-value in ANOVA. From the PCA scores plot of these transitions shown in Figure 2(a), PC1 and PC2 contribute 57% to the total variance. The major separation occurs along PC1. Statistical analysis was also carried out in terms of distinguishing nonresistant and resistant strains by regrouping samples into two sets. We note that, in cases where no antibiotic stress was applied, resistant and nonresistant strains can be well differentiated by PCA. Because PCA is an unsupervised method, the PCA scores plot remains the same regardless of the labels of each sample if the same set of data is used so *t* tests and ROC curves can provide more insight into the differences between strains. The *t* test results (Figure 2(b)) imply that 20 transitions, all of which show up in the 35 MRMs in the previous analysis, are significant for the differentiation. PC1 and PC2 take up 67% of the variance. ROC curves can be used to determine important transitions that are potentially characteristic for each set. As shown in Figure S3, there are seven transitions with AUC above 0.9, including three from saturated fatty acyl chain residues, two from PS, one from PE, and one from PG. Transitions selected from each analysis and their corresponding functional group or lipid class are tabulated in Table S3.

Turning to antibiotic treated bacteria, after elimination of transitions from acyl-carnitines and using the same data filter, 86 MRMs were left. ANOVA and *t* tests produced sets of 34

and 12 transitions with the same cutoff applied, respectively. From the PCA results in Figure S4, transitions selected from ANOVA do not provide perfect separation between ATCC 25922 and CDC 0162. Transitions from *t* tests offer similar separation along PC1 and its first two PCs explain 82% of the total variance. However, the number of features is fewer than in the control set. Among the 12 significant MRMs, three MRMs are found to have AUC above 0.9 from ROC curve, including one from PE, one from 26:0 fatty acyl chain residue, and one from PG, as shown in Figure S5. Details of transitions from each analysis are listed in Table S4. Bacteria treated with amoxicillin/clavulanate at half MIC and the controls have similar lipid transitions determined to be responsible for the separation.

Lipids associated with each MRM are postulated from the characteristic PREC and NL scans, as tabulated in Table S5. Although the exact structure of the lipids associated with each transition could not be decided merely by the MS/MS experiment, it is the pattern of the entire set of selected transitions spread over nine methods that provides reliable differentiation between strains from multiple classes of lipids. The distribution among the lipid classes of the transitions selected from *t* tests is shown in Figure 3. Application of

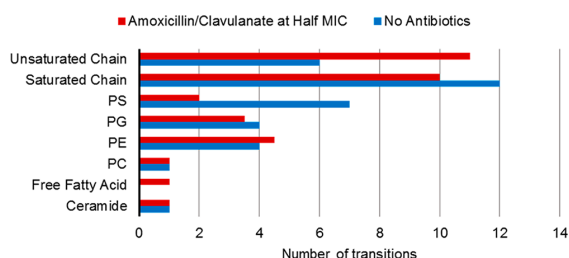


Figure 3. Distribution of transitions selected from *t* test between controls and sample treated with amoxicillin/clavulanate at half MIC. “Saturated Chain” refers to the saturated fatty acyl chain residues. “Unsaturated Chain” refers to fatty acyl chain residues with degree of unsaturation ranging from 1 to 5.

amoxicillin/clavulanate resulted in an increase in the number of informative transitions in unsaturated fatty acyl chain residues and a decrease in those in saturated fatty acyl chain residues. The number of informative transitions from PS dropped significantly after antibiotic treatment. Additionally, the total number of significant transitions from glycerophospholipids is larger when no amoxicillin or amoxicillin/clavulanate are applied, implying that more glycerophospholipids are detected. This is consistent with previous research.⁴³ In spite of these successes at differentiation, samples containing both resistant and nonresistant *E. coli* may be more difficult to distinguish.

Different from exact mass searches in the database as is done in proteomics, MRM-Profilng offers opportunity to investigate changes in functional groups with more confidence. The low resolution of the instrument and the use of direct analysis with MRM methods means that it is still possible that isomeric ion pairs exist. For example, PG (35:1) and PGo (36:1) have monoisotopic masses with close values at 762.5411 (C₄₁H₇₉O₁₀P) and 762.5775 (C₄₂H₈₃O₉P), respectively. In the MRM method, with NH₄Ac introduced into the spray, the ammonium adducts are predominant for PG, making the corresponding transitions appear as 780.5 → 591.5 for both molecules. Nevertheless, when analyzing a lipid extract, the neutral loss of 189 from the headgroup in PG is what one should focus on because both candidate ion pairs are PG. Although the number of antibiotics types is limited in current study, MRM-Profilng might be more sensitive and efficient than existing methods as there are more lipid molecules per cell and analysis of small molecules has advantages in ion transmission and ionization efficiency. This preliminary study has demonstrated the feasibility of distinguishing bacterial strains by carrying out MRM-Profilng to characterize lipid patterns.

CONCLUSIONS

We have demonstrated that MRM-Profilng can be applied to distinguish four different strains of *E. coli*, including two nonresistant and two resistant strains. Different strains are well differentiated by PCA using significant MRMs acquired from *t* test. This indicates that the lipid profiles not only serve to characterize bacterial species, but they also change in resistant strains compared to nonresistant strains and they are sensitive to antibiotic challenge. Lipid biomarker candidates are also determined, and this tool can help zeroing in on the biomarkers most significant for the separation. On the basis of previous studies in other complex biological systems, MRM-Profilng could expedite and improve the identification of lipids related with resistance, virulence, and viability. As such it will help benchmark the gene pathway involved in the phenotypes as a novel approach to identify unique resistance genes.

ASSOCIATED CONTENT

Supporting Information

The Supporting Information is available free of charge on the ACS Publications website at DOI: 10.1021/acs.analchem.9b02465.

Table S1, MIC information; Table S2, details of each scan method in discovery stage; Table S3, MRMs selected from control set; Table S4, MRMs selected from Amox/Clav set; Table S5, postulated formula of MRMs; Figure S1, distribution of positive mode MRMs;

Figure S2, distribution of negative mode MRMs; Figure S3, ROC curves of control set; Figure S4, PCA of Amox/Clav set; Figure S5, ROC curve of Amox/Clav set (PDF)

AUTHOR INFORMATION

Corresponding Authors

*E-mail: mpugia@indianabiosciences.org.

*E-mail: cooks@purdue.edu.

ORCID

R. Graham Cooks: 0000-0002-9581-9603

Notes

The authors declare no competing financial interest.

ACKNOWLEDGMENTS

This work was funded by pilot grants from Indiana Clinical and Translational Sciences Institute, Purdue University Center for Cancer Research, and Indiana Biosciences Research Institute.

REFERENCES

- (1) Fleming-Dutra, K. E.; Hersh, A. L.; Shapiro, D. J.; Bartoces, M.; Enns, E. A.; File, T. M.; Finkelstein, J. A.; Gerber, J. S.; Hyun, D. Y.; Linder, J. A.; et al. *JAMA* **2016**, *315* (17), 1864.
- (2) Mohareb, A. M.; Dugas, A. F.; Hsieh, Y.-H. *Am. J. Emerg. Med.* **2016**, *34* (6), 1059–1065.
- (3) Weiner, L. M.; Webb, A. K.; Limbago, B.; Dudeck, M. A.; Patel, J.; Kallen, A. J.; Edwards, J. R.; Sievert, D. M. *Infect. Control Hosp. Epidemiol.* **2016**, *37* (11), 1288–1301.
- (4) Santajit, S.; Indrawattana, N. *BioMed Res. Int.* **2016**, *2016*, 1–8.
- (5) Pugia, M. J.; Sommer, R. G.; Kuo, H.-H.; Corey, P. F.; Gopual, D. L.; Lott, J. A. *Clin. Chem. Lab. Med.* **2004**, *42* (3), 340–346.
- (6) Foxman, B. *Infect. Dis. Clin. North Am.* **2014**, *28* (1), 1–13.
- (7) Salvatore, S.; Salvatore, S.; Cattoni, E.; Siesto, G.; Serati, M.; Sorice, P.; Torella, M. *Eur. J. Obstet. Gynecol. Reprod. Biol.* **2011**, *156* (2), 131–136.
- (8) Gidengil, C. A.; Mehrotra, A.; Beach, S.; Setodji, C.; Hunter, G.; Linder, J. A. *J. Gen. Int. Med.* **2016**, *31* (8), 918–924.
- (9) Barlam, T. F.; Soria-Saucedo, R.; Cabral, H. J.; Kazis, L. E. *Open Forum Infect. Dis.* **2016**, *3* (1), 1–7.
- (10) Sanchez, G. V.; Master, R. N.; Karlowsky, J. A.; Bordon, J. M. *Antimicrob. Agents Chemother.* **2012**, *56* (4), 2181–2183.
- (11) Aroutcheva, A.; Gariti, D.; Simon, M.; Shott, S.; Faro, J.; Simoes, J. A.; Gurguis, A.; Faro, S. *Am. J. Obstet. Gynecol.* **2001**, *185* (2), 375–379.
- (12) Zowawi, H. M.; Harris, P. N. A.; Roberts, M. J.; Tambyah, P. A.; Schembri, M. A.; Pezzani, M. D.; Williamson, D. A.; Paterson, D. L. *Nat. Rev. Urol.* **2015**, *12* (10), 570–584.
- (13) Hibbing, M. E.; Fuqua, C.; Parsek, M. R.; Peterson, S. B. *Nat. Rev. Microbiol.* **2010**, *8* (1), 15–25.
- (14) Conway, T.; Cohen, P. S. *Microbiol. Spectrum* **2015**, *3* (3) MBP-006–2014 DOI: 10.1128/microbiolspec.MBP-0006-2014.
- (15) Castro-Escarpulli, G.; Alonso-Aguilar, N. M.; Sánchez, G. R.; Bocanegra-García, V.; Guo, X.; Juárez-Enriquez, S. R.; Luna-Herrera, J.; Martínez, C. M.; Guadalupe, A.-A. M. *Imed Pub Journals* **2015**, *7*, 1–10.
- (16) Váradi, L.; Luo, J. L.; Hibbs, D. E.; Perry, J. D.; Anderson, R. J.; Oregana, S.; Groundwater, P. W. *Chem. Soc. Rev.* **2017**, *46* (16), 4818–4832.
- (17) Janda, J. M.; Abbott, S. L. *J. Clin. Microbiol.* **2007**, *45* (9), 2761–2764.
- (18) Köser, C. U.; Ellington, M. J.; Cartwright, E. J. P.; Gillespie, S. H.; Brown, N. M.; Farrington, M.; Holden, M. T. G.; Dougan, G.; Bentley, S. D.; Parkhill, J.; et al. *PLoS Pathog.* **2012**, *8* (8), No. e1002824.

- (19) Larsen, M. V.; Cosentino, S.; Rasmussen, S.; Friis, C.; Hasman, H.; Marvig, R. L.; Jelsbak, L.; Sicheritz-Ponten, T.; Ussery, D. W.; Aarestrup, F. M.; et al. *J. Clin. Microbiol.* **2012**, *50* (4), 1355–1361.
- (20) Geha, D. J.; Uhl, J. R.; Gustafarro, C. A.; Persing, D. H. *J. Clin. Microbiol.* **1994**, *32* (7), 1768–1772.
- (21) Sauget, M.; Valot, B.; Bertrand, X.; Hocquet, D. *Trends Microbiol.* **2017**, *25* (6), 447–455.
- (22) Rodríguez-Sánchez, B.; Cercenado, E.; Coste, A. T.; Greub, G. *Eurosurveillance* **2019**, *24* (4), 1–12.
- (23) Singhal, N.; Kumar, M.; Kanaujia, P. K.; Viridi, J. S. *Front. Microbiol.* **2015**, *6*, 1–16.
- (24) Cheng, K.; Drebot, M.; McCrea, J.; Peterson, L.; Lee, D.; McCorrister, S.; Nickel, R.; Gerbasi, A.; Sloan, A.; Janella, D.; et al. *PLoS One* **2013**, *8* (2), No. e57339.
- (25) Charretier, Y.; Dauwalder, O.; Franceschi, C.; Degout-Charrette, E.; Zambardi, G.; Cecchini, T.; Bardet, C.; Lacoux, X.; Dufour, P.; Veron, L.; et al. *Sci. Rep.* **2015**, *5* (1), 13944.
- (26) Rees, J. C.; Pierce, C. L.; Schieltz, D. M.; Barr, J. R. *Anal. Chem.* **2015**, *87* (13), 6769–6777.
- (27) Guijas, C.; Montenegro-Burke, J. R.; Warth, B.; Spilker, M. E.; Siuzdak, G. *Nat. Biotechnol.* **2018**, *36* (4), 316–320.
- (28) Johnson, C. H.; Ivanisevic, J.; Siuzdak, G. *Nat. Rev. Mol. Cell Biol.* **2016**, *17* (7), 451–459.
- (29) Li, H.; Balan, P.; Vertes, A. *Angew. Chem., Int. Ed.* **2016**, *55* (48), 15035–15039.
- (30) Muhamadali, H.; Weaver, D.; Subaihi, A.; Almasoud, N.; Trivedi, D. K.; Ellis, D. I.; Linton, D.; Goodacre, R. *Analyst* **2016**, *141* (1), 111–122.
- (31) Sohlenkamp, C.; Geiger, O. *FEMS Microbiol. Rev.* **2016**, *40* (1), 133–159.
- (32) Hewelt-Belka, W.; Nakonieczna, J.; Belka, M.; Baczek, T.; Namiesnik, J.; Kot-Wasik, A. *J. Proteome Res.* **2016**, *15* (3), 914–922.
- (33) Strahl, H.; Errington, J. *Annu. Rev. Microbiol.* **2017**, *71*, 519–538.
- (34) Watson, A. D. *J. Lipid Res.* **2006**, *47* (10), 2101–2111.
- (35) Li, M.; Yang, L.; Bai, Y.; Liu, H. *Anal. Chem.* **2014**, *86* (1), 161–175.
- (36) Ferreira, C. R.; Yannell, K. E.; Mollenhauer, B.; Espy, R. D.; Cordeiro, F. B.; Ouyang, Z.; Cooks, R. G. *Analyst* **2016**, *141* (18), 5252–5255.
- (37) Cordeiro, F. B.; Ferreira, C. R.; Sobreira, T. J. P.; Yannell, K. E.; Jarmusch, A. K.; Cedenho, A. P.; Lo Turco, E. G.; Cooks, R. G. *Rapid Commun. Mass Spectrom.* **2017**, *31* (17), 1462–1470.
- (38) Dhillon, J.; Ferreira, C. R.; Sobreira, T. J. P.; Mattes, R. D. *Curr. Dev. Nutr.* **2017**, *1* (9), No. e001545.
- (39) Casey, T.; Harlow, K.; Ferreira, C. R.; Sobreira, T. J. P.; Schinckel, A.; Stewart, K. J. *Appl. Anim. Res.* **2018**, *46* (1), 667–676.
- (40) Franco, J.; Ferreira, C.; Paschoal Sobreira, T. J.; Sundberg, J. P.; HogenEsch, H. *PLoS One* **2018**, *13* (4), No. e0196595.
- (41) de Lima, C. B.; Ferreira, C. R.; Milazzotto, M. P.; Sobreira, T. J. P.; Vireque, A. A.; Cooks, R. G. *J. Mass Spectrom.* **2018**, *53* (12), 1247–1252.
- (42) Bligh, E. G.; Dyer, W. J. *Can. J. Biochem. Physiol.* **1959**, *37* (8), 911–917.
- (43) Schenk, E. R.; Nau, F.; Thompson, C. J.; Tse-Dinh, Y.-C.; Fernandez-Lima, F. *J. Mass Spectrom.* **2015**, *50* (1), 88–94.



Bioanalytics

International Edition: DOI: 10.1002/anie.201909047

German Edition: DOI: 10.1002/ange.201909047

High-Throughput Bioassays using “Dip-and-Go” Multiplexed Electro spray Mass Spectrometry

Zhenwei Wei, Zhuoer Xie, Reshma Kuvelkar, Vinit Shah, Kevin Bateman, David G. McLaren,* and R. Graham Cooks*

Abstract: A multiplexed system based on inductive nano-electrospray mass spectrometry (nESI-MS) has been developed for high-throughput screening (HTS) bioassays. This system combines inductive nESI and field amplification micro-electrophoresis to achieve a “dip-and-go” sample loading and purification strategy that enables nESI-MS based HTS assays in 96-well microtiter plates. The combination of inductive nESI and micro-electrophoresis makes it possible to perform efficient *in situ* separations and clean-up of biological samples. The sensitivity of the system is such that quantitative analysis of peptides from 1–10 000 nM can be performed in a biological matrix. A prototype of the automation system has been developed to handle 12 samples (one row of a microtiter plate) at a time. The sample loading and electrophoretic clean-up of biosamples can be done in parallel within 20 s followed by MS analysis at a rate of 1.3 to 3.5 s per sample. The system was used successfully for the quantitative analysis of BACE1-catalyzed peptide hydrolysis, a prototypical HTS assay of relevance to drug discovery. IC_{50} values for this system were in agreement with LC-MS but recorded in times more than an order of magnitude shorter.

High-throughput, target-based screening has become a staple of the drug discovery process.^[1] The introduction of robotic systems for sample preparation and plate handling enables bioassays to be run in a fully automated fashion, which allows assessment of the functional activity of small molecule compound libraries^[2] at scales in the order of millions of compounds.^[3] Optical detection formats such as absorbance, fluorescence^[4] and luminescence^[5] are well-suited to high-throughput screening (HTS) due to the rapid nature of the measurement (ca. 10–100 ms/sample). Though effective, not all bioassays are inherently suited to optical detection due to labelling reactivity, interference of the biological matrix and the emerging demands for intact molecule bioassays.^[6] For these reasons, mass spectrometry (MS) is widely considered an attractive alternative to optical

detection methods for HTS bioassays,^[1b] due to its inherent selectivity, sensitivity and label-free characteristics. As a result, a number of MS platforms have been applied to screening of bioassays, including LC-MS at rates of ca. 0.5 to 8 min/sample,^[7] RapidFire-MS at rates of ca. 6 to 8 s/sample, MALDI-MS at a rate of ca. 0.3 s/sample^[8] and, acoustic droplet ejection MS at rates of 0.5 to 1 s/sample.^[9] For the above techniques, the sacrifice in separation increases the HTS rate but can lead to loss of specificity and sensitivity in bioassays; methods enabling both high-throughput and efficient separation and analysis remain in high demand.

Nanoelectrospray ionization^[10] (nESI) is highly sensitive^[11] and one of the most robust^[12] sample introduction methods used for MS-based analysis of biological samples. The common implementation of nESI uses tapered emitters pulled from glass tubes.^[10] Nevertheless, the outstanding analytical performance of nESI has not been exploited for HTS analysis because the sample introduction step in nESI has only been done manually. In recent years, our group has developed inductive nESI which enables the ionization of liquid samples using a remote electrode.^[13] Inductive nESI, better termed inductive picelectrospray (pL min⁻¹ flowrate of spray solvent, pESI) can perform reliable analysis from small confined volumes including droplets^[14] and single cells^[13c] with sensitivity down to the zeptomole level.^[13b] When either a static^[13c,15] or alternating electrical field^[13b] is applied to initiate inductive nESI, the polarization of the liquid causes the spatial separation of ions,^[13c,16] allowing *in situ* micro-electrophoresis. This effect becomes particularly significant when: a) sample amounts are at the nanoliter level and b) the electrical field applied to initiate inductive nESI is also used to effect micro-electrophoresis. We hypothesize that the combination of inductive nESI with high performance micro-electrophoresis could constitute a promising approach for HTS bioassays.

Herein, we establish the performance of a dip-and-go multiplex system (Figure 1) for HTS bioassays based on a combination of inductive nESI with field amplified micro-electrophoretic cleaning. Inductive nESI enables the “dip” method of sample introduction for samples of approximately 100 nL volume from a 96-well microtiter plate. The samples are introduced into the emitters by simply immersing the emitter tips into the sample solution, significantly decreasing the time compared to traditional nESI techniques. To fit the format of a 96-well microtiter plate, a 3D printed emitter holder was used for simultaneous introduction of samples from one row of the microtiter plate. We used a DC electrical field to initiate inductive nESI and to perform micro-electrophoresis by simply modulating the electrical field strength.

* Dr. Z. Wei, Z. Xie, Prof. R. G. Cooks
Aston Labs, Department of Chemistry, Purdue University
560 Oval Drive, West Lafayette, IN 47906-1393 (USA)
E-mail: cooks@purdue.edu

R. Kuvelkar, V. Shah, Dr. K. Bateman, Dr. D. G. McLaren
Merck & Co., Inc.
2000 Galloping Hill Road, Kenilworth, NJ 07033 (USA)
E-mail: david.mclaren@merck.com

Supporting information and the ORCID identification number(s) for the author(s) of this article can be found under:
<https://doi.org/10.1002/anie.201909047>.

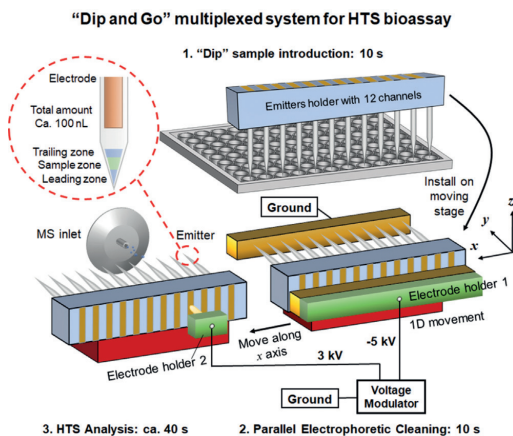


Figure 1. Instrumentation for dip-and-go multiplexed HTS bioassay. The emitter holder has 12 channels which can hold 12 emitters designed to fit the 96-well plate format. Step 1 is the “dip” step used for sample introduction. The emitters are immersed into water, sample solution and water in turn (the Figure only shows dip into sample solution) to load the leading and trailing zones with pure water and the mid zone with sample solution. In step 2 the holder is installed on a 1D moving stage and subjected to 10 s electrophoretic cleaning. In step 3, the emitters are moved into position for inductive nESI-MS analysis.

During the “dip” event we load three separate bands of solutions with different electrical conductivity into the emitter. This allows field amplification,^[17] a method that can dramatically increase the performance of micro-electrophoresis. The high-performance cleaning process takes just 10 s and is applied to the emitters in parallel, resulting in a significantly improved and rapid sample clean-up process. Subsequently, the emitters are subjected to inductive nESI analysis. The emitter holder is moved in front of the mass spectrometer to allow screening at a rate of 1.3–3.5 s/sample. The total analysis time of one row of a 96-well microtiter plate is ca. 2 min, comprised of ca. 10 s for sample loading, 10 s for field amplification micro-electrophoretic cleaning, ca. 40 s for inductive nESI analysis and 50 s for homing the device for measurement of the next row. In order to evaluate the performance of our multiplexed nESI system for application to HTS bioassays we selected BACE1 as a prototypical enzyme of relevance for HTS since it has been successfully screened by mass spectrometry in the past.^[18]

First, we used the multiplexed system to perform chemical reaction screening of samples in a 96-well array to test the basic analytical performance. As a test case, we investigated substituent effects on the Claisen–Schmidt reaction, screening multiple reactions to generate a Hammett plot. Reactions between 6-hydroxyindanone and five benzaldehydes with different substituents were examined in a 96-well plate in a period of 30 minutes. The reactions are quenched using 10 × methanol and, without chemical pretreatment, split into 5 rows for MS analysis. We dipped the emitters into the sample wells for 5 seconds and then performed inductive nESI-MS

analysis at a rate of 1.3 s/sample (Figure S1 in the Supporting Information). The high linearity of Hammett plot indicates the good performance of the dip-and-go system in chemical reaction screening.

For the bioassays, we examined the analytical performance of inductive nESI with field amplification micro-electrophoresis. Figure 2 compares analysis of the reaction

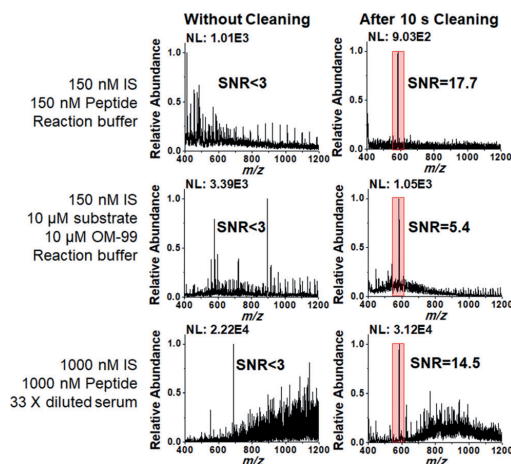


Figure 2. Full scan mass spectra using inductive nESI analysis of KTEEISEVNL (m/z 581.5) with internal standard KTEEISEVN(L- $^{13}\text{C}_7$) (m/z 585.0) in different biological matrices with and without field amplification micro-electrophoretic clean-up. Reaction buffer is 2 nM BACE1 enzyme, 6 mM sodium acetate, 1.5% glycerol, 0.25% DMSO, 3 ppm Brij-27 and 1% formic acid.

product peptide here designated as KTEEISEVNL and its isotopically labeled internal standard (IS) KTEEISEVN(L- $^{13}\text{C}_7$) (stoichiometry is 1:1) in different biological matrices using full m/z scan mass spectra. Spectra obtained without electrophoretic cleaning (left column) show strong ion suppression effects leading to signal to noise ratios (SNR) below 3. This is inadequate even for qualitative analysis. The spectra obtained after 10 s of electrophoretic clean-up (right column) by contrast show SNR of 17.7 and 5.4 in the reaction buffer and in buffer with interfering peptides, respectively. After clean-up, the ratio of KTEEISEVNL and IS remains 1:1 as expected, demonstrating the precision of the technique. An LoQ of 150 nM was obtained for the KTEEISEVNL using full scan MS at SNR > 10 (Figure S2). Plots of the calibration curve acquired by full scan MS after clean-up MS demonstrate a linear dynamic range from 150 nM to 4000 nM ($R^2 = 0.9950$, Figure S3). The results of analyzing 1000 nM KTEEISEVNL in diluted human serum are also encouraging. As shown in full scan spectra, electrophoretic clean-up of human serum sample shows SNR of 14.5 for the target peptide while the peptide peaks are submerged under baseline without cleaning. Ion isolation followed by a mass scan increased the SNR from below 3 to 20–40 and also increased the signal intensity 13.2 to 130-fold (Figure S4). We also interrogated

precision and carryover in high-throughput bioassays (detailed discussion is available in the Supporting Information). Briefly, the relative standard deviation was less than 15% at a scan rate of 2 to 4 s/sample (Figure S5). The carryover between two measurements using the same emitter was less than 2.5% (Figure S6). The above results demonstrate the power of the dip-and-go multiplexed system in bioassays.

Figure 3 shows the operating mode of field amplification micro-electrophoresis. Figure 3a shows the formation of three distinct sample and solvent zones before electrophoresis: the highly conductive sample solution with its complex matrix (zone 2) and the surrounding low conductivity leading (zone 1) and trailing (zone 3) zones of pure water. Electrophoresis (on at 3 s, off at 12 s, Figure 3b) was performed by simply changing the electrode voltage from zero to -5 kV and maintaining this value for ca. 10 s. After electrophoresis (12 s to 45 s, Figure 3b), the electrode voltage was changed to $+3$ kV for inductive nESI analysis. The total ion chromatogram (TIC, Figure 3c) after cleaning is stable while the ion map shows multiple extracted ion chromatograms (Figure 3d). Three typical zones appear after clean-up. Typical mass spectra (Figure 3e) of zone 1 are very noisy; the spectrum of zone 2 is very clean with the analyte peptides displaying very high SNR and enhanced signal intensity, while the spectrum of zone 3 shows matrix peaks. These results are consistent with the following proposed mechanism, based on our prior study of this effect:^[13c,16b,d] during electrophoresis (-5 kV voltage applied to the electrode) a strong static electrical field in the solution pulls small cations and positively charged complexes into zone 3 (they show up later as the interference peaks in the MS of zone 3); the initial negative potential also

pushes small anions into zone 1 so cleaning the analyte in zone 2 of interfering negatively charged ions. By removal of the high mobility ions from zone 2, a commensurate narrowing of the bandwidth and preconcentration of weak electrolytes (e.g. peptides) within zone 2 will occur to compensate for the decrease in conductivity. Since electrical field strength is inversely proportional to conductivity,^[17] an amplified electrical field is created inside zones 1 and 3 which accelerates the separation (additional discussion of the clean-up process is available in the Supporting Information). This special field amplification operating mode for micro-electrophoresis is quite different from traditional field amplification capillary zone electrophoresis,^[19] in which the sample zone has much lower conductivity than the surrounding buffer used for electrophoresis. Indeed, this operating mode is generally not achievable in traditional capillary zone electrophoresis because buffer solution with good conductivity is needed to control the Joule heating that limits performance in electrophoresis.^[20] In the micro-electrophoresis driven by the inductive static electrical field, the current is much lower.^[13c,21] Since the sample volume introduced by our dip-and-go strategy is on the order of 100 nL, a low current generates sufficient electrophoretic separation without excessive Joule heating.

As an example of a prototypical HTS application, we used our dip-and-go multiplexed system to determine the IC_{50} of the well-characterized BACE1 inhibitor OM99-2 by following BACE1 catalyzed hydrolysis of KTEEISEVNLDAEFRHDK to KTEEISEVNL. We spiked 150 nM KTEEISEVNL(L - $^{13}C_7$) into the final assay as internal standard. Since the concentration of the peptide product can be very low in highly inhibited reactions, we used the MS/MS scan mode for quantification and determination of IC_{50} . As shown in Figure 4a, for an artificial solution with 1:1 ratio of KTEEISEVNL:IS, we isolated ions from m/z 578 to 588 and fragmented them before recording product ion spectra. Two pairs of product ions showing a 1:1 intensity ratio for the 7 Da (singly charged) mass difference appear: the pair of m/z 246.2 and 253.2 and the pair of m/z 561.3 and 568.3. As the ion pair m/z 246.2 and 253.2 shows a very low baseline and the very high SNR of 110, this pair was used for quantification. (The advantages of the product ion spectrum vs. simple ion isolation are shown in Figure S7.) Twelve samples were prepared spanning 5-orders of magnitude range of OM99-2 concentrations in order to determine the IC_{50} against BACE1. These samples were placed in 7 rows (7 replicates, 84 samples in total) of a microtiter plate and analyzed by dip-and-go analysis. Figure 4b shows a typical TIC as well as EIC for the IS and target peptide from analysis of one row of samples at a scan

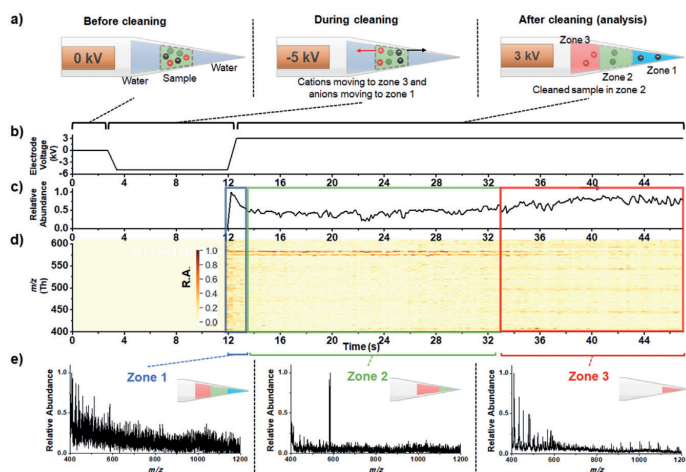


Figure 3. Process of field amplification micro-electrophoresis. a) Ion migration in each step (note that electroneutrality will be maintained over the whole solution volume including zones 1, 2 and 3 while each individual zone can have a net charge). b) Electrode voltage vs. time in the process. c) TIC over course of the process. d) Ion map of the process. e) Typical mass spectra from the three zones.

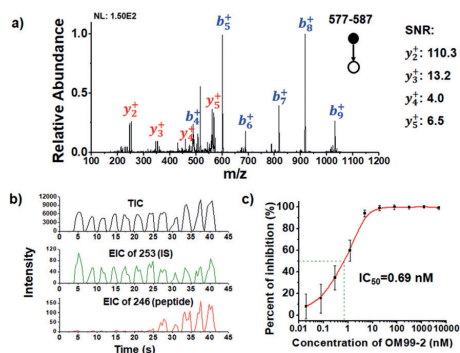


Figure 4. a) MS² spectrum of precursor ions in range of m/z 578 to 588. The collision energy used is 30 (nominal value). This range covers the doubly charged precursor ions of KTEEISEVNL (m/z 581.5) and IS (m/z 585.0). The spiked ratio of the KTEEISEVNL and IS is 1:1. b) Typical TIC and EIC of dip-and-go analysis of one row of samples. c) IC₅₀ of inhibitor OM99-2 to BACE1 determined using the dip-and-go system.

rate of 3.5 s/sample. From left to right the inhibition is 100% to 0. These seven measurements were normalized to plot the IC₅₀ curve shown in Figure 4c.

The IC₅₀ curve determined by our dip-and-go multiplexed system is consistent with that determined by an LC-MS experiment performed specifically to allow this comparison (Figure S8). The total measurement time of these 84 samples by the dip-and-go method was only ca. 14 min while that for LC-MS was 11 hours (8 min/sample).

In summary, we have developed a dip-and-go multiplexed system that is suitable for HTS bioassays. This system uses a novel “dip” sample loading strategy which can be combined with inductive nESI to achieve HTS nESI analysis for the first time. We have developed a new operating mode for field amplification micro-electrophoresis in which small volumes of reaction solution are (i) purified in situ and (ii) preconcentrated. This method enables accelerated sample clean-up and ultra-high sensitivity HTS bioassays. The dip-and-go system shown in this manuscript is a lab prototype; the process of “dip” sample introduction is not fully automated; the voltage control system should also be improved, and data processing software needs to be developed. The screening rate of the prototype is 1.3–3.5 s/sample and the total analysis time for 96 samples is ca. 16 min, representing a significant improvement over the throughput of conventional LC-MS (several min per sample) and competitive with typical “catch and elute” SPE-MS systems used for current HTS bioassays such as the RapidFire platform (ca. 8 s/sample). With the aid of high-resolution MS, the performance of the “dip-and-go” system can be further improved. The current multiplexed system is quite efficient for the analysis of compounds with low electrical mobility, for example, oligosaccharides and peptides, because they can be preconcentrated in the mid zone and separated from matrix components; the clean-up for small metabolites is still challenging since they may move together with the salts. We believe that with further optimization this

system has the potential to play a significant role in accelerating chemical and pharmaceutical discovery.

Experimental Section

Claisen–Schmidt reaction: Reactions are performed at 100 mM with equimolar reactants and 1.8 M KOH. Reactions were quenched by 10× dilution with methanol in 96-well microtiter plate. BACE1 reaction: 2.5 μL of diluted OM99-2 (in DMSO) was added to 4 nM BACE1 enzyme in 300 μL of assay buffer consisting of 20 mM NaOAc, pH 4.5, 5% glycerol, 0.001% Brij-27. The mixtures were subsequently incubated for 30 minutes at ambient temperature. Afterwards, the reaction was initiated by addition of 200 μL of 25 μM peptide substrate (KTEEISEVNLDAEFRHDK; 10 μM final concentration) and incubated for 210 minutes at ambient temperature. The reaction was quenched with 500 μL of quench solution containing 2% formic acid and 300 nM KTEEISEVNL-[L-¹³C] internal standard. More detailed information is available in the Supporting Information.

Acknowledgements

We acknowledge sponsorship of this research by the Merck–Purdue Partnership in Analytical Sciences. Thanks to Richard Hosler of the Jonathan Amy Facility for Chemical Instrumentation for help in fabricating the device.

Conflict of interest

The authors declare no conflict of interest.

Keywords: enzyme inhibition · field amplification · inductive nano-electrospray · micro electrophoresis · pharmacokinetics

How to cite: *Angew. Chem. Int. Ed.* **2019**, *58*, 17594–17598
Angew. Chem. **2019**, *131*, 17758–17762

- [1] a) J. Drews, *Science* **2000**, *287*, 1960–1964; b) D. B. Kassel, *Chem. Rev.* **2001**, *101*, 255–267.
- [2] A. Gaulton, L. J. Bellis, A. P. Bento, et al., *Nucleic Acids Res.* **2012**, *40*, D1100–D1107.
- [3] M. J. Wildey, A. Haunso, M. Tudor, et al., *Annu. Rep. Med. Chem.* **2017**, *50*, 149–195.
- [4] K. H. Shaughnessy, P. Kim, J. F. Hartwig, *J. Am. Chem. Soc.* **1999**, *121*, 2123–2132.
- [5] J. W. Noah, W. Severson, D. L. Noah, et al., *Antiviral Res.* **2007**, *73*, 50–59.
- [6] J. B. Baell, J. W. M. Nissink, *ACS Chem. Biol.* **2018**, *13*, 36–44.
- [7] X. S. Song, J. Zhang, X. Chen, et al., *J. Biomol. Screening* **2016**, *21*, 117–126.
- [8] a) C. Haslam, J. Hellicar, A. Dunn, et al., *J. Biomol. Screening* **2016**, *21*, 176–186; b) M. Winter, T. Bretschneider, C. Kleiner, et al., *SLAS Discovery* **2018**, *23*, 561–573; c) M. Winter, R. Ries, C. Kleiner, et al., *SLAS Technol.* **2019**, *24*, 209–221.
- [9] a) I. Sinclair, R. Stearns, S. Pringle, et al., *J. Lab. Autom.* **2016**, *21*, 19–26; b) G. A. Gómez-Ríos, C. Liu, M. Tascon, et al., *Anal. Chem.* **2017**, *89*, 3805–3809.
- [10] M. Wilm, M. Mann, *Anal. Chem.* **1996**, *68*, 1–8.
- [11] a) I. M. Lazar, R. S. Ramsey, S. Sundberg, et al., *Anal. Chem.* **1999**, *71*, 3627–3631; b) U. Bahr, A. Pfeningner, M. Karas, et al., *Anal. Chem.* **1997**, *69*, 4530–4535.

- [12] X. J. Guo, T. L. Fillmore, Y. Q. Gao, et al., *Anal. Chem.* **2016**, *88*, 4418–4425.
- [13] a) G. M. Huang, G. T. Li, J. Ducan, et al., *Angew. Chem. Int. Ed.* **2011**, *50*, 2503–2506; *Angew. Chem.* **2011**, *123*, 2551–2554; b) G. M. Huang, G. T. Li, R. G. Cooks, *Angew. Chem. Int. Ed.* **2011**, *50*, 9907–9910; *Angew. Chem.* **2011**, *123*, 10081–10084; c) Z. W. Wei, X. C. Xiong, C. A. Guo, et al., *Anal. Chem.* **2015**, *87*, 11242–11248.
- [14] N. Gasilova, Q. L. Yu, L. Qiao, et al., *Angew. Chem. Int. Ed.* **2014**, *53*, 4408–4412; *Angew. Chem.* **2014**, *126*, 4497–4501.
- [15] L. Qiao, R. Sartor, N. Gasilova, et al., *Anal. Chem.* **2012**, *84*, 7422–7430.
- [16] a) G. Y. Li, S. M. Yuan, S. H. Zheng, et al., *Anal. Chem.* **2018**, *90*, 3409–3415; b) Z. W. Wei, S. Han, X. Y. Gong, et al., *Angew. Chem. Int. Ed.* **2013**, *52*, 11025–11028; *Angew. Chem.* **2013**, *125*, 11231–11234; c) X. Y. Gong, X. C. Xiong, Y. C. Zhao, et al., *Anal. Chem.* **2017**, *89*, 7009–7016; d) Z. Z. Zhang, C. J. Pulliam, T. Flick, et al., *Anal. Chem.* **2018**, *90*, 3856–3862; e) H. Y. Zhu, G. C. Zou, N. Wang, et al., *Proc. Natl. Acad. Sci. USA* **2017**, *114*, 2586–2591.
- [17] J. Lichtenberg, E. Verpoorte, N. F. de Rooij, *Electrophoresis* **2001**, *22*, 258–271.
- [18] G. C. Adam, J. Meng, J. M. Rizzo, et al., *J. Biomol. Screening* **2015**, *20*, 212–222.
- [19] a) F. E. P. Mikkers, F. M. Everaerts, T. P. E. M. Verheggen, *J. Chromatogr.* **1979**, *169*, 11–20; b) R. L. Chien, J. C. Helmer, *Anal. Chem.* **1991**, *63*, 1354–1361; c) D. S. Burgi, R. L. Chien, *Anal. Chem.* **1991**, *63*, 2042–2047.
- [20] G. Y. Tang, D. G. Yan, C. Yang, et al., *Electrophoresis* **2006**, *27*, 628–639.
- [21] A. Y. Li, A. Hollerbach, Q. J. Luo, et al., *Angew. Chem. Int. Ed.* **2015**, *54*, 6893–6895; *Angew. Chem.* **2015**, *127*, 6997–6999.

Manuscript received: July 19, 2019

Accepted manuscript online: October 7, 2019

Version of record online: October 23, 2019